UNIVERSITAT POLITÉCNICA DE CATALUNYA

Department of Physics - Division of Aerospace Engineering

Comparison of the response of different configurations of aircraft repair patches under static and dynamic loading

By

Siddharth Pitta

Advisors:

Dr. José I. Rojas

Prof. Daniel Crespo

Escola d'Enginyeria de Telecomunicació i Aeroespacial de Castelldefels

A thesis submitted for the degree of Doctor of Philosophy

Castelldefels, September 2019

Acknowledgements

I would like to acknowledge and thank the huge support and help received from my supervisors Dr. Jose. I. Rojas and Prof. Daniel Crespo. Dr. Rojas had helped me throughout the journey of my PhD from initial days counting from application to the present day.

I would like to thank Prof. Abdel Wahab for supporting me with the research stay at Ghent University, Belgium. I would also like to thank lab technician Francesc Joaquim Garcia without whom I would have troubles finishing experiments.

I would like to thank my friends Swapan Rana and Santhanu Pradhan. Their support was huge at the beginning of my PhD. I would also like to thank my colleagues Enrique, Ruxandra, Georgy, Leila, Chenyang, Tiara, Mitra, Cecilia and Patricia.

At last but not the least, I would like to thank the support received at all the moments from my family Ammaji, VD Rao and Harsha.

The work presented in this thesis is funded by Spanish Ministry of Economy and Competitiveness (MINECO) through the grant FIS2014-54734P, FIS2017-82625-P and Generalitat de Catalunya through grant AGAUR 2017 SGR 42. Also, thanks to mobility grant from Generalitat de Catalunya and Research Foundation Flanders (FWO) project G018916N. Finally, sincere thanks to Generalitat de Catalunya for supporting me through AGAUR grant 2017FI_B 00179, 2018FI_B1 00102 and 2019FI_B2 00097.

Index of contents

Outline and research target

In the present day, the fastest mode of transport is by air. Air transportation demand has increased by two folds in the last decade. Demand for the air transport is increasing because of easy accessibility of airplanes with low flight fares and population growth. Most airlines aim at minimising their operational costs and maximizing aircraft use factor (i.e., make the maximum possible flight hours with the least turn-around time). Operational costs can be reduced, for instance by improving fuel efficiency, reducing drag acting on the aircraft and by reducing maintenance costs.

As an aviation structural engineer, better understanding of repair technologies has significant role in minimising the operational costs. Namely, an expensive, time-consuming process in airline industry is the maintenance of aircraft in between flights, detection of early formation of cracks, monitoring crack growth and fixing the corresponding parts with joints, when necessary. This thesis focusses on repair technologies of aircraft structural parts to regain their operational strength.

In recent aircraft generations, manufacturers have shifted the main structural material from aluminium alloys to composites. For instance, Airbus A350 and Boeing 787 have more than 50% of their structure from composites. Composites have many advantages over conventional aluminium alloys, which made aviation industry to propel their production. Composites have very high specific strength to weight ratio compared to aluminium alloys, but when they are riveted, more than 60% of the material strength is lost due to the presence of the holes. Holes made in the composite structure for riveting introduce damage to the plies and this may cause composite material to fail without any early detection before the scheduled maintenance checks. Riveting process of composite parts is still common practice in airline industry maintenance as a quick and temporary solution. To overcome this far-from-optimum, it is necessary to study various alternative repair technologies to compare their behaviour with conventional riveted method under different load conditions.

Most of the aircraft structures are designed with a safety factor (design load/operational load) of 1.5 for static strength while predominant failures occur due to repetitive or cyclic loads known as fatigue.

In this thesis, repair technologies such as riveted, adhesive bonded and hybrid (riveted + adhesive bonded) methods are presented for two different substrate materials: namely, aluminium alloy 2024- T3 (metal) and carbon fibre reinforced epoxy (composite). Metal and composite substrates are repaired with metal and composite twin doublers under riveted, adhesive bonded and hybrid joint configurations. Hence, metal-metal, metal-composite, composite-composite and composite-metal joint configurations are investigated through experiments and numerical analysis.

Numerical analysis consists of finite element analysis in ABAQUS CAE, and fatigue prediction tools such as FRANC2D/Layered and FRANC3D. In addition, a tool from Autodesk's Helius Composites tool is used to predict various parameters of composite substrate such as ply load distribution, progressive failure analysis and failure mode of composite plies. Experimental results and numerical analysis results are compared and error percentages are smaller than 5%.

List of Figures

List of Tables

List of Publications

- Pitta S, Carles VDLM, Roure F, Crespo D, Rojas JI. On the static strength of aluminium and carbon fibre aircraft lap joint repairs. *Compos. Struct.* 2018; 201(1): 276-290.

- Pitta, S.; Roure, F.; Crespo, D.; Rojas, J.I. An Experimental and Numerical Study of Repairs on Composite Substrates with Composite and Aluminum Doublers Using Riveted, Bonded, and Hybrid Joints. *Materials* 2019, *12*, 2978.

- S Pitta, J I Rojas and D Crespo, "Comparison of fatigue crack growth of riveted and bonded aircraft lap joints made of Aluminium alloy 2024-T3- A numerical study", Journal of Physics: Conference Series, Volume 843. DOI: 10.1088/1742-6596/843/1/012035

- S Pitta, J.I. Rojas, D. Crespo and M. Abdel Wahab, "Fatigue life analysis of un-repaired and repaired metallic substrate using FRANC2D", In: Abdel Wahab M. (eds) Proceedings of the 7th International Conference on Fracture Fatigue and Wear. FFW 2018 2018. Lecture Notes in Mechanical Engineering. Springer, Singapore. https://doi.org/10.1007/978-981-13-0411-8_50

- Siddharth Pitta, J. I. Rojas and Daniel Crespo, "Comparison of the response of different configurations of Aircraft repair patches under Static and Dynamic loading", 13th FEMS Junior EUROMAT Conference, Lausanne, Switzerland, 10-14. July 2016.

- Siddharth Pitta, J. I. Rojas and Daniel Crespo, “Comparison of the performance of aircraft repair patches consisting of riveted lap joints on aluminium and composite substrates”, FEMS EUROMAT 2017, Greece, 17-22 September 2017.

- Siddharth Pitta, J. I. Rojas and Daniel Crespo, “Comparison of fatigue crack growth of riveted and bonded aircraft lap joints made of aluminium alloy 2024-T3 substrates- A numerical study”, International Conference on Fracture Fatigue and Wear 2017, 26-27 July 2017.

- Siddharth Pitta, J. I. Rojas and Daniel Crespo, “Fatigue life analysis of un-repaired and repaired metal substrate in FRANC2D”, Seventh International Conference on Fracture Fatigue and Wear, Ghent University, Belgium 9-10 July 2018.

- Siddharth Pitta, Francesc Roure, Daniel Crespo and Jose I. Rojas, “Investigation on repairs of aircraft composite structures made with various joining techniques”, International Conference on Composite Structures, Bologna, Italy, 4-7 September 2018.

Chapter 1: Introduction

An aircraft is a complex engineering structure often manufactured from many small parts. These small parts are made from sheet, extruded sections, forgings, castings, or machined shapes, which indeed are joined together to form sub-assemblies. These sub-assemblies are joined together to form major components such as the wings, fuselage, engines, horizontal tail plane, vertical tail plane, etc. Thus, an aircraft is an assembly of major assemblies made from different materials as shown in Fig. 1.1. Most parts of the complete aircraft structure must be organised and arranged so that they can be disassembled for logistics, inspection, repairs or replacements, etc. Hence, joining techniques play a major role in aircraft assemblies, and the mechanical properties of the aircraft structure depend on these joining techniques. Most commonly, parts are joined by either rivets or bolts. To facilitate easy assembly and disassembly, it is convenient to have a minimum number of fasteners for bolted or riveted connections.

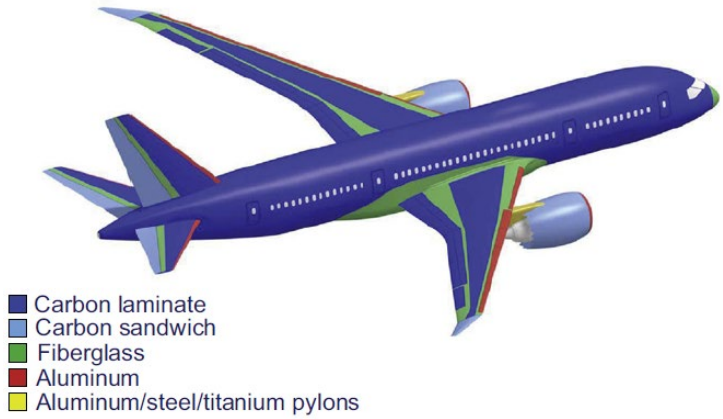

Figure 1.1: *Materials used in Boeing 787 Dreamliner [79].*

Consider the case of a semimonocoque wing structure made from metal. It usually resists bending stresses thanks to numerous stringers and sheet distributed along the wing cross-section. Thus, the wing cannot be made as one continuous riveted assembly from root to tip, but is usually spliced at two

or more cross-sections. Splices are designed so that multiple fasteners can transfer all loads across the splice. The fasteners that connect members are called fittings, and are designed to resist the highly concentrated loads resulting from load transfer process from spars to skin panels and stringers. Many uncertainties exist due to the stress distribution in the fittings. Care should also be taken for manufacturing tolerances such as fastener diameter to hole dimensions, since any small variation in dimensions may affect the desired stress distribution. In order to prevent maximum variations, the fittings are designed with a safety margin of 15%. This factor is generally implemented in the design of the entire fitting, including riveted, bolted, or any welded joints [1].

1.1 Structural design philosophies

Ensuring structural integrity of aircraft structures involves fulfilling fatigue and damage tolerance requirements by Federal Aviation Regulations (FAR) 25.571 [2]. The purpose of fatigue analysis is to ensure that aircraft structures do not crack too soon, while that of damage tolerance analysis (DTA) is to ensure that cracks do not grow too fast once initiated. In addition, that the given component can fulfil its mission under service life conditions even if it is provided by the manufacturer with a given amount of damage (cracks of a given length). Some other important concepts in aircraft design are safe life and fail-safe.

Safe life:

Certain critical components in the airframe must be free of cracks throughout their service life, and any failure of these components would result in a catastrophic structural collapse and/or loss of aircraft. The safe life design criterion is demonstrated by test evidence with appropriate scatter factors to ensure safety [2]. The crash of a General Dynamics F-111 fighter from the US Air Force (USAF) while attempting a 4g steady manoeuvre has forced to develop a new design method called fail-safe.

Fail-safe:

In the Fail-Safe design approach, the structure is designed to be able to continue carrying the service loads following the failure of a component, to ensure local failure to a safe condition, such that there is no catastrophic failure of the aircraft. The rate of fatigue crack growth (FCG) is not monitored but it is necessary to detect when failure has occurred through periodic inspections. Structural repairs are then required to restore the component to serviceable conditions. The failure of a Boeing 707-300 freighter of DAN-Air services lead to DTA design method.

Damage Tolerance Analysis (DTA):

This design approach ensures that the structure is tolerant to serious fatigue, corrosion, and accidental damage that can occur within operational life of the aircraft, and that it can withstand reasonable loads without failure or excessive structural deformation until damage is detected. In 1978, the Damage Tolerance concept is introduced into airworthiness regulations for new aircraft.

When structural components develop cracks of size equal or greater than 12.7 mm, they have to be repaired to restore their strength, as established in FAR 25.1529 (Continuum Airworthiness regulation) and FAR 25.613 (Material strength properties and material design values) [3].

Joints are among the most common locations for failures in the aircraft structure. Therefore, joints are one of the most important aspects to be considered in the design, followed by structural testing. Failures can occur due to various reasons: fatigue is responsible for most failures of metallic materials, for example, but fatigue can also be due to secondary stresses due to eccentricities, stress concentrations, fretting or slippage in connections, or a combination of these phenomena. These factors do not affect the static strength. However, they have a great influence on fatigue life of the joints and the adjacent structure. Some of the most important considerations while designing joints are as follows:

(a) Eccentricities

If eccentricities appear in a joint, they cause secondary bending moments, which is a problem, as the load transfer does not take place in an optimum way. For example, joints are designed to carry tensile, compressive, or shear loads where secondary bending might affect the objective of the joint. One of the reasons for secondary bending is the thickness of joints.

(b) Fatigue resistance

Joints must be designed taking into consideration the fatigue resistance of the resulting repaired structure.

(c) Mixed-fasteners

Generally, it is not good practice to use both rivets and bolts in a same joint. Each joint is designed according to the structural load it has to carry. If the components are changed, it might influence the performance of the structure.

(d) Efficiency of the joint

The efficiency of the joint depends on the number of fasteners, the load it can carry, and the load distribution among fasteners. Joints should be designed uniformly considering both sides of the sheet material to prevent secondary bending.

1.2 Riveted Joints

The most commonly used mechanical fasteners in the air transport are rivets. Rivets are permanent fasteners, which simplifies assemblies. Primary reason for riveting is due to low cost, labour costs and machine time set to rivet parts. Compared to threaded fasteners, rivets are low in cost to manufacture as they are made in large quantities with high-speed machines. Some of the advantages of the rivets are:

- Ability to joint dissimilar materials, metallic or non-metallic parts of various thicknesses.
- Rivets have various finishes such as Parkerizing, plating or paint.
- Rivets can serve for multi-purposes such as fastening, electric contacts, stops or pivot shafts.
- Rivets are light weighted among other mechanical fasteners.

Some of the disadvantages are as follows:

- The tensile and fatigue strengths of rivets are generally lower than screws or bolts.
- Riveted joints cannot be disassembled for maintenance without damaging or destroying the rivets.
- High stress concentrations appear around the rivet holes.

1.2.1 Design of riveted joints

Some of the geometric design parameters that effect the fatigue strength of the riveted joints are discussed in this section:

(a) Number of rivets

The number of rivets in a riveted joint is usually proportional to the load it has to carry. Namely, if the joint must carry high loads, the thickness of the doubler is usually increased, as well as the number of rivets. Results from [4, 5] clearly show that the fatigue strength of lap joints

increases significantly with the number of rivet rows. Moreover, experiments showed that fatigue life increased from 331×10^3 to 500×10^3 cycles when using four rivet rows instead of three [6]. These improvements of fatigue performance with the number of rivet rows can be explained by the reduction of the load transfer through the critical outer rivet rows.

(b) Rivet row spacing

Results for specimens with protruding head rivets demonstrated that increasing the rivet row spacing improves the fatigue properties of joints [4]. Experiments with countersunk rivets suggest also better fatigue performance with increasing rivet spacing [5]. This can be explained by one of the benefits of using longer rivet row spacing in lap joints: the fact that secondary bending is lowered.

(c) Rivet row pitch

The ratio between the rivet pitch from row to row and the rivet diameter (s/D_0) is based on static strength calculations [7]. Low stress concentration factors were observed for joints with s/D_0 of 2.5 [8]. Further experiments suggested that the optimal ratio ranges from 2.5 to 3.75 [9], values that are favourable for both static and fatigue loads.

(d) Rivet-edge distance

The distance between the edge of the joint and the outer-most rivet row appears to have little effect on the fatigue strength [7]. According to [10], the mid-axis of the outer rivet row should be at least twice the diameter of a rivet, which is a static strength requirement. The minimum permissible edge distance is 1.5 times the rivet diameter, if the edge is parallel to the load direction [9].

(e) Rivet pattern

There are two types of rivet patterns: namely, in-line and zigzag. The effect of the rivet pattern on riveted joints was studied in [11]. Further investigations concluded that there is no difference in the fatigue strength of double-row lap joints with in-line and zigzag rivet patterns [5, 12].

(f) Sheet thickness

The sheet thickness must be increased when the joint has to carry higher loads, but the size of the rivets should also be increased as well. Fatigue tests on double-row lap joints with protruding rivets with sheet thickness ranging from 0.8 to 1.6 mm are reported in [13]. S-N data reveal that a small change in thickness from 0.8 to 1 mm has little effect on fatigue properties [13]. Compared to thinner specimens, those plates thicker than 1.6 mm have shorter fatigue lives. From fatigue tests on simple-lap joints with protruding head rivets and countersunk rivets, it was found that, for the same conditions, specimens with larger rivet diameter-to-sheet thickness ratio (D/t) had longer fatigue life [14].

1.2.2 FAR specifications for riveted lap joints

In this section, specifications and regulations established by FAR for installation of rivets in airframe structures are discussed [15]:

(a) Repair layout:

Involves determining the number of rivets needed the size and style of rivets, material properties, temper conditions, size of holes, distance between holes and distance between hole and the edges. All distances are usually established in terms of rivet diameter.

(b) Rivet length:

The total length of the rivet depends on the combined thickness of the plates to be joined (termed as "grip length") and the rivet shank needed to form a proper stop head.

(c) Rivet strength:

For airframe structural purposes, the strength of the replacement rivets is of primal concern. Rivets should not be interchanged based on material type due to differences in thermal expansion.

(d) Stresses on rivets:

Rivets are usually subjected to shear and/or tensile stresses. On one side, the rivet shear strength is the ultimate force required to slice a rivet in a joint. On the other, the rivet bearing strength refers to the tensile force needed to pull a rivet such that the hole in the plate experiences elongation.

(e) Rivet spacing:

This parameter is the measured distance between the revolution axes of two successive rivets in the same row. The minimum spacing between protruding rivets should not be less than 3.5 times the rivet diameter.

(f) Edge distance:

Also called "edge margin" by some manufacturers, it refers to the distance from the centre of the first river to the edge of the sheet. Standards suggest that it should not be less than 2 and more than 4 times the rivet diameter.

(g) Rivet pitch:

It is the distance between the centres of neighbouring rivets in the same row. The smallest allowable rivet pitch is 3 rivet diameters, but the average pitch ranges from 4 to 6 rivet diameters. The minimum rivet pitch depends also on the number of rivet rows: for one and three rivet rows, the minimum pitch is 3 rivet diameters, and, for two rows, a minimum pitch of 4 rivet diameters is usually applied.

(h) Transverse pitch:

It is the distance between the rivet columns. The smallest allowable transverse pitch is 2.5 times the rivet diameter, and it is common practice to use 75% of the rivet pitch.

1.2.3 Parameters affecting fatigue strength

Some of the parameters that affect fatigue strength of riveted lap joints, such as the sheet and fastener materials, fastener types, manufacturing process, and squeeze force, are discussed in this section.

(a) Sheet material

The material used for the sheet in riveted joints has a predominant effect on the fatigue strength of the joint. Typically, aluminium alloys (AA) 2024-T3 and 7075-T6 are used for the fuselage and wing skin. The minimum mechanical properties required for the sheet materials, as specified by US regulations [16] are shown in Table 1.1. Either sheet material can be provided with a cladding of soft pure aluminium layer with thickness about 5% of the plate thickness. This aluminium cladding (Alclad) layer will provide protection from corrosion to the sheet [17].

Sheet material	**Thickness (mm)**	S_y **(MPa)**	S_u **(MPa)**	δ **(%)**	**Specification**
2024-T3	0.25-1.57	276	414	15	AMS-QQ-A-250/5
Alclad	1.6-3.25	289	427	15	MIL-HDBK-5H
7075-T6	0.3-0.99	482	538	7	AMS-QQ-A-250/13
Clad	1.06-3.18	482	551	8	MIL-HDBK-5H

Table 1.1: *Minimum mechanical properties for sheet materials set by US standards [16].*

Static mechanical properties such as the yield and tensile strength are slightly higher when tested in a direction aligned with the grain direction, but the elongation at fracture does not depend on the rolling direction. Schijve [18] tested the anisotropy of AA 2024-T3 sheet from seven manufacturers and reported an average ratio of yield stress in transverse to longitudinal direction of 0.9.

The effect of directionality is observed under fatigue loading. For AA 2024-T3 Alclad sheet, crack propagation requires 40% more time if loaded in the rolling direction, compared to specimens loaded in the transverse direction [19]. AA 2024-T3 Alclad has slightly better fatigue properties than AA 7075-T6 (see Fig. 1.2), but the static strength is higher for AA 7075-T6.

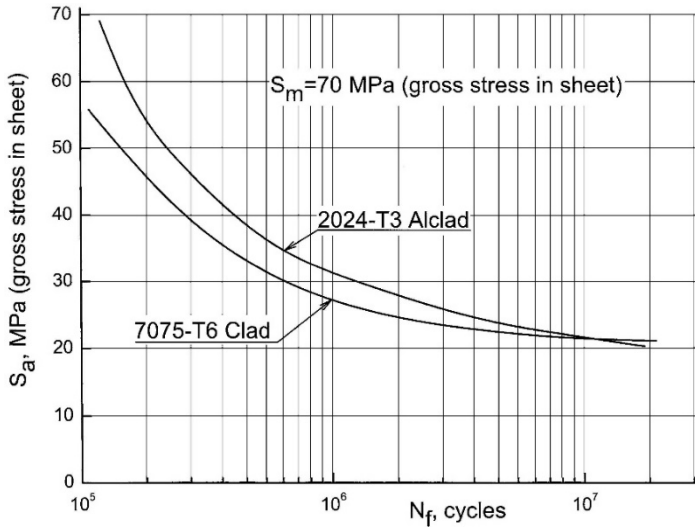

Figure 1.2: *Fatigue life comparison of AA 2024-T3 and 7075-T6 [20].*

(b) Fastener material and type

There are two types of rivets: solid and blind or pop rivets. Solid rivets are used when both sides of the sheet are accessible. Mostly, aluminium alloys are used for manufacturing solid rivets. While installing solid rivets, the driven head is formed by using a hand hammer, compressed air hammer, or rivet press. During this process, known as direct riveting, the manufactured head is supported by an anvil. While indirect riveting, the hammer is applied to the manufactured head and the driven head is shaped by a holding-up tool. For aerodynamic reasons, counter-sunk rivets are introduced to obtain a flat outer side of the joint. Any small gap between the countersunk rivet head and the countersunk hole must be sealed to prevent corrosion.

Blind rivets are another type of rivets that are used when access to both sides of the sheet is not possible or impractical [21-22]. The static strength of blind rivets is lower than solid rivets.

(c) Manufacturing parameters

In this section, various manufacturing process errors and tolerances are discussed. The fatigue behaviour of a joint depends on the fit between the rivet shank and the rivet hole, the clamping force of the rivets, and the friction between mating sheet surfaces [23].

(i) Riveting method

There are different riveting methods, such as hand, pneumatic, and hydraulic riveting. The effect of the riveting method on the fatigue properties of lap joints was investigated in [7-8]. In aviation industry, a light pneumatic rivet gun, in combination with a heavy stationary rivet die, is commonly used in assemblies. Fig. 1.3 shows a comparison of the influence of riveting methods on the fatigue strength.

Blind rivets are placed in the sheet in their corresponding positions and fastened with a pop rivet gun. Pop rivet guns can also be hand, pneumatic, or hydraulic driven.

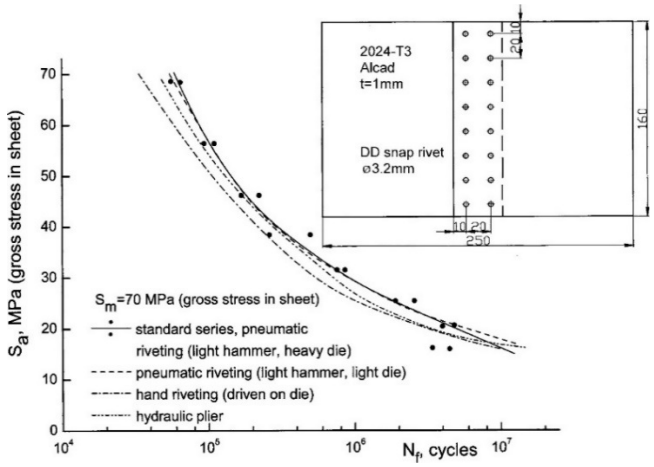

Figure 1.3: *Effect of riveting methods on fatigue strength of lap joints [24].*

(ii) Rivet holes

Laboratory specimens are usually produced under ideal conditions but in practice, such conditions are not always achievable, and fasteners may be installed in defective holes. Fatigue tests were carried out on rivet holes drilled when two sheets were clamped [24]. Specimens from a longitudinal fuselage lap joint of a Fokker 100 aircraft were investigated under full scale testing [25]. Countersunk and cylindrical hole mismatch caused gapping of the rivet head. Fatigue cracks were noticed at the rivets with extensive head gapping and inferior hole filling [25]. Smaller driven rivet head diameters are found near frames that are under stringer heads due to the poor accessibility to rivets for riveting tools. These imperfections are considered a main factor leading to poor fatigue properties of the joint compared to laboratory specimens. The effects of over deep countersinking and mismatched holes have also been investigated [26], as well as the application of finite element methods (FEM) to riveting for mismatched rivet holes [27, 28].

(iii) Cold working of holes

Cold working (CW) of the holes in repairs or new designs involving riveted or bolted lap joints is performed to improve their fatigue properties and damage tolerance characteristics [29]. CW introduces compressive residual stresses in the material surrounding the rivet hole, which improves the fatigue life. Compressive stresses in the tangential direction are created by provoking radial expansion of the material with an oversized tapered pin drawn through the hole [30].

FEM was used to simulate the residual stresses for 1 mm thick AA 2024-T3 sheet when rivet holes of 2.9 mm are tapered to 3.04 mm, using a tapered pin [31]. Moreover, it was reported that expansions of 2-3% are sufficient to obtain significant improvements in fatigue

strength [17]. This is confirmed by recent experiments on 4.5 mm thick AA 7075-T6 sheet with oversized steel pins inside holes of 5 mm diameter, with interference values ranging from 1.5% to 4% [32].

There are two common techniques of CW: split-sleeve method [29] and split-mandrel method [33]. Theoretical and experimental investigations have been devoted to CW, to quantify the residual stress field around the hole, and to determine the time required for crack initiation and propagation in aircraft components [34, 35].

(iv) Surface treatment of sheet

The most common surface treatment of aircraft parts is anodizing. In this case, an artificial oxide layer is grown, which serves as a pre-treatment for corrosion protection and better adhesive bonding [36]. Fatigue tests were performed on AA 2024-T3 Alclad single-lap joints with two rows of snap rivets of 3.2 mm diameter. Bare specimens, as well as specimens with chromic acid anodizing and sulphuric acid anodizing were studied, and their fatigue strength was compared, as shown in Fig. 1.4 [36]. At present day, the aviation industry uses phosphoric acid anodizing; chromic acid anodizing is no longer in use to reduce damage to the environment caused by chromates [37].

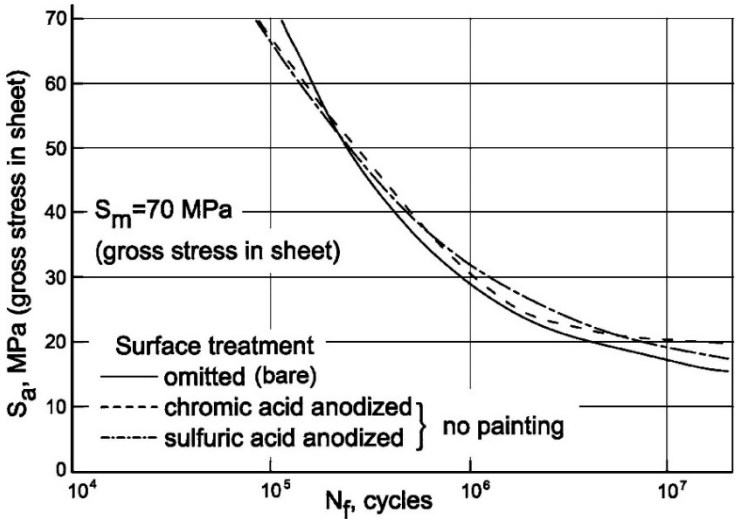

Figure 1.4: *Effect of surface treatment methods on fatigue strength of lap joints [36].*

Anodizing on top of cladding is detrimental for the properties of AA 2024-T3 sheet, but beneficial for aluminium with no cladding [38]. Another type of surface treatment consists in applying water-displacing fluids to avoid corrosion problems. The basic idea of this method is that the inter-faying fluid prevents entry of water into the joints, which prevents electrolytic corrosion [39].

(v) Squeeze force

The most important factor in riveted lap joints is probably the rivet installation process. It consists in squeezing the rivets with a sufficiently large force, resulting in plastic flow of the rivet, and leading to formation of the rivet driven head, as shown in Fig. 1.5.

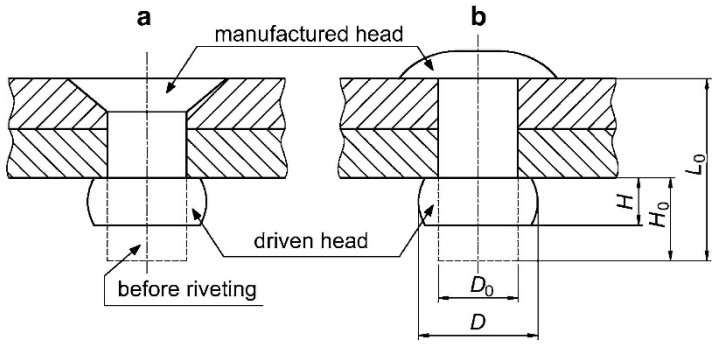

Figure 1.5: *Rivet dimensions before and after formation (a) countersunk and (b) protruding head [23]*

1) Effect of squeeze force on fatigue performance

Experimental results have shown that the driven head dimensions significantly influence the fatigue performance of riveted joints [8]. Namely, for double-row lap joints, fatigue properties have been reported to decrease with reductions of the driven head diameter of snap rivets [40]. On the other side, for anti-symmetric riveted lap joints, it was observed that fatigue cracks initiate at both end rivet rows if rivets had been squeezed equally [41]. Experiments also revealed that the rivet head diameter increases with the squeeze force. This leads to better filling of the hole and thus increased clamping between the plates of the joint. Some other advantages of applying higher squeeze force are:

- Increase in load transfer by friction
- The location of secondary bending stresses shifts away from the rivet holes
- Increases rivet hole expansion, implying lower local mean stress and a reduction in local stress amplitude

For riveted lap joints used in Airbus A340, fatigue life increased when rivet squeeze force was increased from 16.95 to 36 kN, as shown in Fig. 1.6 [41].

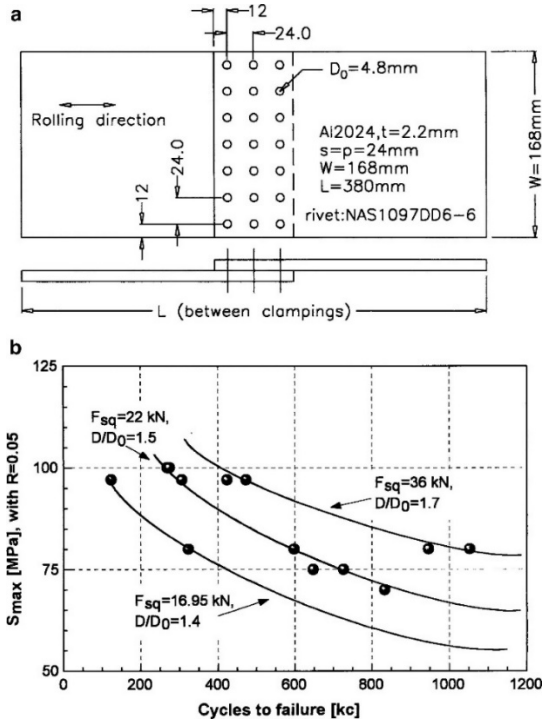

Figure 1.6: *Effect of rivet squeeze force on the fatigue life of Airbus A340 configuration (a) specimen dimensions and (b) S-N curve for 16.95, 22 and 36 kN [41].*

2) Effect of rivet driven head dimensions on squeeze force

The dependence of the rivet driven head dimensions on squeeze force has been thoroughly investigated [41, 42]. A very good correlation between the rivet driven head dimensions and the squeeze force was obtained in [43], where two countersunk rivet dimensions and three sheet thicknesses were studied, with the rivets made of AA 2117-T4 and the plates made of AA 2024-T3. AA 2024-T3 riveted lap joints with rivets of different lengths installed with same squeeze force have different driven head dimensions, but the fatigue lives are very similar for the same squeeze force. These results imply that the driven head dimensions affect fatigue performance only if identical rivets are used [41].

3) Effect of rivet hole expansion on the squeeze force

In addition to formation of the rivet driven head due to the riveting process, the radial expansion of the rivet shank deforms the sheet material near the rivet hole. Based on the conditions of the sheet material adjacent to the hole, three stages can be distinguished:

Filling the hole: Rivet holes are initially made 0.1 mm larger than the rivet diameter to ease fitting the rivet in the hole. Then, the axial compression due to the squeeze force results in radial expansion. When the rivet shank makes contact with the rivet hole, the rivet deforms plastically due to transverse strain.

Hole expansion: This phenomenon is quite complex due to the plastic deformation of both the sheet and rivet shank. When this happens, rivets exert radial pressure on the holes and thus the sheet deforms elastically initially, and then plastically. Due to this, part of the rivet squeeze force is transferred to the sheet, which further deforms plastically.

Springback: Upon removal of the squeeze force after formation of the rivet driven head, the sheet relaxes elastically in the radial and thickness direction, which results in residual stresses in the rivet-sheet system.

Rivets were cut vertically close to the centre line for measuring and comparing dimensions of squeezed rivet shank to the original hole [41].

4) Effect of residual stresses due to riveting

A residual stress field is created due to the riveting. Its impact on the loading of the joints plays an important role on nucleation and growth of fatigue cracks near the rivet hole. As explained earlier, squeezing of rivet leads to plastic deformation of the sheet material around the rivet. This process is similar to CW to some extent, though some differences exist:

- After CW, as the hole is open, the radial residual stresses on the hole must be zero. After riveting, however, the rivet shank in the hole will exert radial pressure
- The rivet head exerts clamping pressure in the thickness direction of the sheet, which results in a 3D residual stress state

Radial residual stresses are highly influenced by the squeeze force. For larger squeeze forces, significant compressive stress flows around the rivet hole edges are induced [44]. FEM simulations of countersunk rivets installation shows residual stress distributions at the hole edge [41]. The residual stresses around countersunk rivets and protruding heads were also modelled and studied with FEA [31].

1.2.4 Failure modes of riveted joints

A lap joint as shown in Fig. 1.7, with two plates of thickness t, connected by a single line of rivets, is the simplest type of joint used in construction of structures. Suppose that the plates carry an edge load of P/Unit width, with rivets of diameter d, which are spaced a distance b, and with a distance a from the line of rivets to the edge of the plate.

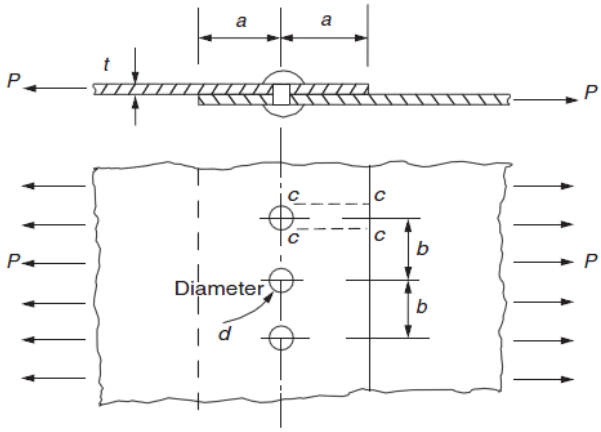

Figure 1.7: *Simple riveted lap joint [45].*

For such a simple riveted lap joint design, four possible failure modes must be considered: rivet shear, bearing pressure, plate failure in tension, and plate failure in shear, as explained below [45].

(a) Rivet Shear

Rivets may fail due to shear across their diameter, which typically occurs at the interface of the plates. In this case, if the maximum shear stress that the rivet can withstand is τ_1, failure occurs when:

$$Pb = \tau_1 \left(\frac{\pi d^2}{4} \right) \qquad 1\text{-}1$$

from which:

$$P = \tau_1 \left(\frac{\pi d^2}{4b} \right) \qquad 1\text{-}2$$

(b) Bearing Pressure

Either the plate or the rivet may fail under bearing pressure failure mode. In this case, if the bearing pressure is p_b, failure occurs when:

$$p_b = \left(\frac{Pb}{td}\right) \quad \text{1-3}$$

So that:

$$P = \left(\frac{p_b td}{b}\right) \quad \text{1-4}$$

(c) Plate failure in tension

This mode of failure occurs due to the reduction in cross-sectional area of the plate in tension along the line of rivets due to presence of rivet holes. In this case, if the ultimate tensile stress (UTS) in the plate is σ_{ult}, failure occurs when:

$$\sigma_{ult} = \left(\frac{Pb}{t(b-d)}\right) \quad \text{1-5}$$

From which:

$$P = \left(\frac{\sigma_{ult} t(b-d)}{b}\right) \quad \text{1-6}$$

(d) Shear failure in a plate

When rivets are dragged out of the plate, shearing of the plates occur on the plane cc. In this case, if the maximum shear stress at failure of the plates is τ_2, failure occurs when:

$$Pb = 2at\,\tau_2 \quad \text{1-7}$$

Which gives

$$P = \frac{2at\,\tau_2}{b} \quad \text{1-8}$$

(e) Joint Efficiency

The efficiency of riveted joints is measured by comparing their actual failure load with the failure load if there were no rivet holes in

the plate. For the joint shown in Fig. 1.6, the joint efficiency ɳ defined by:

$$\eta = \frac{\sigma_{ult}\, t(b-d)/b}{\sigma_{ult}\, t} = \frac{b-d}{b} \qquad 1\text{-}9$$

1.3 Adhesive bonded joints

Adhesive bonding in aircraft construction is an accepted means of attaining high structural strength, efficiency, and improved fatigue life. Particularly, adhesive bonding is extensively used in construction of secondary structures. However, only a few aircrafts have employed adhesive bonding for primary structures such as wing stiffeners, fuselage longerons, and fuselage skin panels [46]. In recent years, the use of adhesive bonding in aircraft structures has expanded greatly as advanced composite materials are being developed and implemented.

1.3.1 Adhesive bonded vs riveted repairs

In this section, the merits of adhesive bonded and riveted repairs are discussed. One advantage of riveted joints is that they can be disassembled and can be made in an uncontrolled environment. Unfortunately, the holes in mechanical fastened joints weaken the load carrying capabilities of the corresponding plates and gives rise to high stress concentrations.

On the other side, adhesive bonding should not be performed unless stringent cleaning and processing steps are previously conducted on the surfaces to be adhered in a controlled environment. The cleaning area should not be subjected to any operation such as sanding or grinding, and should be free from oil vapours or any other contaminants. Once the surfaces are cleaned, the parts should be sealed in non-contaminating oil-free paper or polyethylene film. Most importantly, the joint should be designed such that the adhesive is

stressed in the direction of its maximum shear strength and tension or minimal peel stresses.

With controlled processing steps and properly prepared bonding surfaces, adhesive bonded joints are very efficient, with the load being distributed over a large area, and thus eliminating high stress concentrations. For instance, research showed that the breakeven point of boron/epoxy doubler lap joints was 1900 kN/m [47]. Other researches showed that symmetrical-step lap joints or scarf joints could increase breakeven point over 7000-8700 kN/m [48, 49]. Thick structures have a remarkable tolerance for large bond imperfections associated with adhesive bonding of thicker adherends and has sensitivity to large voids [50]. However, any flaws in thick adhesive bonded structures can propagate catastrophically compared to mechanical fasteners from a fail-safe load path [51].

The curing of adhesives that require curing temperatures above 120^0C has the disadvantage of causing potential damage to the surrounding structure [52]. Moreover, adhesives that only cure at temperatures above 120^0 C tend to be more brittle and have lower peel strength. On the other hand, adhesives that cure in the range 93-120^0 C have good strength and stiffness [52], and may not cause so much damage in the surrounding structure.

1.3.2 Adhesives

The selection of proper adhesives for adhesive bonded joints should be based on static strength requirements, operational temperature range, and curing temperature. In this section, various types of adhesives and their properties are discussed.

Based on their applications, structural adhesives can be classified into three categories: films, pastes, and foams [53]. Films are easier to use and provide more uniform bondline thickness compared to pastes and foams. If repair parts are inaccessible, paste adhesives are used. Foam adhesives are used for, namely, splicing pieces and stabilizing honeycomb cores.

Film adhesives are made from high molecular weight polymers with curing agents and other compounding elements, which are cast into thin films.

These are available in thicknesses ranging from 0.127 to 0.508 mm, with weights ranging from 0.15 to 1 kg/m^3. For repairs, it is recommended to use 0.127-0.508 mm thick adhesive films for composite to metal or metal to core applications. For metal-metal and composite-composite adhesive bond repairs, 0.154-1.524 mm thick films are recommended [54].

Film adhesives are usually easier to apply than other adhesive types and do not require mixing equipment. They also have more uniform viscosity and composition, and hence provide uniform bondline thickness in joints compared to paste adhesives. A major disadvantage of these films is that they require refrigeration for storage, and the fact that films are more expensive and require heat and pressure to achieve the desired bonds [54].

Paste adhesives are also relatively easy to apply with a spatula or other spreading equipment. They are commercially available in the form of one- or two-component adhesives, which are cured either at room temperature (RT) or at higher temperatures (thermal curing). Two-component paste adhesives consist of liquid epoxy resin and a cross-linking agent. These adhesives have a long shelf life and do not need any refrigeration for storage. However, the two components have to be mixed thoroughly before application because any incomplete mixing or improper weighting would result in lower strength of the adhesive bond [54].

Foam adhesives for structural bonding are implemented with epoxy resin systems, which contain also a foaming agent so they can expand during the curing step. Foam adhesives are used, for instance, in honeycomb core repairs, to fill gaps or between edge members. They are available in either paste or tape form with an expansion ratio ranging from 1.3 to 5.0, and with densities ranging from 192 to 720 kg/m^3. Generally, foam tapes are available in thicknesses ranging from 0.35 to 0.508 mm [54].

1.3.3 Adhesive testing

Adhesives are usually tested to evaluate standard properties such as their tensile strength, elongation, and shear strength. Some of the usual tests employed in testing of adhesives are lap shear (performed at RT and at the highest operational temperature of the adhesive), metal peel, honeycomb peel,

and film weight. These tests will provide information about the uniformity of the adhesive, but not direct data about design allowables for adhesive bonded repairs. Standard lap shear tests are more commonly focused on joint deflection and induced peel stresses than on the shear strength of the adhesive.

Hence, it is important to generate data for establishing design allowables on how the adhesive will be loaded in structurally configured repair joints. Testing of adhesive bonds at high frequency loading should be avoided as these tests usually lead to misleading results [55]. Indeed, adhesives should never fail at high frequency loading because they have no time for experiencing creep. For example, thick adherends with short bonding overlap showed no evidence of damage after 10^7 loading cycles at high loading frequency. However, when the same specimens were tested at low frequency, the joints failed after only a few hundreds of cycles for the same stress amplitude. Low loading frequencies caused creep accumulation and fracture in short overlap joints but in long overlap joint's creep is stabilised.

1.3.4 Surface preparation

Generally, achieving high performance structural adhesive bonding requires great care throughout the bonding process to ensure highest quality of the adhesive bonded repair [56]. This is necessary because, for example, the shear strength of adhesive bonded repairs is highly dependent on surface preparation of the adherends. Namely, surface preparation of metal adherends is the most important factor in achieving high adhesive bond strengths of these adherends. Failure analyses of both aluminium and titanium alloys have repeatedly demonstrated that adhesive bond durability and longevity are dependent on bondability and stability of the adherend surfaces [57, 58]. Pre-bond surface treatments for aluminium and titanium alloys are presented in [59].

The basic steps in surface preparation of metals are- descale, degrease, deoxidize, chemical etching or anodizing, and prime [60]. Structural aerospace grade aluminium and titanium alloys rarely need descaling treatments. If necessary, sometimes titanium alloys are abraded mildly prior to chemical treatment. Degreasing to remove traces of soluble contaminants consists of hot

water detergent and condensing solvent vapour cleaning treatments. Once the surfaces are free from soluble contaminants, deoxidation is performed with the use of buffered alkaline or acid solutions. In this processes, the oxide layer of metal adherends is removed, exposing fresh metal surface. For aluminium alloys, phosphoric acid anodizing (PAA) treatment, in combination with a corrosion-inhibited primer, is superior in all aspects compared to any other surface preparation method [61].

1.3.5 Environmental behaviour

Adhesive bonded repairs are sensitive to environmental effects such as corrosion and moisture that may affect the bond performance. From service records of adhesive bonded metallic structures, they failed in most cases due to inadequate surface preparation or the use of environmentally sensitive adhesives without corrosion inhibiting primers, but not due to the various possible flaws in the bond [50].

Particularly, humidity is one of the detrimental environmental effects that can significantly affect the bond quality. The moisture content of the structures being repaired must be low to achieve high strength of the repairs. Carbon and boron fibre reinforced epoxy composites can absorb as much as 1.2% of their weight in moisture during service. Moisture may cause local delamination or blistering in parent laminates, reducing the strength of the repair patch. Furthermore, expanding moisture in honeycomb cells may create sufficient pressure to separate covering skins from the core, ultimately reducing the effectiveness of non-destructive testing (NDT) due to discrepancies in signal detection.

1.3.6 Failure of adhesive joints

In this section, the four failure modes of adhesive bonded joints are presented:

Adhesive failure: Occurs at the interface of the adhesive and substrate. After failure adhesive is remains on one side of substrate.

Cohesive failure: Occurs when adhesive fails. In this mode of failure, failed adhesive remains on both the substrate surfaces.

Mixed failure: This failure mode is when both adhesive and cohesive failure takes place.

Substrate failure: Occurs when substrate fails. In this mode of failure, adhesive interface between the substrates is stronger than the strength of the substrates.

1.4 Hybrid Joints

The combination of mechanical fasteners and adhesive bonding is known as hybrid joint, which provides a fine solution to making joints and repairs. There are a few research works on hybrid joints in the literature [62-69], particularly on their load paths. Initial failure of hybrid joints is mostly due to debonding. The effect of the presence of mechanical fasteners in adhesive bonded joints is one of the most interesting research areas, but, in many cases, it is found that mechanical fasteners have no active role in the load transfer in hybrid joints unless there is initiation of bondline failure [64] which is also presented by [65].

Mechanical fasteners in hybrid joints are not subjected to sufficient relative motion between substrate and doublers while the adhesive layer is intact. The most critical location of mechanical fasteners is the first fastener hole. Adhesive bonded structures under low loads should not need rivets, as they can never experience any load even after the structure has damaged. However, for heavily loaded adhesive bonded structures, the rivets can arrest any initial damage in the bondline, and thus helping to prevent catastrophic failure [65]. In most cases, the adhesive bond is stronger than the rivets, but if the rivets are stronger than the adhesive bond, then damage in rivets can be prevented thanks to the adhesive bond.

Finite element analysis on load transfer in a hybrid joint is investigated by [66]. Load transfer paths in these joints is quite complex due to the differences in stiffness of the adhesive layer and the rivets. Some of the analysed factors that affect the behaviour of hybrid joints are [66]:

- The fact that the fastener load transfer increases with the adherend thickness and with the adhesive thickness
- The fact that the fastener load transfer decreases with the overlap length, with the fastener pitch distance, and with the adhesive elastic modulus

1.4.1 Advantages of hybrid joints

- Excellent fatigue properties: Compared to mechanically fastened joints and adhesive bonded joints, hybrid joints have improved fatigue life as rivets can stop sudden crack propagation, preventing catastrophic failure
- Higher stiffness compared to riveted or adhesive bonded joints
- Additional residual strength compared to adhesive bonded joints thanks to the fasteners
- Reduction in peel and through-thickness stresses compared to adhesive bonded joints
- Supress any defects in the bondline
- Better load distribution than riveted joints thanks to load sharing between fastener and adhesive

1.4.2 Disadvantages of hybrid joints

- Fastener holes can damage the substrates, especially for composite materials
- Inspection of hybrid joints is difficult
- Increase in weight of the joint compared to riveted and adhesive bonded joints
- Need for proper preparation and surface treatments, compared to pure riveted joints

Relative to mechanically fastened joints and adhesive bonded joints, hybrid joints have an advantage of improved fatigue life as it can stop sudden crack propagation by avoiding catastrophic failure.

Chapter 2: Materials and Methodology

In this section, the materials used in the preparation of the specimens are briefly presented, together with their mechanical properties and specifications. The components for making all the specimens are the substrate, doublers, rivets, adhesive, and tabs.

2.1.1 AA 2024 T3 (Aluminium alloy)

Metallic substrates and doublers for experiments are prepared from sheet of commercial AA 2024-T3. The T3 temper consists in solution heat-treatment at 480^0C for 1 hour, followed by rapid water quenching to room temperature (RT), cold working, and natural ageing [70]. The mechanical properties and composition (in wt.% and at.%) of AA 2024-T3 are shown in Tables 2.1 and 2.2, as supplied by Kaiser Aluminium fabricated products, Spokane, USA. The substrates, doubler 1, and doubler 2 are machine cut to dimensions 171.4 mm x 25.4 mm x 3.175 mm, 215.9 mm x 25.4 mm x 1.5875 mm, and 165.1 mm x 25.4 mm x 1.5875 mm, respectively.

Al alloy	Yield stress	UTS	% Area Reduction	Brinell Hardness
2024-T3	316 MPa	464 MPa	20.2%	HB 123

Table 2.1: *Mechanical properties of AA 2024-T3, as provided by the manufacturer, Kaiser Aluminium fabricated products, Spokane, USA.*

Al alloy	Units	Si	Fe	Cu	Mn	Mg	Zn	Ti	Cr	Al
2024-T3	wt.%	0.5	0.5	4.9	0.9	1.8	0.25	0.15	0.1	90.9
2024-T3	at.%	0.5	0.25	2.16	0.46	2.7	0.11	0.09	0.05	94.31

Table 2.2: *Chemical composition in wt. % and at. % of AA 2024-T3, as provided by the manufacturer, Kaiser Aluminium fabricated products, Spokane, USA.*

2.1.2 Carbon Fibre Reinforced Epoxy (CFRE)

Composite substrates and doublers are made from plain 3K 200 gr/m^2 carbon fibre fabric with SR 8100 epoxy system. SR 8100 is a two-component epoxy system specially formulated for resin transfer processes, such as infusion or injection. The cured system gives temperature resistance up to 80^{o}C. Substrates and doublers are manufactured and supplied by Composites Ate, S.L., Barcelona, Spain. The mechanical properties of the composite fibre lamina, as provided by the manufacturer, are shown in Table 2.3. The substrates are made of 12 layers of carbon fibre lamina, while doublers are made of 6 layers, each with a thickness of 0.25 mm. The stacking sequence of the substrate is [(45/-45), (0/90), (0/90), (0/90), (0/90). (45/-45)]s, while for doublers it is [(45/-45), (0/90), (0/90)]s. These stacking sequences are designed based on the golden rules for lay-up of composite laminates [70]. The dimensions of the substrates, doubler 1, and doubler 2 are 226 mm x 25.4 mm x 3 mm, 215.9 mm x 25.4 mm x 1.5 mm, and 165.1 mm x 25.4 mm x 1.5 mm, respectively.

Composite	E_{11} (GPa)	E_{22} (GPa)	G_{12} (GPa)	G_{13} (GPa)	ν_{12}	Tensile Strength (MPa)			Compressive Strength (MPa)	
						$+S_{11}$	$+S_{22}$	$+S_{12}$	$-S_{11}$	$-S_{22}$
CFRE	67.6	67.6	4.2	4.2	0.04	885	885	97	835	835

Table 2.3: *Mechanical properties of the composite lamina, as provided by the manufacturer, Composites Ate, S.L., Barcelona, Spain.*

2.1.3 Rivets

Blind rivets for riveted and hybrid joint specimens are made from simple aluminium alloy with steel mandrel, diameter 3/16 of an inch (4.75 mm). The rivets were supplied by Rapid rivets, Hestra, Sweden.

2.1.4 Adhesive

The commercial adhesive used for the adhesive bonded and hybrid joints is Araldite 2031, manufactured by Huntsman Advanced Materials, GmbH, Switzerland. Araldite 2031 is a two-part thixotropic adhesive consisting of resin and hardener. This toughened adhesive is chosen because of its capabilities to bond similar and dissimilar materials with high chemical resistance and low shrinkage. The best performance of the adhesive is obtained when the adhesive bonded surfaces are abraded well and cured at 40^0C for 16 hours. The mechanical properties of Araldite 2031 are shown in Table 2.4.

Adhesive	$\boldsymbol{E}$ (GPa)	$\boldsymbol{\sigma_{fracture}}$ (MPa)	$\boldsymbol{\varepsilon_{fracture}}$ (%)
Araldite 2031	1.057	21.38	6.39

Table 2.4: *Material properties of Araldite 2031, as provided by the manufacturer.*
*$\sigma_{fracture}$ is the fracture stress and $\varepsilon_{fracture}$ is the fracture strain.

2.1.5 Tabs

Tabs are attached to the ends of the composite substrates for smooth load transfer between substrate and doublers. In addition, the tabs prevent breaking at the ends of the composite substrate, i.e., they prevent failure at grips. Particularly, the tabs are made of epoxy resin reinforced with glass fibre fabric in 0/90 plies, with dimensions 80 mm x 25.4 mm x 2.5 mm.

2.2 Experiment specimens and test conditions

In this section, details on specimen preparation and experimental conditions are described. Specimens are prepared for the experiments with the following substrate-doublers combinations: metal-metal, metal-composite, composite-composite and composite-metal. Here metal corresponds to AA 2024-T3 and composite corresponds to Carbon Fibre Reinforced Epoxy (CFRE). For each of the mentioned substrate-doublers combinations, six specimens of riveted, adhesive bonded, and hybrid (riveted + adhesive bonded) joint configurations were prepared. Three specimens are used for static tests

and three for fatigue tests, for each type of joint configuration. In total, 36 static tests and 36 fatigue tests are performed and results are mentioned in this thesis. Glass fibre tabs are adhesively bonded to the composite substrate at its ends, as shown in Fig. 2.1, to prevent breakage of substrate at grips and to have a smooth load transfer. Fig. 2.2 and Fig. 2.3 indicate the dimensions for all the studied joint configurations.

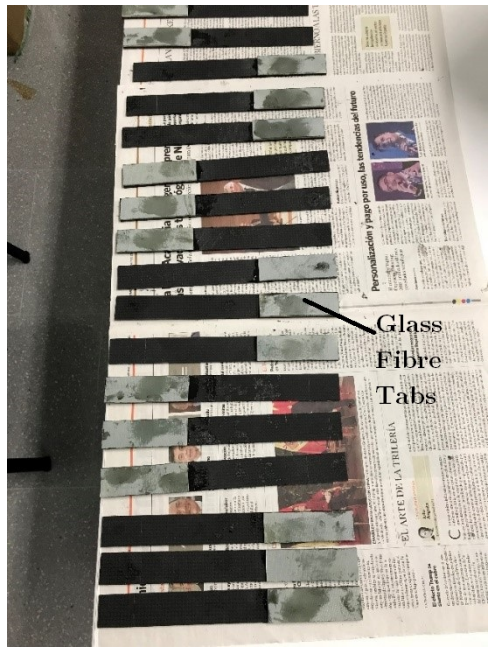

Figure 2.1: *Glass fibre tabs adhesively bonded to ends of composite substrates.*

2.2.1 Riveted joint specimens

The riveted specimens used in this work are designed in accordance with Federal Aviation Administration (FAA) regulations of aircraft maintenance [15]. In these regulations, the design of aircraft riveted joints is based on rivet diameter (D). In this research, all the specimen types (i.e., metal-metal, metal-composite, composite-composite, and composite-metal) consist of eight rivets distributed throughout the joint, as shown in Fig. 2.2 and Fig. 2.3. The standards set by the FAA suggest a minimum rivet pitch of 3D, but an average of 4D to 6D between rivets. A minimum rivet-edge distance of 2.5D should be maintained between edges of the joint and rivets.

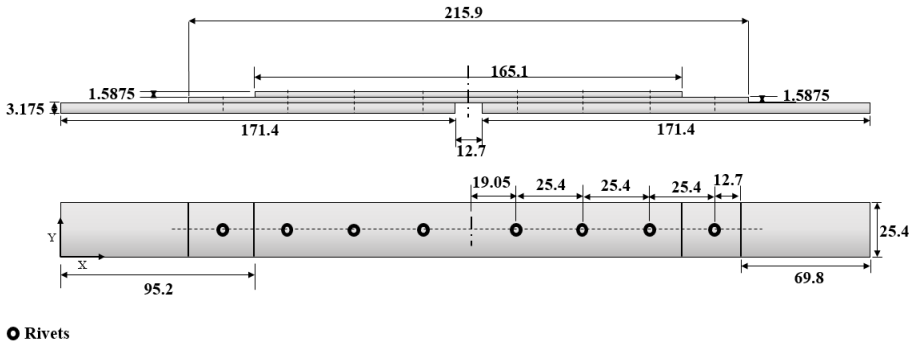

Figure 2.2: *Dimensions of riveted specimens of metal substrate-metal doublers and metal substrate-composite doublers (all units in mm) [70].*

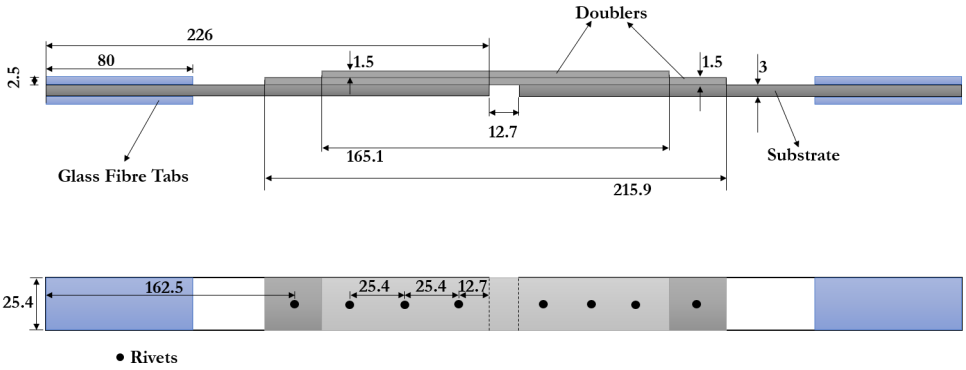

Figure 2.3: *Dimensions of riveted specimens of composite substrate-composite doublers and composite substrate-metal doublers (all units in mm).*

In this study, the riveted specimens have a rivet pitch of 5.3D and a rivet-edge distance of 2.5D and hence comply with FAA safety regulations for aircraft maintenance. Rivet holes at specific locations on the substrates, doubler 1, and doubler 2 are made using a carbide drill bit of diameter 5 mm. Once holes are drilled, rivets are placed in position and fastened with a rivet popgun.

2.2.2 Adhesive bonded joint specimens

In this section, the preparation of adhesive bonded joint specimens is described. Before applying the adhesive on the specimens, the surfaces of the

metal and composite substrates and doublers are abraded with sand paper with a grit size of 80 and then of grit size 40, to remove the oxidation layer for metal surfaces and create abrasion at 45° to improve the shear strength of adhesive bond. After abrasion, the surfaces are cleaned with acetone to remove traces and impurities, which can affect the quality of the bond. Finally, a thin finite layer of araldite 2031 is applied in between the surfaces to be adhesive bonded. Adhesive bonded surfaces of joints are prepared in steps: first, left substrate is adhesive bonded to doubler 1; then, doubler 2 is adhesive bonded to doubler 1, finally followed by bonding of the right substrate. Each time adhesive is applied the surfaces, the bond is cured at 40°C for 16 hours.

2.2.3 Hybrid joint specimens

In this section, the preparation of the hybrid joint specimens is described. This process consists in the following steps: the first steps are the same as for preparation of adhesive bonded specimens, discussed in section 2.2.2, and the last step is to drill holes of diameter 5 mm using a carbide drill bit into the adhesive bonded specimens at the locations shown in Fig. 2.2 and Fig. 2.3. Once holes are drilled, rivets are placed in positions and fastened with a rivet popgun. The prepared specimens of riveted, adhesive bonded and hybrid joint configurations of metal-metal and metal-composite are shown in Fig. 2.4, and composite-composite and composite-metal are shown in Fig. 2.5.

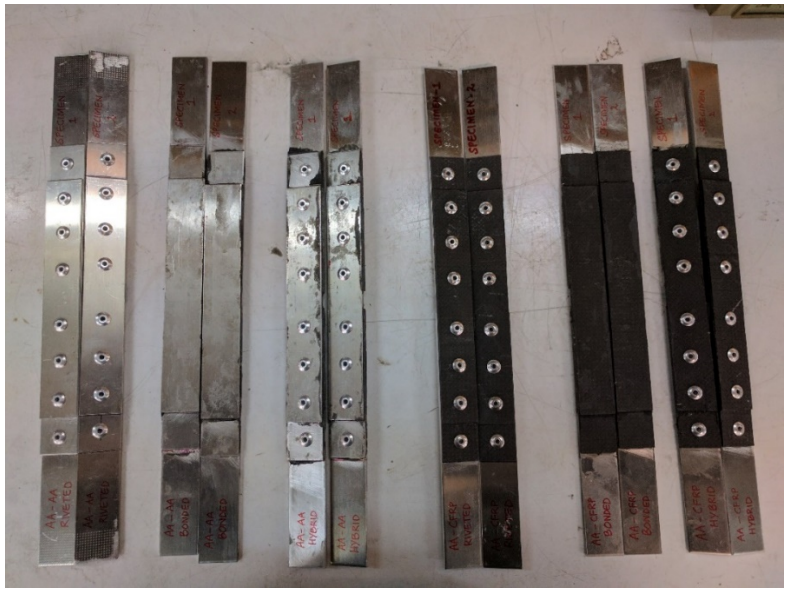

Figure 2.4: *From left to right, specimens of metal-metal and metal-composite with riveted, adhesive bonded, and hybrid joints.*

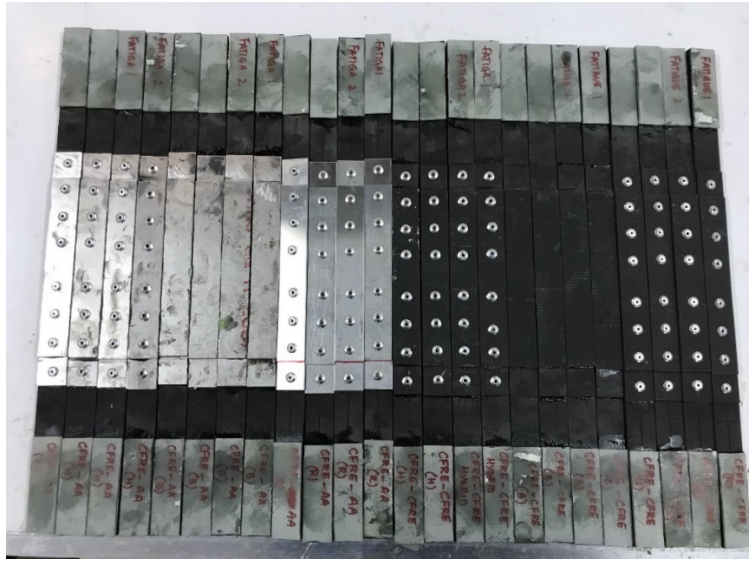

Figure 2.5: *From left to right, specimens of composite-composite and composite-metal with riveted, adhesive bonded, and hybrid joints.*

2.2.4 Static tests

The static tensile tests of specimens are conducted using Metrotest 810 UTM machine under displacement control at a rate of 6mm/min controlled by

a personal computer shown in Fig. 2.6. Crosshead displacement and load from load cell is recorded during the tests with a sampling rate of 10 readings/second. Three specimens of each type of joint configuration are tested under static loads.

Figure 2.6: *Static test machine with personal computer (left) and with loaded joint (right)*

2.2.5 Fatigue Tests

The fatigue tests of specimens are conducted using the same machine as for the static tests. Unlike static tests, fatigue tests are not simple to perform and are mostly a time consuming process. Fatigue tests can be performed using load control, suitable for high cycle fatigue (HCF), or displacement control, suitable for low cycle fatigue (LCF). Since these tests are HCF, load/force control is adopted. Fatigue loads are divided into three steps depending on number of cycles, as shown in Table 2.5. Three specimens of each type of joint configurations is tested under fatigue loads.

Substrate	**Step 1** **Up to 200,000 cycles**	**Step 2** **Up to 400,000 cycles**	**Step 3** **Up to failure**
Metal	$F_{amplitude}$ =4410 N F_{mean} =2695 N	$F_{amplitude}$ =5733 N F_{mean} =3504 N	$F_{amplitude}$ =7453 N F_{mean} =4555 N
Composite	$F_{amplitude}$ =4482 N F_{mean} =2739 N	$F_{amplitude}$ =5827 N F_{mean} =3561 N	$F_{amplitude}$ =7575 N F_{mean} =4629 N

Table 2.5: *Fatigue test conditions in the three steps used in this work.*

2.3 Numerical methodology

In this section, we present the numerical modelling and analysis of riveted, adhesive bonded, and hybrid joints using FEA and other tools. In particular, FEA is performed with the commercial tool ABAQUS CAE. On the other side, open source fatigue-life prediction tool developed by Fracture Analysis Consultants (FRANC), such as Fracture Analysis 2D Layered (FRANC2D/L) and FRANC3D, is also used, as well as Helius Autodesk Composite tool.

2.3.1 Finite element analysis

ABAQUS CAE is used for numerical analysis of metal-metal, metal-composite, composite-composite, and composite-metal configurations of riveted, adhesive bonded, and hybrid joints. 3D finite element models are created using shell elements for both the substrate and doublers. Shell elements provide optimised solutions without compromising computational time and accuracy [70]. The metals are modelled as homogeneous solids, while composites are modelled as composite layups with the orientations discussed in Section 2.2.

The substrate and doublers are modelled as 4-node doubly curved thin shells (S4R) with reduced integration elements. For meshing the substrates and doublers, quad-dominated medial axis meshing is used. All the joint configurations were symmetric about the X-axis, and hence only half-model is analysed by applying symmetry boundary condition in the YZ plane. Obviously, simulating half models of the joints requires less computational time compared to simulating full-scale models, thus increasing efficiency.

Surface-to-surface contact algorithm is used to generate contact interactions between the substrates and doublers. Particularly, all the joint models have a common contact interaction called “general”, defined as frictionless and hard contact with no penetration.

The half-joint models consist of 4275 elements for the substrate, 2700 for doubler 1, and 2075 for doubler 2. The loading and boundary conditions are equivalent to the experimental conditions. An equation constraint is implemented using two node sets; namely, the load node (a single node on the joint edge), and the follower nodes (all other nodes except the load node, which are tied to the later node). That is, the follower nodes are connected to the load node using an equation constraint, in a way that the load on the former is the same as the load applied on the load node. Thus, the response of the joint at the node set gives the response of the complete joint.

In the following subsections, we briefly present the modelling techniques for the riveted, adhesive bonded, and hybrid joints implemented in this study.

(a) Riveted joints

Mechanical fasteners, and especially rivets, can be modelled in many ways [70] for example, by using multi-point constraints, solid rivets, or point-based fasteners with attachment points or lines. In this analysis, the rivets are modelled as point-based fasteners. Their stiffness values in six different degrees of freedom are calculated using Eqns. (2-1 to 2-5) [70]. The first three equations are used to calculate the stiffness in translational directions, while the later three equations are used to calculate the rotational stiffness values. The effect of the fastener or radius of influence of the rivet is 2.5 mm, with continuum distribution.

$$K_1 = \left\{\frac{k}{m}\left[\left(\frac{t_{shell1} + t_{shell2}}{2d}\right)^{\lambda}\left(\frac{1}{E_{11,shell1}t_{shell1}} + \frac{1}{m.E_{11,shell2}t_{shell2}} + \frac{1}{2.E_{fast}t_{shell1}} + \frac{1}{2m.E_{fast}t_{shell2}}\right)\right]\right\}^{-1} \quad \textit{2-1}$$

$$K_2 = \left\{\frac{k}{m}\left[\left(\frac{t_{shell1} + t_{shell2}}{2d}\right)^{\lambda}\left(\frac{1}{E_{22,shell1}t_{shell1}} + \frac{1}{m.E_{22,shell2}t_{shell2}} + \frac{1}{2.E_{fast}t_{shell1}} + \frac{1}{2m.E_{fast}t_{shell2}}\right)\right]\right\}^{-1} \quad \textit{2-2}$$

$$K_3 = \frac{\pi d^2 E_{fast}}{4(t_{shell1} + t_{shell2})} \quad \text{2-3}$$

$$K_4 = K_5 = \frac{\pi d^2}{16}\left(\frac{E_{fast} d^2}{4L} + G_{fast}.L\right) \quad \text{2-4}$$

$$K_6 = \frac{G\pi d^4}{32L} \quad \text{2-5}$$

where k is 2.2 and λ is 0.4 for solid rivets, m is 1 for single-shear joints, t_{shell1} and t_{shell2} are the thicknesses of shell 1 and shell 2, respectively, d is the diameter of rivet holes, E_{11}, E_{22}, and E_{fast} are the elastic moduli of the metal plates, composite plates, and fasteners, respectively, G_{fast} is the fastener shear modulus, and L is the fastener length. From the joint dimensions shown in Section 2.1, one can notice that the first rivet row has only substrate and doubler 1, while the subsequent rivet rows have thickness of substrate, doubler 1, and doubler 2.

(b) Adhesive bonded and hybrid joints

The adhesive bond in adhesive bonded joints is modelled using the cohesive zone model (CZM). CZM involves a cohesive contact interaction/interface between the adhesive bonded surfaces. This interface layer has no physical thickness, but has the same effect as an adhesive layer of thickness 0.25 mm. From the literature [71, 72] apparently there are no significant differences between CZM with physical layer or with cohesive contact interaction.

The CZM algorithm uses linear elastic traction-separation behaviour to simulate the behaviour of the adhesive. It has been reported that traction-separation criteria provide good accuracy with low error margin compared to experiments [70]. The traction-separation model used in ABAQUS has linear elastic behaviour, which can be extended with damage initiation and evolution. The elastic behaviour of the adhesive is defined in terms of nominal stresses and

nominal strains across the interface. The nominal stresses (force components divided by area at each integration point) consist of three components: t_n, t_s and t_t, in the normal, shear, and traction directions, respectively. The same occurs for the nominal strains: ε_n, ε_s, and ε_t as shown in Eq. 2-6 [70]. The latter components are obtained from the nominal separations δ_n, δ_s, and δ_t divided by the original thickness of the cohesive element T_0:

$$\varepsilon_n = \frac{\delta_n}{T_0},\ \varepsilon_s = \frac{\delta_s}{T_0} \text{ and } \varepsilon_t = \frac{\delta_t}{T_0} \qquad 2\text{-}6$$

The elastic behaviour of cohesive elements is defined as:

$$t = \begin{Bmatrix} t_n \\ t_s \\ t_t \end{Bmatrix} = \begin{bmatrix} k_{nn} & k_{ns} & k_{nt} \\ k_{sn} & k_{ss} & k_{st} \\ k_{tn} & k_{ts} & k_{tt} \end{bmatrix} \begin{Bmatrix} \varepsilon_n \\ \varepsilon_s \\ \varepsilon_t \end{Bmatrix} = K\varepsilon$$

Where K is the matrix of stiffness values in the normal, shear, and traction directions. In this research, uncoupled behaviour between traction and separation of the adhesive is assumed, and so the off-diagonal terms are zero. Hence, only k_{nn}, k_{ss}, and k_{tt} are calculated, where k_{nn} is the Young's modulus of the adhesive divided by T_0, and k_{ss} and k_{tt} are the shear moduli of the adhesive divided by T_0. From the information provided by the manufacturer, adhesive stiffness is 4E+12 N/m in normal, traction and separation directions.

The damage of the adhesive in the CZM is modelled with progressive failure of cohesive elements, which is defined in terms of traction-separation terms. The failure mechanism in this model consists of three stages: damage initiation, damage evolution, and, finally, complete failure, as shown in Fig. 2.7. The initial response of the cohesive elements is linear and, once a damage initiation criterion is satisfied, damage evolution/propagation occurs, following the damage evolution law shown in Fig. 2.7.

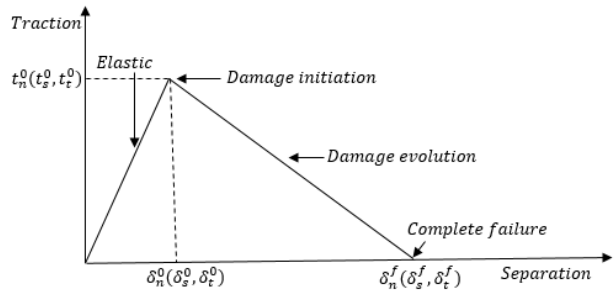

Figure 2.7: *Traction-separation response with failure mechanism [70].*

As mentioned, damage initiation begins when the cohesive elements satisfy a specified criterion. In this analysis, we used the quadratic nominal stress criterion (for instance, the Araldite 2031 adhesive used in this research has a maximum nominal stress of 25 MPa, as provided by manufacturer), which states that damage initiates when the nominal stress ratios are such that the following quadratic interaction function exceeds 1 (see Eq. 2-7) [70]:

$$\left\{\frac{\langle t_n \rangle}{t_0^n}\right\}^2 + \left\{\frac{t_s}{t_0^s}\right\}^2 + \left\{\frac{t_t}{t_0^t}\right\}^2 = 1 \qquad 2\text{-}7$$

For deformations in purely normal direction to the interface, the terms t_0^n, t_0^s, and t_0^t are the peak values of nominal stress. The term $\langle t_n \rangle$ is to signify that no damage is initiated if the deformation is compressive in nature.

After damage initiation, damage evolution takes place, based on the aforementioned damage evolution law, which defines the rate of degradation of the cohesive elements. A scalar quantity D represents the level of cohesive element damage, ranging from 0 (state where no damage has occurred in the cohesive elements) to 1 (associated with complete failure of the cohesive elements). The damage for the traction-separation model consists then of the following three components shown in Eqns. 2-8, 2-9 and 2-10 [70]:

$$t_n = \begin{cases} (1-D)\bar{t}_n, & \bar{t}_n \geq 0 \\ \bar{t}_n \; otherwise\,, \end{cases} \qquad 2\text{-}8$$

$$t_s = (1 - D)\,\bar{t}_s, \qquad 2\text{-}9$$

$$t_t = (1 - D)\,\bar{t}_t \qquad 2\text{-}10$$

Where $\bar{t}_n$, $\bar{t}_s$, and $\bar{t}_t$ are the stress components for the current strains without damage, as predicted by the elastic traction-separation behaviour.

Indeed, damage evolution is based on the energy dissipated as a result of a damage process called fracture energy. The fracture energy is the area under the traction-separation curve. For Araldite 2031, the fracture toughness is $1.6\ MPa \cdot mm^{1/2}$, and the fracture energy in mode I, G_{Ic}, is $2\ kJ/m^2$. The fracture energies in mode II and mode III were not provided by the manufacturer. Hence, these values were obtained based on a previous work by Campilho et al. [74], stating that, for brittle adhesives, the fracture energies in mode II and mode III are twice the fracture energy in mode I. In Campilho's work, adhesives are defined as brittle if their failure strain is less than 0.1, and thus the adhesive used in our study can be assumed brittle, since its failure strain is 0.05, as provided by the manufacturer. Therefore, due to the lack of experimental data or information from the adhesive manufacturer, the fracture energies G_{IIc} and G_{IIIc} are assumed as $2G_{Ic}$.

As mentioned before, hybrid joints comprise both mechanical fasteners and adhesive bond. Thus, for modelling the hybrid joints in the frame of this research, we combined the rivet and adhesive models just commented, that is, point-based fasteners and CZM.

2.3.2 FRANC 3D

FRANC3D, from Fracture Analysis Consultants, Inc. group, USA, has a simple graphical user interface, where mesh models can be imported from ABAQUS in .inp file format. Cracks can then be inserted at desired locations in the models, and allowed to grow for the applied boundary conditions. M-integral stress intensity factors (SIF) are then calculated for these cracks. Finally, based on these SIF and the mechanical properties of the material, the

fatigue life of the structure can be obtained. Moreover, it is possible to insert multiple cracks, multiple crack fronts, and multiple load steps.

In this study, a simple 3D finite element mesh model of the metal substrate generated in ABAQUS was imported to FRANC3D. Substrates with crack lengths of 1, 2, 5, 10, and 12.7 mm inserted at their centres, as shown in Fig 2.8 and 2.9, were studied. The material properties and boundary conditions were defined in the meshed model. Finally, the load was applied at the ends of the metal substrate.

FRANC3D has an inbuilt mesh algorithm to mesh the crack front. Initially, a static analysis of the substrate is performed. Afterwards, the crack is allowed to grow under the given loading conditions, following a quasi-static power law criterion. NASGRO version 3 equation (Eq. 2-11) implemented in the tool is used to compute the fatigue life [75]:

$$\frac{da}{dN} = C\left[\frac{1-f}{1-R}\Delta K\right]^{n}\frac{\left(1-\frac{\Delta K_{th}}{\Delta K}\right)^{p}}{\left(1-\frac{K_{max}}{K_c}\right)^{q}} \qquad 2\text{-}11$$

Where $C, n, p,$ and q are curve fitting constants. For AA 2024 T3, the UTS is 455 MPa, the yield stress is 365 MPa, and the fracture toughness K_c is 36.3 MPa.mm$^{0.5}$, C is 1.832e-12 mm/cycle, n is 3.284, p is 0.5, and q is 1 [75].

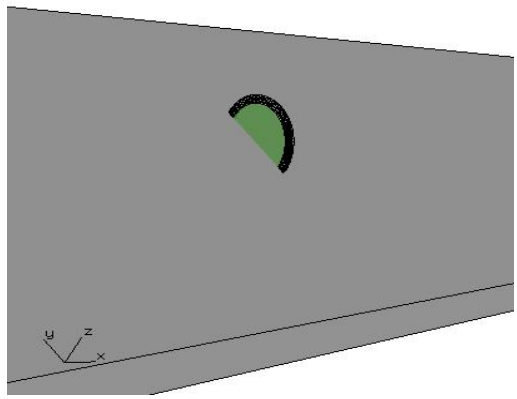

Figure 2.8: *Crack insertion in the substrate-FRANC3D [75].*

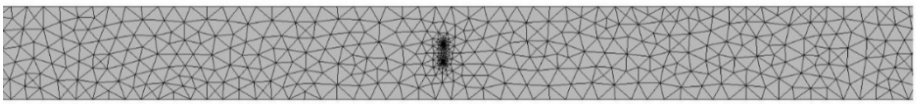

Figure 2.9: *Mesh generated by FRANC3D mesh algorithm [75].*

2.3.3 FRANC2D/L

FRANC2D/L is a two-dimensional fracture and fatigue analysis tool, where 'L' stands for layered. To perform fatigue analysis of joints with layers in FRANC2D/L, initially a mesh file for each layer is generated in a tool called CASCA [76]. CASCA allows the users to design joint layers and save the file in .inp format. Then, all the layers can be merged into a complete model with the help of a translator called Castofranc. Once a final model has been generated with all these layers, it is saved and imported to FRANC2D/L tool.

In FRANC2D/L, pre-processing information is required, such as material properties (e.g., elastic modulus, Poisson's ratio, density, and fracture toughness), thickness of the layers, etc. At one end of the model, a fixed constraint is applied, while, on the other end, a force is applied in the form of traction. The rivets in FRANC2D/L are defined and added at the desired location on the joint. Huth's formulae [76] is used to calculate the rivet stiffness as shown in Eqns. 2-12 and 2-13 [76]:

$$K_{huth} = 1/C \qquad 2\text{-}12$$

$$C = \left(\frac{t_1 + t_2}{2d}\right)^a . \frac{b}{n}\left(\frac{1}{t_1 E_1} + \frac{1}{n t_2 E_2} + \frac{1}{2 t_1 E_3} + \frac{1}{2 n t_2 E_3}\right) \qquad 2\text{-}13$$

where a and b are rivet constants, n is 1 for single-shear joints, t_1 and t_2 are the thickness of the plates, and E_1, E_2, and E_3 are the Young's modulus of plate 1, plate 2, and the rivets, respectively. For riveted metal joints, a is 0.4 and b is 2.2. Finally, the SIF for crack lengths ranging from 1 to 24 mm in step increments of 1 mm were computed in this work using FRANC2D/L.

For adhesive bonded joints, adhesive shear stiffness is 1000 MPa (Araldite 2031) with a thickness of 0.25 mm defined between substrate and doublers.

2.3.4 Helius composite

Helius Autodesk Composite tool is a simple software package designed for analysing the properties of composite laminates. When a load is applied on such laminates, knowing the load distribution among plies is important to understand local stress concentrations. Once the ply load distribution is known, first-ply failure analysis can provide which ply is vulnerable to the applied load. Indeed, Helius Autodesk Composites tool can be used for computing the ply load distribution, first-ply failure with progressive failure analysis (PFA), and the failure envelopes in the longitudinal and transverse directions of the composite substrate. From the first-ply failure analysis with PFA, the failure mode of the composite substrate ply can be obtained. In this case, Christensen's failure criterion is used to predict the failure of the composite substrate. According to this criterion, shown in Eq. 2-14 and 2-15, the failure mode can be classified as either fibre failure or matrix failure [77]:

$$\left(\frac{1}{S_{22}^{+}}-\frac{1}{S_{22}^{-}}\right)(\sigma_{22}+\sigma_{33})+\frac{1}{S_{22}^{+}S_{22}^{-}}(\sigma_{22}+\sigma_{33})^2+\frac{1}{S_{23}^{2}}(\sigma_{23}^2-\sigma_{22}\sigma_{33})+\frac{1}{S_{12}^{2}}(\sigma_{12}^2+\sigma_{13}^2)\geq 1.0 \qquad 2\text{-}14$$

where $S_{23}\geq\frac{1}{2}\sqrt{S_{22}^{+}+S_{22}^{-}}$ and:

$$\left(\frac{1}{S_{11}^{+}}-\frac{1}{S_{11}^{-}}\right)\sigma_{11}+\frac{\sigma_{11}^2}{S_{11}^{+}S_{11}^{-}}\geq 1.0 \qquad 2\text{-}15$$

where S_{11}^{+} and S_{11}^{-} are the values of σ_{11} in longitudinal tensile and compressive failure, S_{22}^{+} and S_{22}^{-} are the values of σ_{22} in transverse tensile and compressive failure, and S_{12} and S_{23} are the absolute values of σ_{12} and σ_{23} in shear direction. The values of the parameters in Eqns. 2-14 and 2-15 are described in Table 2.3.

Chapter 3: Results and Discussion- Experiments

In this chapter, the results obtained from the experiments are first described. These results are divided into subsections based on the substrate material and type of loading.

3.1 AA 2024-T3 substrates- Static tests

In this section, the experimental results for AA 2024-T3 (metal) substrates with AA 2024-T3 (metal) and CFRE (composite) doublers with riveted, adhesive bonded, and hybrid joint are presented. Three specimens of each of these six types of joint configuration are tested in the UTM machine. Hence, results of 18 experiments are presented in this chapter.

The load-displacement curves obtained from these experiments on metal-metal and metal-composite configurations are shown in Fig. 3.1 and 3.2. Table 3.1 and 3.2 show the peak strength of each of the tested specimens, as well as the average and standard deviation of the peak strength of the three tested specimens for each joint configuration.

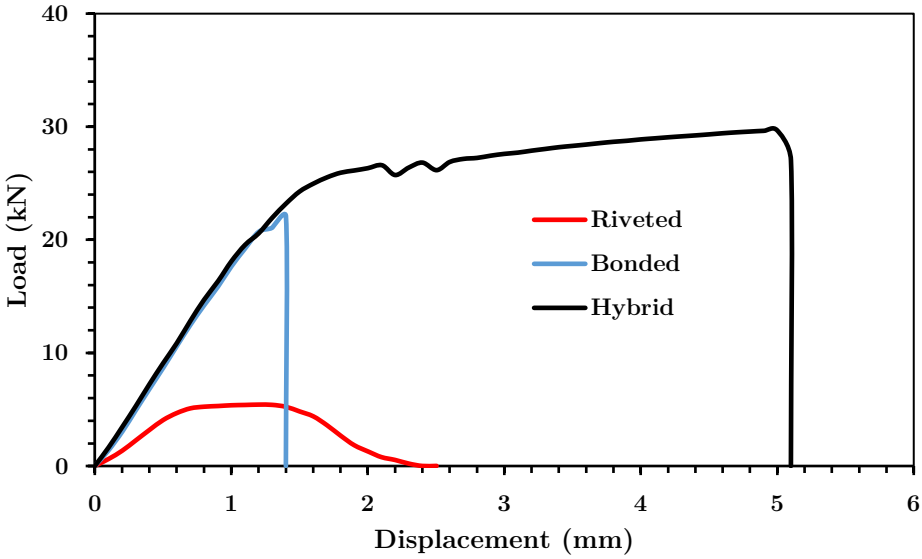

Figure 3.1: *Load vs. displacement curves for metal-metal joints of riveted, adhesive bonded and hybrid configurations.*

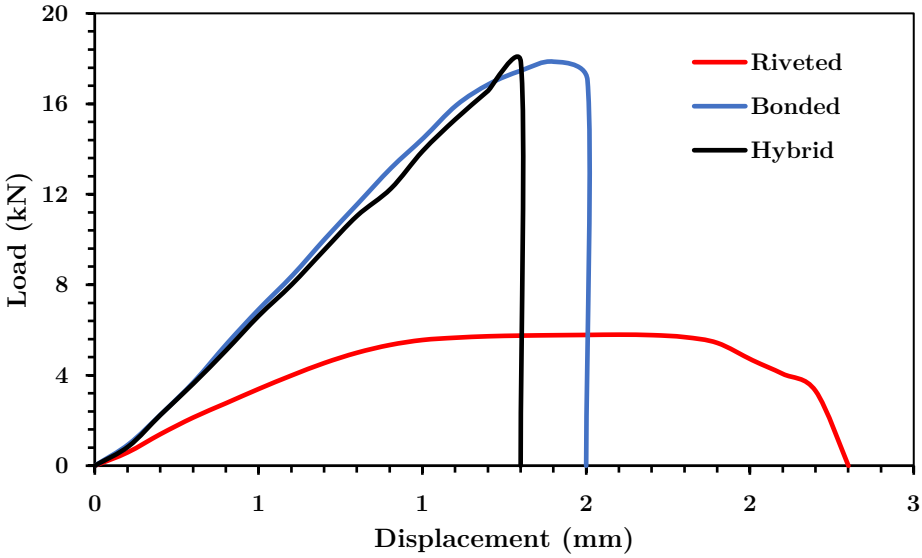

Figure 3.2: *Load vs. displacement curves for metal-composite joints of riveted, adhesive bonded and hybrid configurations.*

Joint Configuration	AA 2024T3-AA2024 T3				
	Strength of Specimen 1 (kN)	Strength of Specimen 2 (kN)	Strength of Specimen 3 (kN)	Average Strength (kN)	Standard Deviation (kN)
Riveted Joint	5.43	5.46	5.51	5.47	0.04
Adhesive Bonded Joint	22.08	26.05	21.02	23.11	2.58
Hybrid Joint	29.31	29.67	26.05	28.34	1.99

Table 3.1: *Joint strengths of metal-metal configurations of riveted, adhesive bonded, and hybrid joints.*

Joint Configuration	AA 2024T3-CFRE				
	Strength of Specimen 1 (kN)	Strength of Specimen 2 (kN)	Strength of Specimen 3 (kN)	Average Strength (kN)	Standard Deviation (kN)
Riveted Joint	5.85	5.80	5.88	5.84	0.04
Adhesive Bonded Joint	22.55	18.49	17.29	19.44	2.76
Hybrid Joint	17.25	17.84	15.00	16.70	1.50

Table 3.2: *Joint strength of metal-composite configurations of riveted, adhesive bonded, and hybrid joints.*

Metal-metal riveted joints failed at an average peak load of 5.5 kN with a total final displacement of 1.3 mm at failure. No plasticity is observed at rivet holes in the substrate and doublers. This suggests that the displacement is mainly due to rivet shearing, where each rivet carried a load of 1.36 kN (also called rivet value). Pure rivet shear (see Fig. 3.3 left) caused the failure of all three riveted joints. From Fig. 3.1, one can notice that the load-displacement curve of the riveted joints has two parts: it shows elastic behaviour up to 4 kN, while above 4 kN yielding of rivets (plastic behaviour) is observed. From the experiments, it can be said that the metal-metal riveted joints have a limit load (i.e., ultimate load/safety factor) of 3.6 kN, when a safety factor of 1.5 is applied. The standard deviation in peak strength of these specimens is very low (0.04 kN).

Metal-composite riveted joints failed at an average peak load of 5.8 kN, which is slightly higher (6.9% higher) than the peak strength of metal-metal riveted joints. This can be due to difference in stiffness of composite doublers compared to metal doublers, as composite doublers are stiffer than metal doublers, and this effect is slightly noticed in the load carrying capacity of the

joint. Slightly higher yielding of rivets is observed for composite doublers compared to metal doublers. At failure, each rivet carried a load of 1.46 kN, with a total final displacement of 2.3 mm. All these specimens failed also due to pure rivet shear (See Fig. 3.3 right). The load-displacement behaviour of these joints shows that the elastic limit is around 4.2 kN. Finally, the limit load for metal-composite riveted joints, as obtained from experiments with safety factor of 1.5, is 3.9 kN. The standard deviation in peak strength is again 0.04 kN.

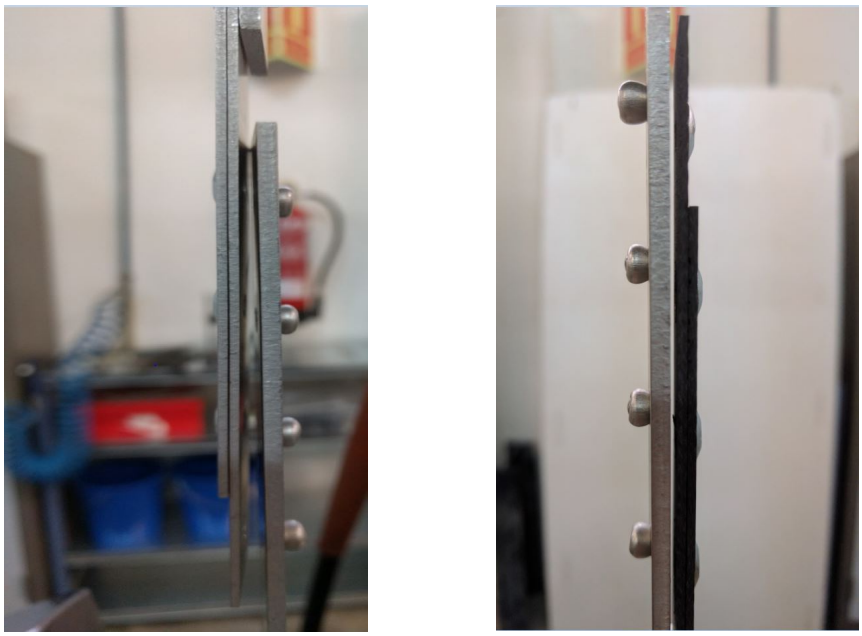

Figure 3.3: *Rivet shear failure of metal-metal (left) and metal-composite (right) riveted joints [70].*

Adhesive bonded joints are stiffer compared to pure riveted joints, which can be observed in load-displacement curves shown in Fig. 3.1 and 3.2. The average peak strength of metal-metal adhesive bonded joints is 23 kN, with final displacement of 1.6 mm at failure. When a safety factor of 1.5 is applied, metal-metal adhesive bonded joints have a safe limit up to 15.3 kN for operations. Load-displacement curve has high slope with no yield behaviour of adhesive. Adhesive bonded joints tend to be brittle in nature as the failure happens quickly without any indication. Standard deviation of 2.6 kN is observed for metal-metal adhesive bonded joints. Secondary bending is

observed in these joints and can be due to thickness of the joint (see Fig. 3.4 left).

Average strength of metal-composite adhesive bonded joints is 19.4 kN, which is 15.6% lower than metal-metal adhesive bonded joints. Though the bonding area and adhesive are the same for both joints, still a difference is noticed. This may be due to a lower load transfer between metal-composite adhesive bonded joints through the adhesive layer. The failure mode of metal-composite adhesive bonded joints is adhesive failure, with the adhesive remaining on the substrate (see Fig. 3.4 right). Standard deviation of 2.8 kN is observed for specimens of metal-composite adhesive bonded joints. Considering a safety factor of 1.5, this joint configuration can carry loads up to 13 kN.

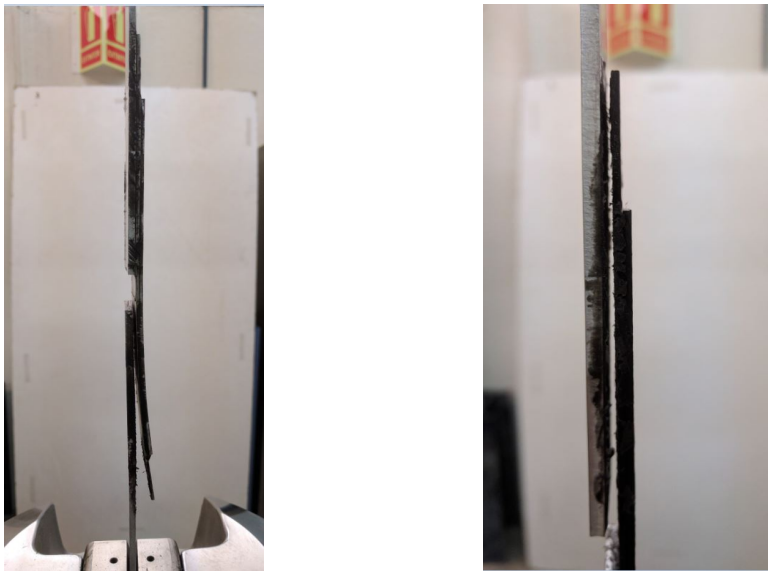

Figure 3.4: *Failure of metal-metal (left) and metal-composite (right) adhesive bonded joint [70].*

From the load-displacement curves shown in Fig. 3.1 and 3.2, metal-metal hybrid joints have highest average peak strength compared to all other joint configurations: 28.3 kN, with standard deviation of 2 kN, which is slightly lower than adhesive bonded joints and much higher than riveted joints, and a final displacement of 5 mm at failure. With a safety factor of 1.5, this joint configuration can carry loads up to 19 kN. The failure of all three specimens occurred in two stages: initially, adhesive failure, followed by rivet shear. This

suggests that, in hybrid joints, most of the load is carried/transferred by the adhesive layer and, once the adhesive fails, then the rivets carry the load up to final failure. Interestingly, one can observe yielding behaviour of metal-metal configuration in the load-displacement curve. This may be due to the adhesive behaviour between metal surfaces, and the fact that it tends to shear more. Secondary bending is observed only for these joints, which can be due to the bigger thickness of the metal substrate and doublers (see Fig. 3.5 left).

Metal-composite hybrid joints have an average peak strength of 16.7 kN, which is 41% lower compared to metal-metal configuration, and a final displacement of 1.3 mm at failure. The standard deviation in peak strength of the specimens is 1.5 kN. The failure mode of all three specimens is net-section failure of the doublers, which happened at the fourth rivet as shown in Fig. 3.5 right. Although composite doublers are much stiffer than aluminium alloy doublers, the net-section failure of the composite doublers suggests vulnerability of these composite structures to the presence of rivet holes, which has deteriorated by 11% the joint strength compared to the joint without holes (i.e., the pure adhesive bonded joint).

Metal-composite hybrid joint has similar load-displacement behaviour compared to metal-composite adhesive bonded joint. No yield is observed for hybrid metal-composite joint when compared to metal-metal hybrid joint.

Figure 3.5: *Failure of metal-metal (left) and metal-composite (right) hybrid joints [70].*

3.2 AA 2024-T3- Fatigue tests

In this section, fatigue test results for metal-metal and metal-composite configurations of riveted, adhesive bonded, and hybrid joints are discussed. Three specimens of each joint configuration are tested under fatigue loading, as discussed in Chapter 2. All fatigue tests are performed under load control mode at stress ratio of 0.1, which means that the experiments are tension-tension fatigue tests. Fatigue loads are applied in three regimes based on the number of cycles specimens have undergone without failure (see Table 3.3).

For the first 2×10^5 loading cycles, the fatigue load is based on the static strength of the riveted joint, that is, the force amplitude in this first regime is 4.4 kN, which is 80% of the average peak static strength of the riveted joints.

- Once the tested joints reach 2×10^5 cycles, an increase in the load amplitude is applied to prevent strain relaxation of the specimens: particularly, for the next 2×10^5 cycles, the applied load amplitude increases by 30%.

- Finally, if the specimens reach 4×10^5 cycles without failure, a further increase of the load amplitude of 30% is applied up to joint failure.

Initially, tests are started with a frequency of 5 Hz and, once the specimens have stabilised, the frequency is increased to 7 Hz. This process is followed consistently for all fatigue specimens throughout the tests.

Regime	**Up to 2×10^5 cycles**	**From 2×10^5 to 4×10^5 cycles**	**From 4×10^5 cycles up to failure**
Conditions	$F_{amplitude}$ =4410 N F_{mean} =2695 N	$F_{amplitude}$ =5733 N F_{mean} =3504 N	$F_{amplitude}$ =7453 N F_{mean} =4555 N

Table 3.3: *Fatigue loading conditions in the three regimes for metal-metal and metal-composite joints.*

Table 3.4 presents the fatigue life of joints with metal substrate and metal doublers. The fatigue life of metal-metal riveted joint specimens was 50×10^3, 52×10^3, and 84×10^3 cycles, respectively. Specimens 1 and 2 have consistent fatigue life but the third specimen has higher fatigue life by 55-60% and possible reason can be due to higher residual stresses during riveting process. If only first two specimens are considered, then the average fatigue life of riveted joints is 51×10^3 cycles. Thus, all these joints failed in the first load regime, that is, before reaching 2×10^5 cycles, with an average fatigue life of 62×10^3 cycles for three specimens. Rivet shear caused all these specimens to fail (see Fig. 3.6 top-left), and no damage to substrate or doublers is observed. However, secondary bending is observed in these specimens, which may be due to the load path/transfer between the substrate and doublers. Finally, from the experimental results it can be said that, the fatigue life of riveted joints solely dependent on rivets: higher rivet strength provides higher fatigue life.

Joint configuration	**Specimen 1**	**Specimen 2**	**Specimen 3**	**Average**	**std. dev**
Riveted joint	50725	52843	84225	62598	15317
Adhesive Bonded joint	85510	73092	11385	56662	32415
Hybrid joint	202200	231800	223000	219000	12411

Table 3.4: *Fatigue life of metal-metal joint configurations.*

The fatigue life of metal-metal adhesive bonded joint specimens was 85×10^3, 73×10^3, and 11×10^3 cycles. Thus, all adhesive bonded joints failed in

the first load regime. Specimens 1 and 2 were tested within a week after preparation, while specimen 3 was tested three weeks later. Aside from this, the discrepancy in the fatigue life observed for the third specimen can be due to unexpected/unnoticed defects in the bondline. The average fatigue life of these specimens was 56×10^3, but this value is significantly affected by the third specimen. If the result for specimen 3 is disregarded, the average fatigue life is 79×10^3 cycles for specimens 1 and 2. In this regard, adhesive bonded joints have an average life higher than riveted joints (average of specimens 1 and 2) by 53%. Adhesive failure caused adhesive bonded joints to fail under fatigue loading, with the failed adhesive remaining on the substrate as shown in Fig. 3.6 top-right.

The fatigue life of metal-metal hybrid joint specimens was 2.02×10^5, 2.32×10^5, and 2.23×10^5 cycles. Thus, all these specimens exceeded 2×10^5 cycles and failed in the second regime, with an average fatigue life of 2.19×10^5 cycles. The failure mode was as follows: first, the rivet close to the mid-plane failed due to rivet shear, followed by doubler debonding at the mid plane; finally, the adhesive between substrate and doubler failed with all rivets shearing at load amplitude of 6.4 kN (see Fig. 3.6 bottom). The test results clearly show the superiority of hybrid joints for metal-metal specimens.

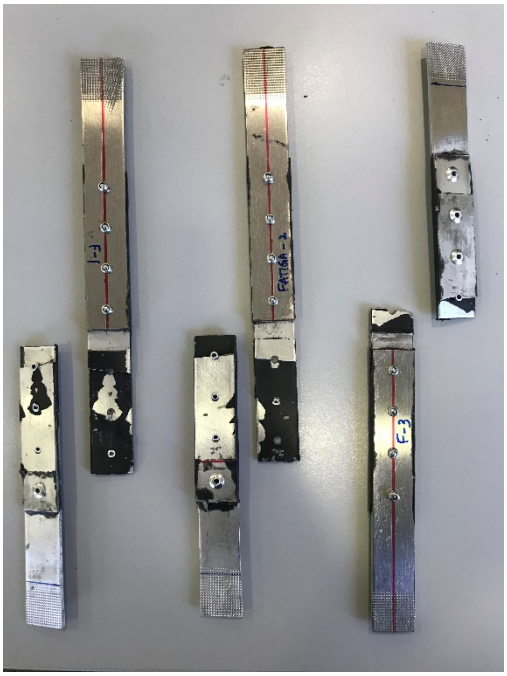

Figure 3.6: *Fatigue failure of metal-metal riveted (top-left), adhesive bonded (top-right) and hybrid joints (bottom).*

Table 3.5 presents the fatigue life of joints with metal substrate and composite doublers. The fatigue life of riveted specimens was 56×10^3, 57×10^3, and 41×10^3 cycles, averaging 52×10^3 cycles. Rivet shear caused failure in all three specimens (see Fig. 3.7 top-left). The average fatigue life of metal-composite riveted joints is 17% lower than that of metal-metal riveted joints. The influence of dissimilar doubler material might have affected the performance of metal-composite riveted joints. However, if only specimens 1 and 2 are considered, then the fatigue life of metal-composite and metal-metal riveted joints is nearly identical. Secondary bending effects are not observed in these joints, probably because composite doublers are thinner than metal doublers.

Joint configuration	**Specimen 1**	**Specimen 2**	**Specimen 3**	**Average**	**std. dev**
Riveted joint	56988	57280	41780	52016	7239
Adhesive Bonded joint	69904	65074	33065	56014	16347
Hybrid joint	442732	441000	442958	442230	875

Table 3.5: *Fatigue life of metal-composite joint configurations.*

The fatigue life of metal-composite adhesive bonded joint specimens was 69×10^3, 65×10^3, and 33×10^3 cycles, averaging 56×10^3 cycles. Specimens 1 and 2 have consistent fatigue lives compared to specimen 3, as occurred for metal-metal configuration. Specimens 1 and 2 were tested within one week of preparation, but specimen 3 was tested a month later. Deterioration of the adhesive due to storage environmental conditions, and/or unnoticed damage in bondline, might explain the lower fatigue life of the third specimen. If specimen 3 is disregarded, then the average fatigue life of specimens 1 and 2 is 67×10^3 cycles, which is 30% higher compared to that of riveted joints. Again, adhesive failure was responsible for the failure of all three specimens, with the failed adhesive remaining stuck to the substrate (see Fig. 3.7 top-right).

The fatigue life of metal-composite hybrid joint specimens was the highest observed in this research: 4.43×10^5, 4.41×10^5, and 4.42×10^5 cycles, averaging 442×10^5 cycles, and with the lowest standard deviation. Specimens 1 and 2 were tested within one week of preparation, but again specimen 3 was tested after a month later. However, the effect of bond deterioration with time is not observed for this hybrid specimen. Net-section failure is observed for two of three specimens and third failed due to adhesive and rivet shear (see Fig. 3.7 bottom and centre specimen).

Therefore, among metal and composite doublers, the performance of composite doublers with hybrid joint is the best, being the only specimens that exceeded 4×10^5 cycles and failed in the third load regime, with a load amplitude of 7.5 kN. Rivet shear and adhesive failure caused all three specimens to fail.

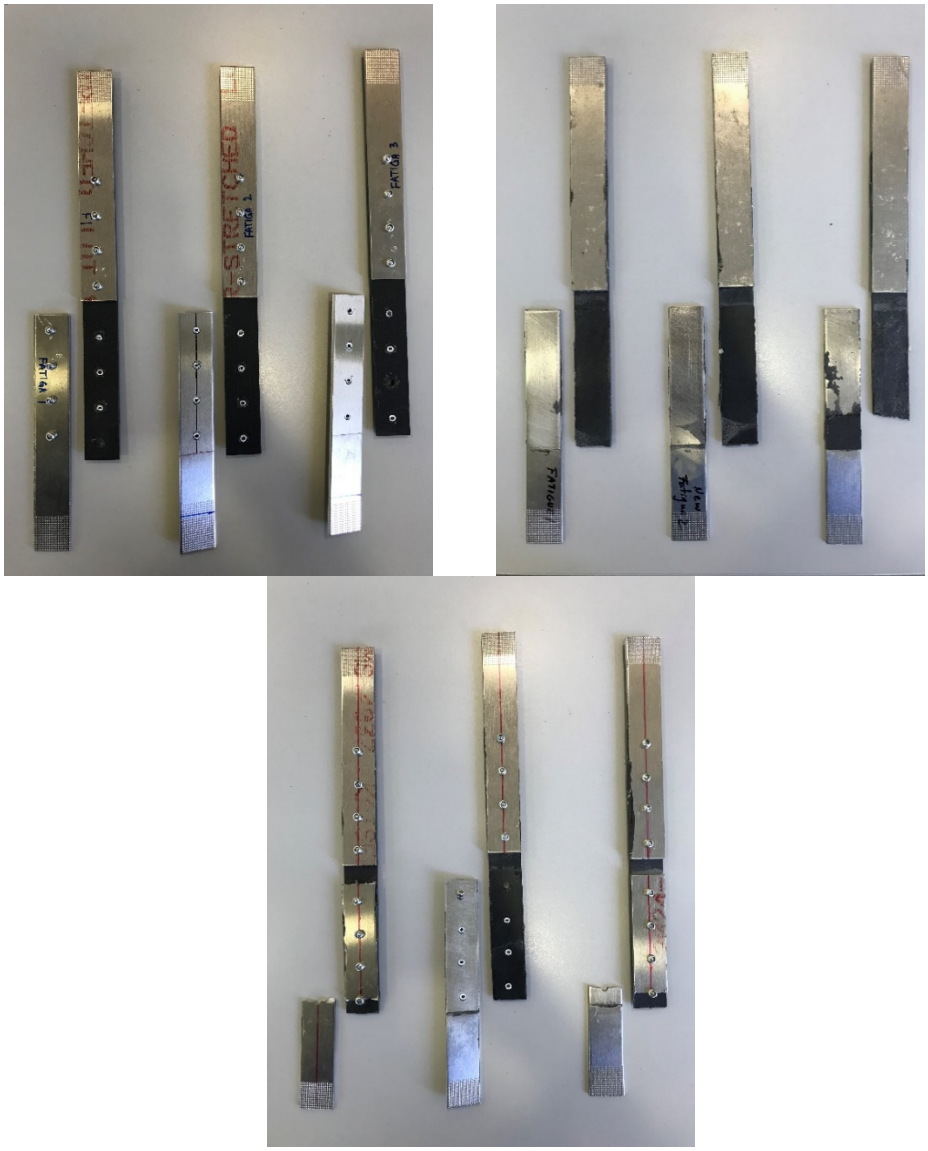

Figure 3.7: *Fatigue failure of metal-composite riveted (top-left), adhesive bonded (top-right) and hybrid joints (bottom).*

3.3 CFRE substrate- Static tests

In this section, the results of static tests on samples with CFRE substrate and CFRE and metal doublers are presented. The load-displacement curves obtained from the experiments for composite-composite and composite-metal configurations of riveted, adhesive bonded, and hybrid joints are shown

in Fig. 3.8 and 3.9. As mentioned in Section 2.2, three specimens of each type of joint configuration were tested. Tables 3.7 and 3.8 show the peak strength of each of the tested specimens, as well as the average and standard deviation of the peak strength of the three tested specimens for each joint configuration.

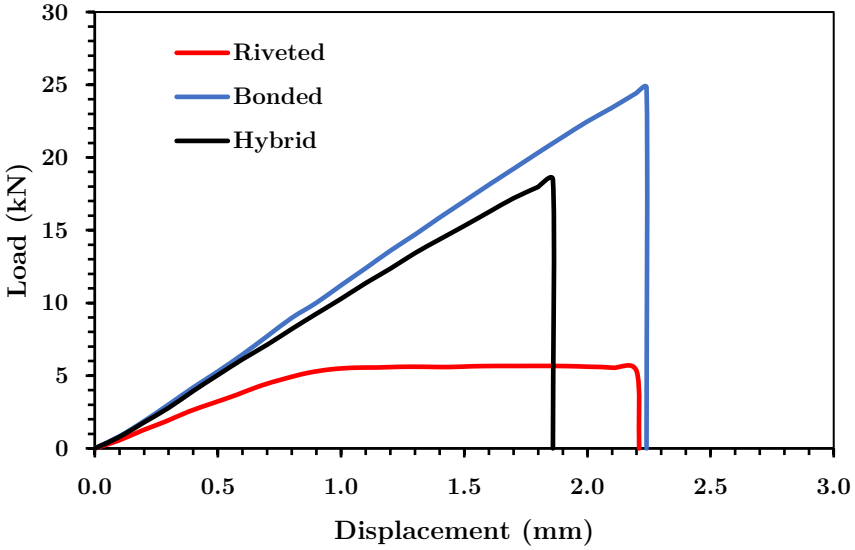

Figure 3.8: *Experimental load vs. displacement curves for composite-composite riveted, adhesive bonded, and hybrid joint configurations.*

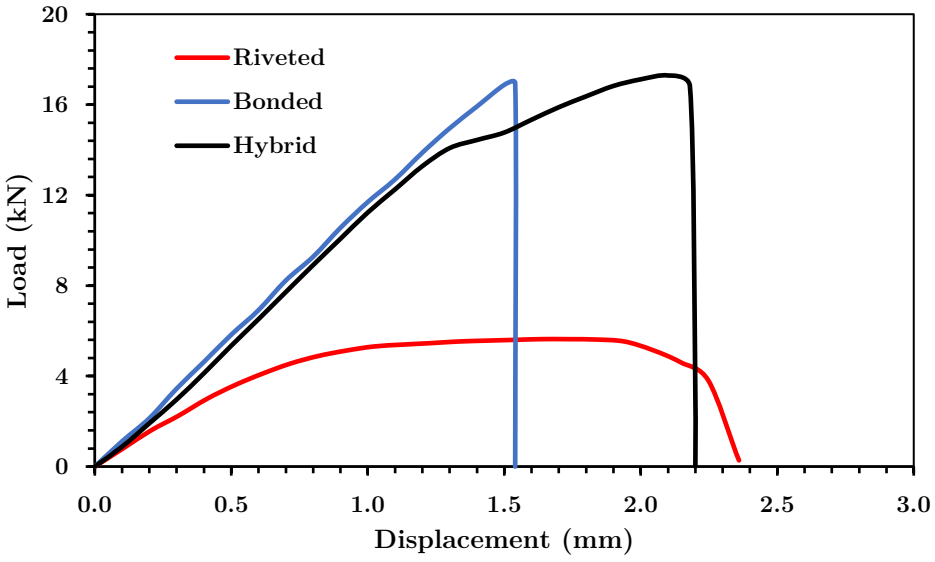

Figure 3.9: *Experimental load vs. displacement curves for composite-metal riveted, adhesive bonded, and hybrid joint configurations.*

Joint configuration	Composite-Composite joint					
	Load of specimen 1 (kN)	Load of specimen 2 (kN)	Load of specimen 3 (kN)	Average load (kN)	Standard deviation (kN)	Standard deviation to av. load (%)
Riveted joint	5.72	5.75	5.73	5.74	0.02	0.4
Adhesive Bonded joint	26.0	25.4	23.0	24.8	1.6	6.5
Hybrid joint	18.1	19.0	18.3	18.5	0.4	2.2

Table 3.6: *Experimental results from static tests on riveted, adhesive bonded, and hybrid joints of composite-composite configuration.*

As shown in Fig. 3.8 and Table 3.6 for composite-composite configuration, riveted joints have the lowest average peak load (5.74 kN), with low standard deviation of 0.02 kN, and peak displacement of 2.1 mm at failure. The failure mode observed for all three specimens of riveted joint is rivet shear, showing that the rivets are the weakest points of these joints and that their failure causes the joints to fail (see Fig. 3.10(a)). The load-displacement curve shows elastic and plastic behaviour: linear elasticity is observed up to a load of 4.3 kN, beyond which rivets sheared plastically up to failure. The shear strength of the rivets is calculated as rivet load divided by cross-sectional area of the rivet, where the rivet load is the joint failure load divided by the total number of rivets. In this case, the rivet load is 717 N, and the shear strength of each rivet is 40 MPa.

For composite-composite configuration, adhesive bonded joints have the highest average peak load (24.8 kN), with standard deviation of 1.6 KN (6.5% of the average load), and peak displacement of 3 mm at failure. Although the adhesive bonded specimens were prepared and tested under the same conditions, the standard deviation is significant. This is because improper or unequal surface treatment or presence of voids in the adhesive bond may have affected the specimens, explaining such dispersion in the results. Unlike riveted joints, adhesive bonded joints are stiffer and show only linear elastic behaviour. Among the three tested specimens of composite-composite adhesive bonded joint, two experienced cohesive failures, with traces of failed adhesive on both the substrate and doubler 1 (see Fig. 3.10(b)), while the third specimen showed doubler failure (see left specimen in Fig. 3.10(b)). The shear strength of adhesive is 4.8 MPa, calculated as the peak load divided by area of the bond.

Finally, composite-composite hybrid joints have an average peak load of 18.5 kN, with relatively low standard deviation of 0.4 kN (2.2% of the average load), three times lower than pure adhesive bonded joints. This may be due to the presence of rivets, thus sharing load transfer between adhesive and rivets and mitigating the impact of uneven performance of the adhesive bonds due to adhesive application conditions. Net-section failure (see Fig. 3.10(c)) is observed in all the three specimens, which, as mentioned before, suggests vulnerability of the composites to fastener holes. As a summary for composite-composite joints, the average peak load of adhesive bonded joints is four and a half times higher than that of riveted joints, and 34% higher than that of hybrid joints.

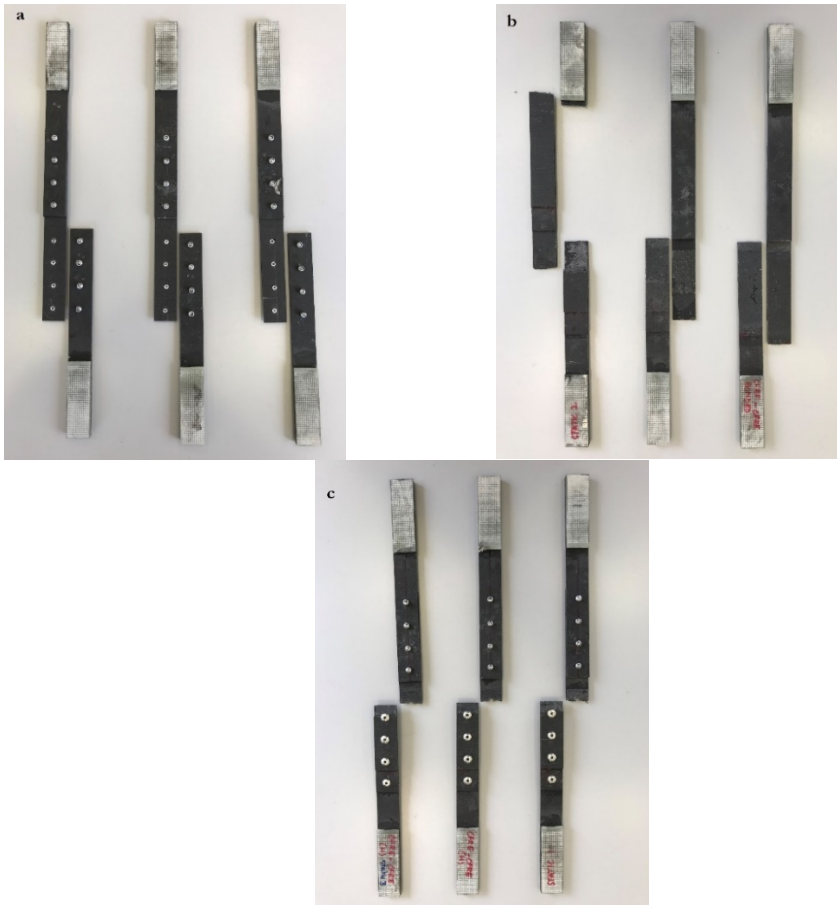

Figure 3.10: *Failure of composite-composite specimens of (a) riveted, (b) adhesive bonded, and (c) hybrid joints.*

Joint configuration	Composite-Metal joint					
	Load of specimen 1 (kN)	Load of specimen 2 (kN)	Load of specimen 3 (kN)	Average load (kN)	Standard deviation (kN)	Standard deviation to av. Load (%)
Riveted joint	5.53	5.65	5.65	5.61	0.07	1.3
Adhesive Bonded joint	17.3	17.7	15.8	16.9	1.02	5.9
Hybrid joint	17.6	16.6	17.7	17.3	0.6	3.5

Table 3.7: *Experimental results from static tests on riveted, adhesive bonded, and hybrid joints of composite-metal configuration.*

As shown in Fig. 3.9 and Table 3.7 for composite-metal configuration, riveted joints have an average peak load of 5.6 kN, with standard deviation of 0.07 kN. Linear elastic behaviour is observed for these joints up to 0.7 mm, which is lower than the elastic limit of composite-composite riveted joints (see Fig. 3.11(a)). The low elasticity of rivets can be due to the dissimilar substrate and doubler material might have caused less elongation of rivets in linear elastic region. As for composite-composite configuration, rivet shear caused the failure of all three composite-metal riveted joint specimens. Hence, the rivets are also the weakest points of these riveted joints, with each rivet carrying a load of 707 N, with rivet shear strength of 40 MPa (virtually equal values to those for composite-composite configuration).

For composite-metal configuration, adhesive bonded joints have an average peak load of 16.9 kN (which is 32% lower than for composite-composite adhesive bonded joints), with standard deviation of 1 kN (6% of the average peak load). Adhesive failure was the failure mode of all three adhesive bonded joint specimens, with the failed adhesive remaining on the substrate (see fig. 3.11(b)). Adhesive failure is common in specimens with dissimilar materials for substrate and doubler [70]. The shear strength of this joint is 3.3 MPa, which is only 68% of the composite-composite adhesive bonded joint. This lower shear strength can be due to the behaviour of the adhesive between dissimilar materials.

Finally, composite-metal hybrid joints, with average peak load of 17.3 kN, and standard deviation of 0.6 kN, have slightly higher load carrying capacity than composite-metal and composite-composite adhesive bonded joints. Two out of three composite-metal hybrid joint specimens failed due to

net-section failure of the substrate, while the third specimen failed due to adhesive failure and rivet shear (see Fig. 3.11(c)). Net-section failure mode suggests vulnerability of composite substrate to high-stress concentrations around fastener holes. The low standard deviation in the strength of these specimens suggests high reliability of these joints for practical purposes. When comparing riveted, adhesive bonded, and hybrid joints, riveted joints show the low standard deviation, followed by hybrid joints. When it comes to applications in the air transport and aviation industries, in general, reliability of joints is a major concern, but adhesive bonded joints can still be considered, as for these joints, the standard deviation is reasonably low (just 5.9% of the average peak load). However, proper NDT inspections to detect cracks or debonding play an important role in maintaining the standards of the adhesive bonded joints.

Figure 3.11: *Failure of composite-metal specimens of (a) riveted, (b) adhesive bonded, and (c) hybrid joints.*

Studying the energy absorption (EA) of the joints provides the necessary energy required to break the joints, given by the area under load-displacement curve. Table 3.8 shows EA for composite-composite and composite-metal configurations. One can notice that composite-composite adhesive bonded joints have highest EA. A simple superposition rule [73] cannot be applied for estimating EA of hybrid joints based on riveted and adhesive bonded energies.

Joint configuration	Composite-composite EA in [J]	Composite-metal EA in [J]
Riveted joint	9.9	10.1
Adhesive joint	28	13.7
Hybrid joint	17.6	23.4

Table 3.8: *Experimental results for energy absorption (EA) by the riveted, adhesive bonded, and hybrid joints in composite-composite and composite-metal configurations.*

3.4 CFRE substrate- Fatigue tests

In this section, we present experimental results of composite-composite and composite-metal configurations under riveted, adhesive bonded, and hybrid joints. The fatigue loading conditions used for testing composite substrate joints (see Table 3.9) are slightly different from those used for testing metal substrate joints:

- The conditions in the first regime (up to 2×10^5 loading cycles) are now calculated based on the static strength of composite-composite and composite-metal riveted joints: the force amplitude in this first regime is 4.5 kN, which is 80% of the average peak static strength of the riveted joints.
- Once the tested joints reach 2×10^5 cycles, the applied load is increased by 30% in the second regime (up to 4×10^5 loading cycles).
- Finally, if the specimens reach 4×10^5 cycles without failure, a further increase of the load amplitude of 30% is applied up to joint failure.

Regime	Up to 2×10^5 cycles	From 2×10^5 to 4×10^5 cycles	From 4×10^5 cycles up to failure
Conditions	$F_{amplitude}$ =4482 N F_{mean} =2739 N	$F_{amplitude}$ =5827 N F_{mean} =3561 N	$F_{amplitude}$ =7575 N F_{mean} =4629 N

Table 3.9: *Fatigue loading conditions in the three regimes used for testing composite-composite and composite-metal joints.*

Table 3.10 shows the fatigue life of joints with composite substrate and composite doubler. In this case, the fatigue life of the tested riveted joint specimens was 57×10^3, 52×10^3 and 51×10^3 cycles, thus averaging 53×10^3 cycles. All three specimens failed due to rivet shear (see Fig. 3.12 top-left). Lower dispersion is observed in the results for these joints, compared to the cases with metal substrates. The average fatigue life of composite-composite riveted joints is lower than metal-metal and metal-composite riveted joints. Thus, for riveted joints, the performance of composite substrates is lower than that of metal substrates.

Joint configuration	Specimen 1	Specimen 2	Specimen 3	Average	std. dev
Riveted joint	57614	52252	51691	53852	2670
Adhesive Bonded joint	266785	247153	272200	262046	10760
Hybrid joint	600000*	600000*	600000*	600000*	--

Table 3.10: *Fatigue life of composite-composite joint configurations. (* indicates samples have not broken)*

The fatigue life of composite-composite adhesive bonded joint specimens was 2.6×10^5, 2.4×10^5, and 2.7×10^5 cycles. Thus, all specimens failed after 2×10^5 cycles, with an average of 2.6×10^5 cycles, and showing low dispersion in fatigue life. In this case, cohesive failure was responsible for the failure of all three tested specimens (see Fig. 3.12 top-right). From these results, composite-composite adhesive bonded joints exhibit higher fatigue life compared to metal-metal and metal-composite adhesive bonded joints.

Composite-composite hybrid joint specimens show the best fatigue response among the 12 tested configurations, with fatigue life in excess of 6×10^5 cycles for all tested specimens. Indeed, the specimens did not fail (see Fig. 3.12 bottom) and, after 6×10^5 cycles, the fatigue tests were terminated as the time needed to perform the tests exceeded the machine's operational range.

Moreover, there was no sign of damage on the tested hybrid joint specimens after the 6×10^5 loading cycles. To sum up, fatigue performance of composite-composite hybrid joints is the best compared to all studied joints.

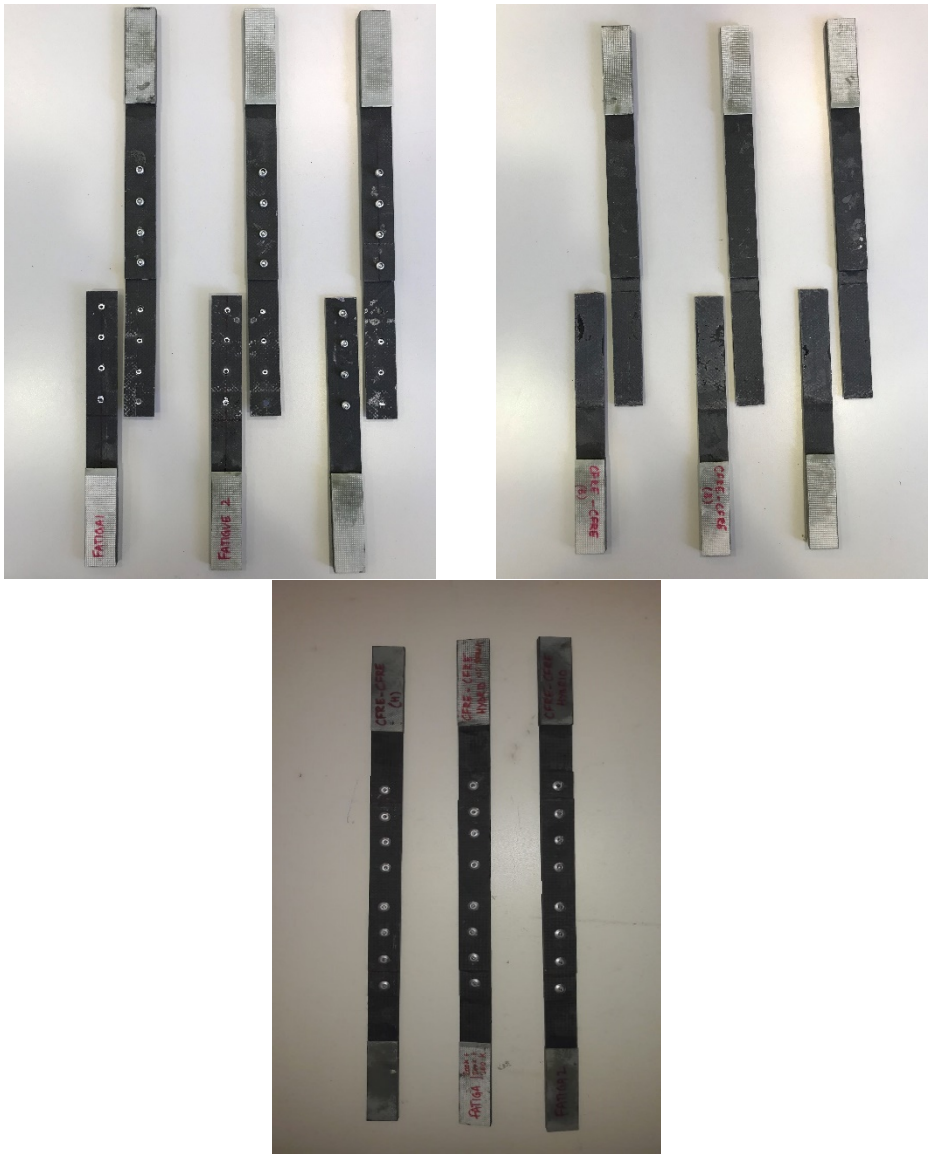

Figure 3.12: *Fatigue failure of composite-composite riveted (top-left), adhesive bonded (top-right) and hybrid joints (bottom).*

Table 3.11 shows the fatigue life of joints with composite substrate and metal doubler. The fatigue life of the tested composite-metal riveted joints was

59×10^3, 45×10^3, and 52×10^3 cycles, averaging 52×10^3 cycles. Rivet shear was responsible for the failure of all tested specimens (see Fig. 3.13 top-left), suggesting that the rivets are, again, as for all studied configurations of riveted joint, the weak spots in these joints. No significant difference is noticed between the response of composite-composite riveted joints and composite-metal riveted joints.

Joint configuration	Specimen 1	Specimen 2	Specimen 3	Average	std. dev
Riveted joint	59915	45525	52725	52722	5875
Adhesive Bonded joint	5814	6810	4314	5646	1026
Hybrid joint	94134	88780	132517	105144	19479

Table 3.11: *Fatigue life of composite-metal joint configurations.*

The fatigue life of composite-metal adhesive bonded joint specimens was 5.8×10^3, 6.8×10^3, and 4.3×10^3 cycles, averaging 5.6×10^3 cycles. These joints were tested 5 weeks after preparation, and the poor results suggest deterioration of the adhesive bond. All tested specimens failed due to adhesive failure, with the failed adhesive remaining stuck to the composite doubler (see Fig 3.13 top-right). There are other possible explanations for these poor results, which include metal surface interaction with composite substrate, suggesting that adherence of the adhesive is better to the composite rather than to the metal (as expected, since epoxy adhesives generally adhere very well to the old epoxy resin of the composite material).

The fatigue life of composite-metal hybrid joint specimens was 94×10^3, 88×10^3, and 13×10^3 cycles, averaging 105×10^3 cycles. Rivet shear and adhesive failure were responsible of the failure of all three tested specimens (see Fig. 3.13 bottom). Among riveted, adhesive bonded, and hybrid configurations, the hybrid joints show higher fatigue life, being nearly twice as large as that of the riveted joints and eighteen times that of the adhesive bonded joints.

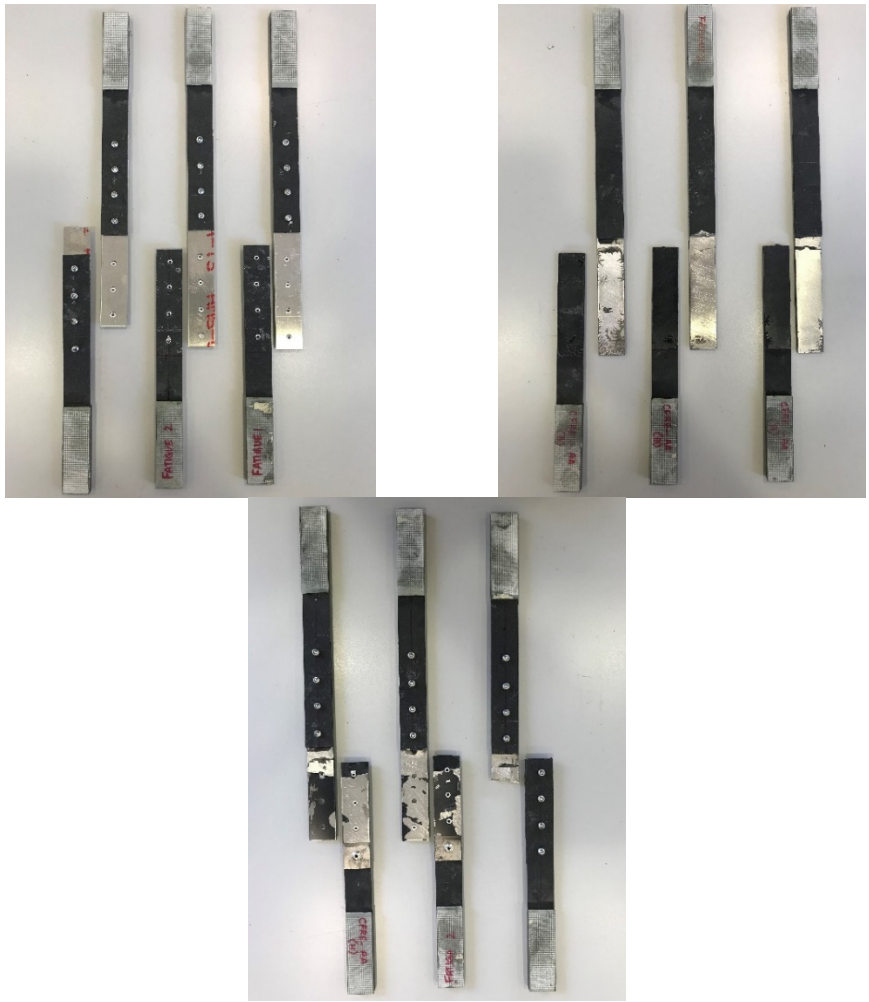

Figure 3.13: *Fatigue failure of composite-metal riveted (top-left), adhesive bonded (top-right) and hybrid joints (bottom).*

3.5 Summary of static tests

In this section, a summary of the static tests results for all specimens is discussed. Table 3.12 shows a comparison of the average peak strength of metal-metal and metal-composite joints. Similarly, Table 3.13 shows a comparison of the average peak strength of composite-composite and composite-metal joints. The percentages shown in these tables correspond to the strengths of the joint configurations on the columns compared with the strengths of the joint configurations on the rows.

Joint configuration		AA 2024-T3–AA 2024-T3			AA 2024-T3–CFRE		
		Riveted	Adhesive Bonded	Hybrid	Riveted	Adhesive Bonded	Hybrid
AA 2024-T3–AA 2024-T3	Riveted	X	423%	519%	107%	355.7%	305.5%
	Adhesive Bonded	24%	X	123%	24%	84%	72%
	Hybrid	19%	82%	X	19%	69%	59%
AA 2024-T3–CFRE	Riveted	94%	396%	485%	X	333%	286%
	Adhesive Bonded	28%	119%	146%	30%	X	86%
	Hybrid	33%	138%	170%	35%	116%	X

Table 3.12: *Comparison table of average strengths of AA 2024-T3–AA 2024-T3 and AA 2024-T3–CFRE joints of riveted, adhesive bonded, and hybrid joints [70].*

For metal substrates with metal doublers, hybrid joints shown highest average peak strength, which is 519% and 123% of the strength of metal-metal riveted and adhesive bonded joints. Hybrid joints also showed highest peak failure displacement: around 5 mm (see Fig. 3.1). This is because the load transfer between substrate and doublers of same material under hybrid joining is better, that is, load transmission/sharing through adhesive layer and rivets is better. Secondly, the strength of metal-metal adhesive bonded joints is 423% of the strength of metal-metal riveted joints. This shows the superiority of the joint strength with adhesive layer compared to just rivets.

On the other side, the strength of adhesive bonded joints of metal substrate with composite doublers is 333% and 116% that of the riveted and hybrid joints. This suggests adhesive bonding is better for dissimilar substrate and doubler materials. Secondly, metal-composite hybrid joints are better than riveted joints by 286% where hybrid joints are better than riveted joints because of the adhesive layer.

It can be concluded from Table 3.12, that hybrid joining is the most suitable joining method for high strength repairs of metal substrate with metal doublers, while for repairs of metal substrate with composite doublers, adhesive bonding shows the best static performance. Overall performance of metal-metal hybrid joints is highest among all metal substrate repairs. Hybrid joints are advantageous with rivets providing additional level of protection in case of premature or early adhesive failure.

Joint configuration		CFRE–CFRE			CFRE–AA		
		Riveted	Adhesive Bonded	Hybrid	Riveted	Adhesive Bonded	Hybrid
CFRE–CFRE	Riveted	X	432%	322%	98%	294%	301%
	Adhesive Bonded	23%	X	75%	23%	68%	70%
	Hybrid	31%	134%	X	30%	91%	94%
CFRE–AA	Riveted	102%	442%	330%	X	301%	308%
	Adhesive Bonded	34%	147%	109%	33%	X	102%
	Hybrid	33%	143%	107%	32%	98%	X

Table 3.13: *Comparison table of average strengths of CFRE–CFRE and CFRE-AA 2024 joints of riveted, adhesive bonded, and hybrid joints.*

From the Table 3.13, it can be observed that composite substrate with adhesive bonded composite doublers have highest strength about 432% and 134% that of composite-composite riveted and hybrid joints. The superiority of adhesive bonded joints is because of the uniform distribution of load by adhesive overlap area. Secondly, the strength of composite-composite hybrid joints is 322% higher than composite-composite riveted joints, which is mainly due to the presence of adhesive layer thereby load distribution takes place by the adhesive layer and rivets.

The results for all the riveted joint configurations (that is, metal-metal, metal-composite, composite-composite, and composite-metal) are very similar because of the use of the same rivets for all these configurations. The peak strength of riveted joints is just around one-fourth or one-fifth of the peak strength of the adhesive bonded and hybrid joints. Among the studied joints, the results for the riveted joints had the lowest standard deviation, making these results reliable when it comes to practical applications, despite their disadvantages.

The main cause of failure of the riveted joints is rivet shear. From this, it can be concluded that rivets with higher shear strength can prevent rivet shear failure and thus joint failure.

Among the adhesive bonded joints, composite-composite showed the highest average peak strength that is 7.3% higher than metal-metal, 27.5% higher than metal-composite, and 46.8% higher than composite-metal.

The main cause of failure of the adhesive bonded joints is adhesive failure. However, a few specimens failed due to cohesive failure, especially for composite-composite joints. The overall performance of adhesive bonded joints is relatively superior to riveted joints for all the studied configurations. The higher standard deviation makes the average peak strength obtained for adhesive bonded joints less reliable compared to that obtained for riveted or hybrid joints.

On the other side, hybrid joints are comparable to adhesive bonded joints but much superior to riveted joints. The presence of adhesive in addition to rivets made hybrid joints nearly three to five times stronger than simple riveted joints. Among the studied hybrid joint configurations, metal-metal showed highest average peak strength, 70% higher than metal-composite, 53.2% higher than composite-composite, and 64% higher than composite-metal configurations.

The main cause of failure for hybrid joints is rivet shear plus adhesive failure, and the other most common failure mode was net-section failure. The specimens showing rivet shear and adhesive failure suggest that substrates and doublers have higher stiffness compared to the adhesive. Net-section failure is seen in specimens with either composite substrate or doublers. This mode of failure suggests vulnerability of composites to stress intensity factors around the fastener holes. Hybrid joints have quite low standard deviation of peak strength, together with higher average peak strength, making them the best choice, in view of the results of this research.

3.6 Summary of fatigue tests

In this section, a summary of the fatigue tests results for all specimens of metal-metal, metal-composite, composite-composite, and composite-metal joints is presented and discussed. Tables 3.14 and 3.15 show a comparison of the average fatigue life in two cases: 1) considering the results of all three

specimens for each studied configuration, and 2) considering only the results of two specimens, if the results for the third specimen show very large deviation with respect to the other two, which is probably, due to experimental error. Note that, in these tables, metal is AA (2024-T3 aluminium alloy) and composite is represented by CFRE (Carbon fibre reinforced epoxy).

	Joint	Specimen 1	Specimen 2	Specimen 3	Av. Life	Std. deviation
AA–AA	Riveted	50725	52843	84225	62598	15317
	Adhesive Bonded	85510	73092	11385	56662	32415
	Hybrid	202200	231800	223000	219000	12411
AA–CFRE	Riveted	56988	57280	41780	52016	7239
	Adhesive Bonded	69904	65074	33065	56014	16347
	Hybrid	442732	441000	442958	445530	875
CFRE–CFRE	Riveted	57614	52252	51691	53852	2670
	Adhesive Bonded	266785	247153	272200	262046	10760
	Hybrid	600000*	600000*	600000*	600000*	--
CFRE–AA	Riveted	59915	45525	52725	52722	5875
	Adhesive Bonded	5814	6810	4314	5646	1026
	Hybrid	94134	88780	132517	105144	19479

Table 3.14: *Fatigue life, average life and standard deviation of all three specimens of joint configurations. (* indicates samples have not broken)*

The average fatigue life of the riveted joints ranges from 52×10^3 to 63×10^3 cycles, if we consider the three tested specimens for each studied configuration (see Table 3.14), while it ranges from 52×10^3 to 57×10^3 cycles if we disregard the fatigue life results that are too deviated from the average (see Table 3.15). It is worth noting that riveted joints show very similar fatigue lives irrespective of the substrate or doubler material. Given this, and the fact that all riveted joints had same failure mode under static loading, also irrespective of the substrate and doubler material, it can be concluded that the rivets are dominant in both the static and fatigue response of the riveted joints. That is, the static failure of riveted joints depends mostly on rivet strength, while the fatigue life of these joints depends mostly on the fatigue life of the rivets.

Unlike riveted joints, the fatigue life of adhesive bonded joints shows high dispersion, because it depends on many parameters that are more difficult to control, such as surface preparation, adhesive bondline, and curing phase. The average life of adhesive bonded joints for the tested configurations ranges from 6×10^3 to 262×10^3 cycles (see Table 3.14). If again we disregard the results that are too deviated, the average life of the adhesive bonded joints now ranges from 6×10^3 to 269×10^3 cycles (see Table 3.15).

	Joint	**Specimen 1**	**Specimen 2**	**Specimen 3**	**Av. Life**	**Std. deviation**
AA-AA	Riveted	50725	52843	--	51784	1059
	Adhesive Bonded	85510	73092	--	79301	6209
	Hybrid	--	231800	223000	227400	4400
AA-CFRE	Riveted	56988	57280	--	57134	146
	Adhesive Bonded	69904	65074	--	67489	2415
	Hybrid	442732	441000	442958	445530	875
CFRE-CFRE	Riveted	57614	52252	51691	53852	2670
	Adhesive Bonded	266785	--	272200	269493	2708
	Hybrid	600000*	600000*	600000*	600000*	--
CFRE-AA	Riveted	59915	--	52725	56320	3595
	Adhesive Bonded	5814	6810	4314	5646	1026
	Hybrid	94134	--	132517	113326	19192

Table 3.15: *Fatigue life, average life and standard deviation of specimens after disregarding most deviated result.*

Among all hybrid joints, the composite-composite configuration shows the highest fatigue life: specimens have not failed even after 6×10^5 cycles. These joints exhibit fatigue life ten times that of simple composite-composite riveted joints, and more than two times that of composite-composite adhesive bonded joints. Composite substrate with aluminium doublers shows the lowest fatigue life among the studied hybrid joint configurations, with an average fatigue life of 105×10^3 cycles for three specimens and 113×10^3 cycles for two specimens. The higher fatigue life of hybrid joints is explained by the load sharing between rivets and adhesive layer, which appears to be better compared to either just rivets or adhesive layer alone.

Joint configuration		AA–AA			AA–CFRE		
		Riveted	Adhesive Bonded	Hybrid	Riveted	Adhesive Bonded	Hybrid
AA–AA	Riveted	X	153%	439%	110%	130%	860%
	Adhesive Bonded	65%	X	286%	72%	85%	561%
	Hybrid	23%	35%	X	25%	30%	196%
AA–CFRE	Riveted	91%	139%	398%	X	118%	780%
	Adhesive Bonded	77%	118%	337%	85%	X	660%
	Hybrid	12%	18%	51%	13%	15%	X

Table 3.16: *Comparison table of average fatigue life of AA 2024-T3–AA 2024-T3 and AA 2024-T3–CFRE joints of riveted, adhesive bonded, and hybrid joints.*

Table 3.16 shows a comparison of average fatigue lives of metal-metal and metal-composite joints. One can observe that, for metal-metal joints, hybrid joints have better average fatigue life than the riveted joints by 439% and adhesive bonded joints by 286%. Metal-metal hybrid have better performance not just in static conditions but also in fatigue conditions. Next to hybrid joints, adhesive bonded joints have average fatigue life higher by 153% that of riveted joints.

On the other side, the average fatigue life of metal-composite hybrid joints is higher than that of riveted joints by 780% and higher than that of adhesive bonded joints by 660%. The higher fatigue lives of hybrid joints shows the strength of adhesive bond and rivets is superior to just adhesive bond or rivets. Secondly, adhesive bonded joints have an average fatigue life, which is 118% higher than riveted joints.

Among metal substrate joints, metal-composite hybrid joints have highest average fatigue life, which is 196% higher than that of metal-metal hybrid joints. This suggests composite doublers have better performance than metal doublers under hybrid joining. Secondly, metal-metal adhesive bonded joints have 118% better average fatigue life than that of metal-composite adhesive bonded joints. The higher average fatigue lives of adhesive bonded joints is due to uniform load distribution over the wide area of adhesive. Though the shear strength of the adhesive is lower than that of the rivets, in adhesive bonded joints the load is distributed in a wide bond area, instead of being concentrates in the rivets, which explains fatigue life of adhesive bonded

joints is higher. When hybrid joints are compared with adhesive bonded joints, results proved that hybrid joints have higher fatigue lives. Finally, riveted joints have lowest fatigue lives.

Joint configuration		**CFRE–CFRE**			**CFRE–AA**		
		Riveted	Adhesive Bonded	Hybrid	Riveted	Adhesive Bonded	Hybrid
CFRE–CFRE	Riveted	X	500%	1114%	105%	10%	210%
	Adhesive Bonded	20%	X	223%	21%	2%	42%
	Hybrid	9%	45%	X	9%	0.009%	189%
CFRE–AA	Riveted	96%	479%	1065%	X	10%	201%
	Adhesive Bonded	954%	4773%	10627%	998%	X	2007%
	Hybrid	47%	238%	529%	50%	5%	X

Table 3.17: *Comparison table of average fatigue life of CFRE–CFRE and CFRE-AA 2024 joints of riveted, adhesive bonded, and hybrid joints.*

Table 3.17 shows a comparison of average fatigue lives of composite-composite and composite-metal joints. Highest average fatigue life is observed for composite-composite hybrid joints that is 1114% higher than riveted joints and 223% higher than adhesive bonded joints. Secondly, composite-composite adhesive bonded joints have average fatigue lives higher by 500% than that of riveted joints. From the results, it is said that the role of adhesive bond in the joints have significant improvement of fatigue lives.

Among composite-metal joints, hybrid joints have an average fatigue lives higher than that of riveted joints by 201% and 2007% higher than that of adhesive bonded joints. Secondly, riveted joints have an average fatigue lives higher by 998% than that of adhesive bonded joints. Only in the case of composite-metal adhesive bonded joints, lowest life is observed.

For all composite substrate joints, composite-composite hybrid joints are the best, as the joints have not failed even after 600×10^3 cycles. Secondly, composite-composite adhesive bonded joints have better performance than composite-composite riveted joints and composite-metal riveted and adhesive bonded joints.

Finally, for metal or composite substrates, hybrid joints have better fatigue lives than their riveted and adhesive bonded configurations. For repairs of metal substrates with composite doublers, hybrid joints are the most performing in terms of highest fatigue life. On the other hand, for repairs of composite substrates with composite doublers, as well, hybrid joints have higher fatigue life compared to riveted and adhesive bonded joints. From this analysis, it can be concluded that metal substrates perform well with both metal and composite doublers, whereas composite substrates perform well with composite doublers.

Chapter 4: Results and Discussion-Numerical Analysis

In this chapter, we discuss the numerical results obtained from FEA (ABAQUS CAE), Fracture Analysis Corp. 2D (FRANC2D/L), FRANC3D, and Autodesk Helius Composites tool. FEA consists of two different analyses: static and fatigue loading.

4.1 AA 2024-T3 substrates

In this section, we present FEA results on static and fatigue loading for AA 2024-T3 substrates.

4.1.1 Static analysis

Riveted, adhesive bonded, and hybrid joints are modelled and analysed in ABAQUS tool. The methodology used for modelling the joints was explained in Chapter 2. In the FEA, the numerical models are tested with the same loading conditions as in the experiments. One end of each joint is set as symmetry boundary condition and displacement is applied in the other end. The load-displacement curves obtained from the experiments and FEA for the studied metal-metal and metal-composite joints are shown in Fig. 4.1, 4.2, and 4.3.

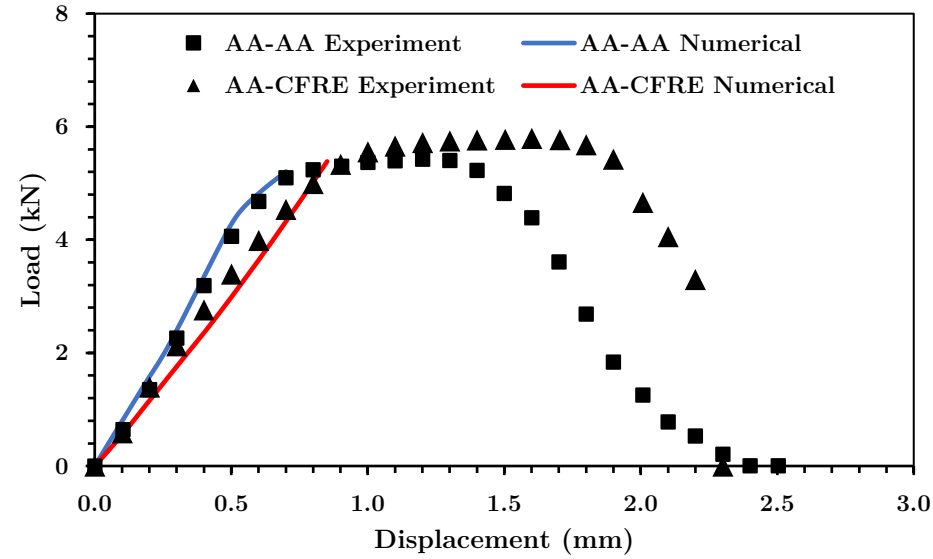

Figure 4.1: *Experiment and FEA load-displacement curves for riveted joints of metal-metal and metal-composite.*

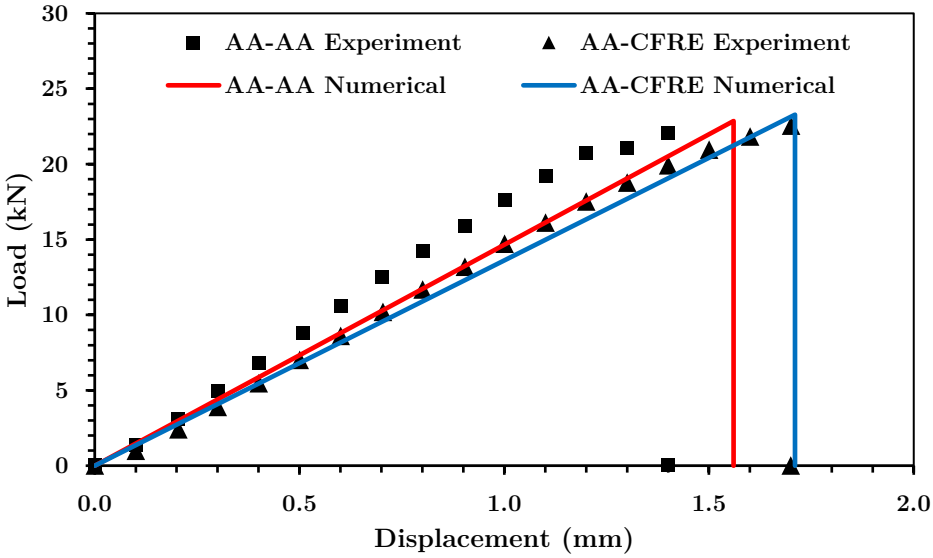

Figure 4.2: *Experiment and FEA load-displacement curves for adhesive bonded joints of metal-metal and metal-composite.*

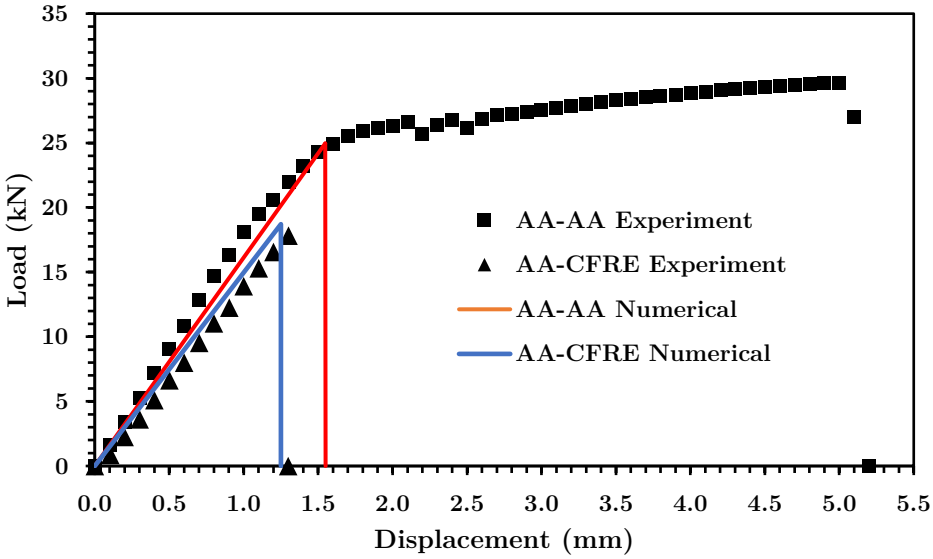

Figure 4.3: *Experiment and FEA load-displacement curves for hybrid joints of metal-metal and metal-composite.*

Rivets in the riveted and hybrid joints are modelled as point-based fasteners with radius of influence of 4.75 mm. Compression and plasticity effects are not modelled as part of point-based fasteners and because of this, numerical curves for riveted and hybrid joints in Fig. 4.1 and Fig. 4.2 are linear and are shorter than experimental curves. This approach is close to the common practice in the aviation industry, as there are numerous fasteners in airframe structures, and point-based fasteners provide a quick and reliable approach to modelling these large numbers of rivets in these structures.

Small differences are observed between numerical and experimental results in the previous figures. Particularly, Table 4.1 compares the numerical and experimental results. As mentioned before, plasticity of rivets is not considered in riveted and hybrid joints; hence, the maximum elastic strength values are reported for comparison in Table 4.1. Namely, the error between FEA and experimental results for riveted, adhesive bonded, and hybrid joints of metal-metal configuration is 2.1%, 3.5%, and 2.8%, respectively. Similarly, for riveted, adhesive bonded, and hybrid joints of metal-composite configuration, the error between FEA and experimental results is 1.5%, 3.2% and 4.9%, respectively. This is because numerical models are ideal models whereas in reality lower performance and properties are usual due to

imperfections in the manufacturing or riveting process of the materials. The strength values obtained from numerical analysis are higher than those from experiments by small fraction and this is because numerical models are ideal models, whereas in reality lower performance and properties are usual due to defects in the materials, as well as imperfections in the manufacturing or riveting process.

Joint Configuration		Numerical Strength (kN)	Experimental Average Strength (kN)	% difference
AA 2024-T3–AA 2024-T3	Riveted Joint	5.21	5.10	2.1%
	Adhesive Bonded Joint	22.86	22.08	3.53%
	Hybrid Joint	24.96	24.27	2.84%
AA 2024-T3–CFRE	Riveted Joint	5.39	5.31	1.5%
	Adhesive Bonded Joint	23.28	22.55	3.23%
	Hybrid Joint	18.71	17.84	4.88%

Table 4.1: *Comparison of numerical and experimental results for strength of the studied joints, and percentage difference between these results.*

Detailed stress analysis

A detailed stress analysis on metal-metal and metal-composite configurations of riveted, adhesive bonded, and hybrid joints is performed with FEA tool ABAQUS. A safety factor of 1.5 is applied for airframe structures to ensure safety operation conditions. In this investigation, the performance of metal-metal and metal-composite configurations of riveted, adhesive bonded, and hybrid configurations are compared at the design load of metal-metal riveted joints. All the models in this analysis use the same methodology as described in Chapter 2. All joints have symmetry boundary condition on one end and 3.6 kN load on the other end. Stresses on substrate and doublers are computed at locations shown on Fig. 4.4. Locations on the substrate and doublers are mid-points in between the rivet rows.

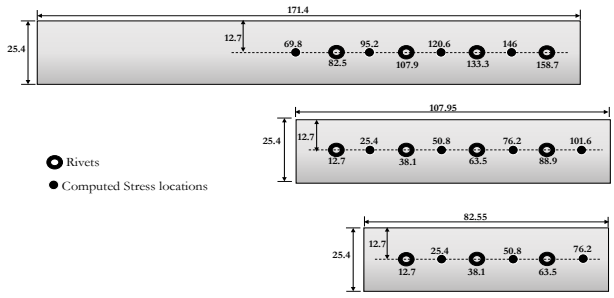

Figure 4.4: *Locations at which Von-Misses stresses are computed on (a) substrate, (b) doubler 1 and (c) doubler 2 (all units are in mm) [70].*

Riveted and hybrid models of metal-metal and metal-composite consist of holes on substrate and doublers as shown in Fig. 4.5. The presence of holes on substrate and doublers allowed visualising stress concentrations around rivet holes and in between the rivet rows. Rivets in this analysis are modelled using multiple point constraints (MPC's) discussed in [70]. MPC's are connected to a reference point using wire feature with bushing elements with stiffness in six directions. Stiffness of bushing elements are calculated using Eq. (2-1) to (2-5). Adhesive bonded and hybrid models use Cohesive Zone Modelling (CZM) and no holes are present in adhesive bonded models.

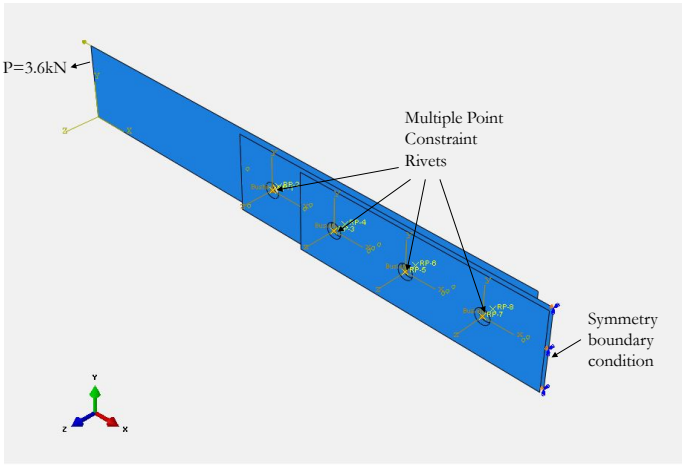

Figure 4.5: *FEA model of riveted joint for detailed stress analysis [70].*

Von-misses stresses on substrate for metal-metal and metal-composite are shown in Fig. 4.6 and 4.7.

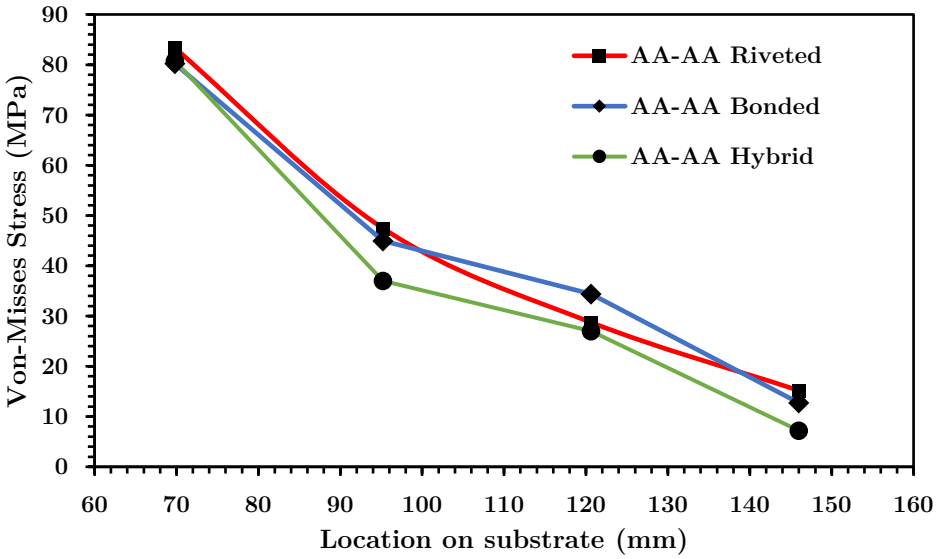

Figure 4.6: *Von-Misses stresses on substrate for metal-metal joint configurations.*

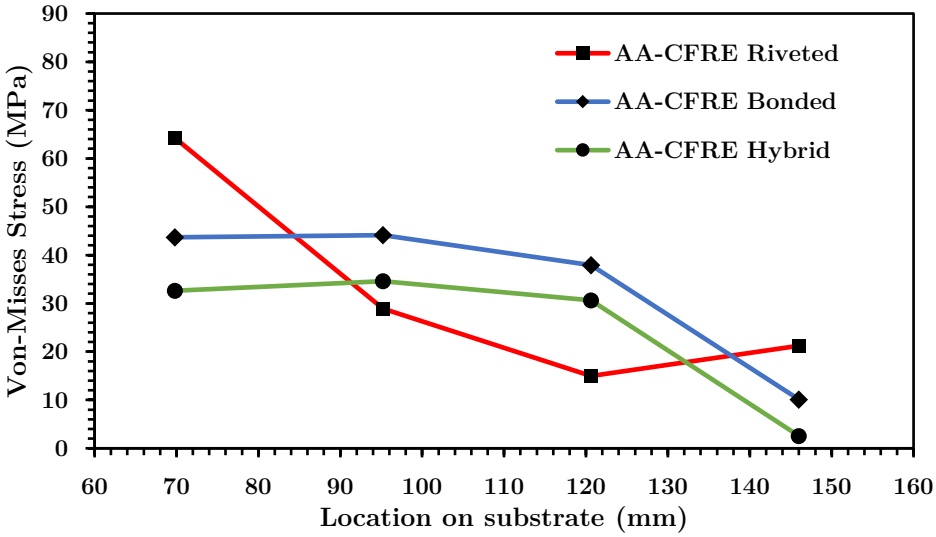

Figure 4.7: *Von-Misses stresses on substrate for metal-composite joint configurations.*

Metal-metal joints of riveted, adhesive bonded, and hybrid have nearly same magnitude of stress (80 MPa) at 69.8 mm. From 69.8 mm to 146 mm, reduction in Von-Misses stress is observed on substrate for all configurations as shown in Fig. 4.6 and 4.7. Reduction of stresses on substrates implies the

load transfer to doublers wither through rivets, adhesive bond or both rivets and adhesive bond. Hybrid joint have lowest Von-Misses stress at 146 mm, which is 57% of adhesive bonded joint and 47% of riveted joint. No much significant change in Von-Misses stress is observed for adhesive bonded and hybrid configurations at any of the four locations on substrate.

In case of metal-composite joints, a different stress patterns are observed on substrates. Von-Misses stress at 69.8 mm is lowest for riveted, adhesive bonded, and hybrid metal-composite joints compared to metal-metal joints of riveted, adhesive bonded, and hybrid (See Fig. 4.7). This effect may be due to high stiffness of composite doublers compared to metal doublers. Among riveted, adhesive bonded, and hybrid configurations of metal-composite joints, riveted joints have highest Von-Misses stresses, which is 1.5 times of adhesive bonded joint and 2 times of hybrid joint. From 69.8 mm to 120.6 mm, riveted metal-composite joint shows reduction in Von-Misses stress and a sudden spike is observed at 146 mm, which is close to crack edge. Least magnitude of Von-Misses stress is observed for hybrid joint at 146 mm. From, the substrate point of view, hybrid joints have low Von-Misses stress concentrations for same boundary conditions.

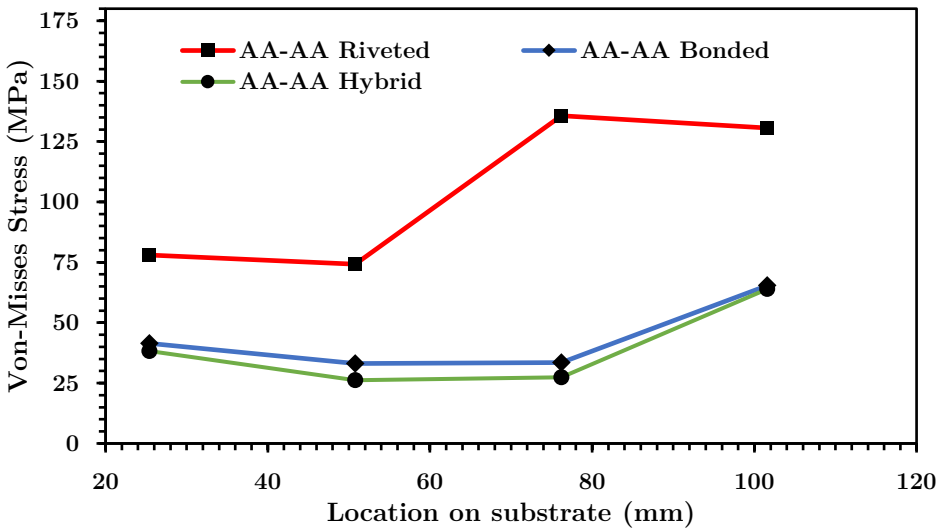

Figure 4.8: *Von-Misses stresses on doubler 1 for metal-metal joint configurations.*

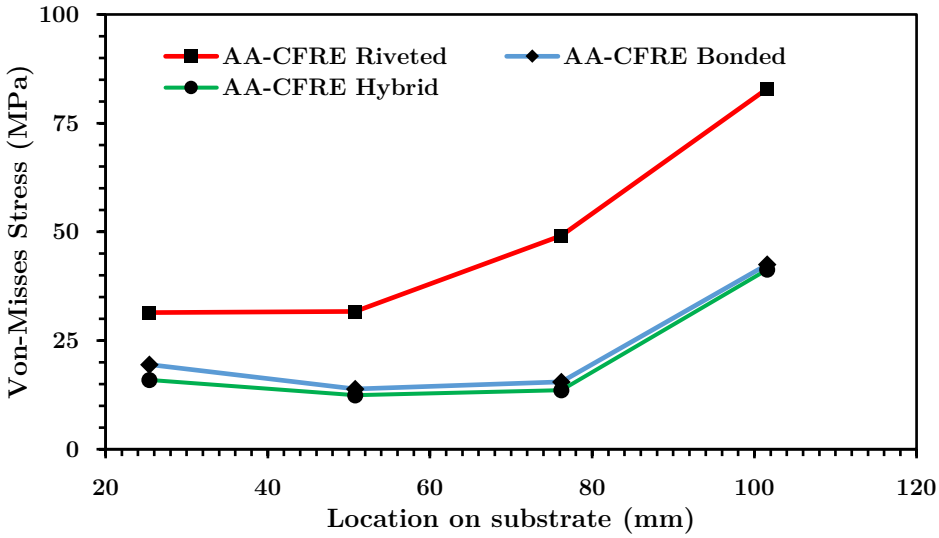

Figure 4.9: *Von-Misses stresses on doubler 1 for metal-composite joint configurations.*

Von-Misses stresses on doubler 1 is shown in Fig. 4.8 and 4.9, for metal-metal and metal-composite joints. Locations at which Von-Misses stresses are computed are 25.4, 50.8, 76.2 and 101.6 mm. Highest magnitude of Von-Misses stresses on doubler 1 is noticed for riveted joint at 76.2 mm, which is 1.7 times of magnitude at 25.4 mm. Nearly similar magnitudes of Von-Misses stresses are noticed for adhesive bonded and hybrid joints.

Metal-composite joints have relatively lower Von-Misses stresses on doubler 1 compared to metal-metal joints (shown in Fig. 4.9). Among metal-metal and metal-composite joints, results suggest metal substrate with composite doublers are better and have smooth load transfer. Magnitude of Von-Misses stresses on composite doubler 1 is nearly half of metal doubler.

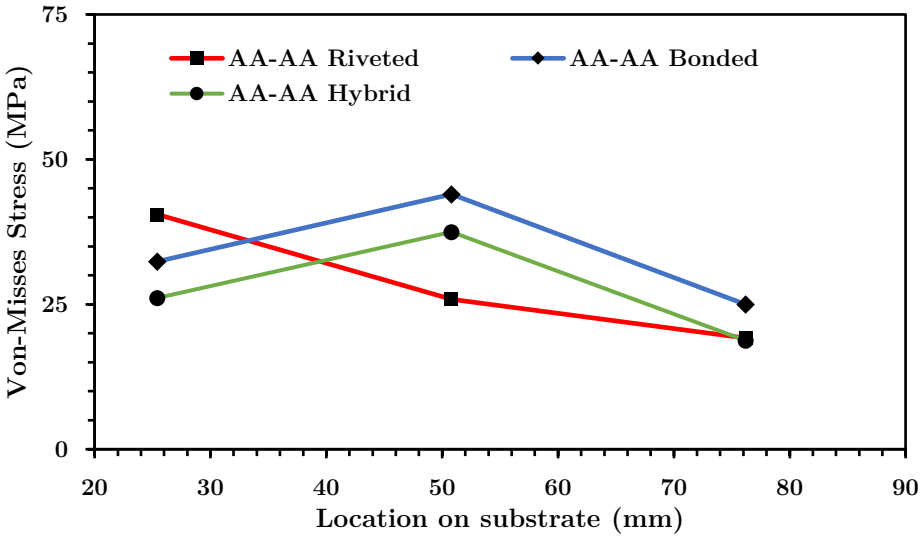

Figure 4.10: *Von-Misses stresses on doubler 2 for metal-metal joint configurations.*

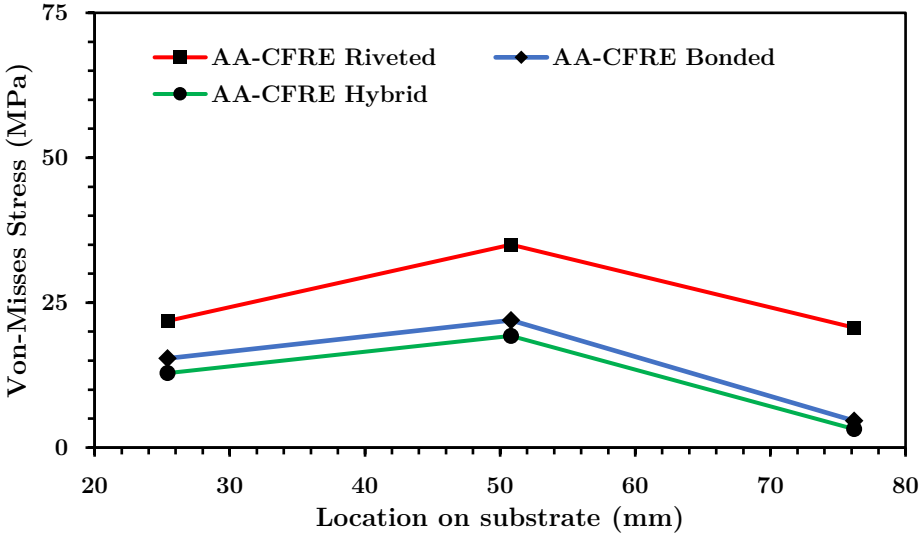

Figure 4.11: *Von-Misses stresses on doubler 1 for metal-composite joint configurations.*

Von-Misses stresses is computed at 25.4, 50.8 and 76.2 mm for metal and composite doubler 2 (See Fig. 4.10 and 4.11). At 25.4 mm, doubler 2 of metal and composite have highest stresses for riveted joint. From 50.8 mm to 76.2 mm, an increase in magnitudes of Von-Misses stresses are observed for all joint configurations of metal-metal and metal-composite. On comparison of performance of metal doublers to composite doublers for repairs of metal substrate, composite doublers performance is better. The better performance

is due to high stiffness of composite doublers and are able to transfer loads between substrate and doublers effectively.

Numerical analysis of reinforced cracked substrates

In this section, repairs/reinforcements performed on cracked structures are analysed numerically. When a crack in a structure reaches a critical limit, the flawed structure has to be repaired. According to aviation maintenance rules, when a crack reaches a size of 12.7 mm, repairs should be conducted [15]. In this analysis, cracked metal substrates with pre-induced crack lengths of 1, 5 and 10 mm (shorter than the critical length), and reinforced with metal doublers under riveted and adhesive bonded joint, are studied. The cracked substrates and reinforcement doublers have the same dimensions as those of the samples used in the previous experiments. Contour-integral cracks of 1, 5 and 10 mm are inserted in the substrate (see Fig. 4.12), and SIF are computed with ABAQUS. The load conditions and boundary conditions are the same for all configurations: one end of the joint is fixed and a load of 3.6 kN is applied at the other end. This load corresponds to the limit load of the riveted joints with eight rivets, as obtained from the experiments. SIF solution obtained from FEA tool ABAQUS is shown in Table 4.2.

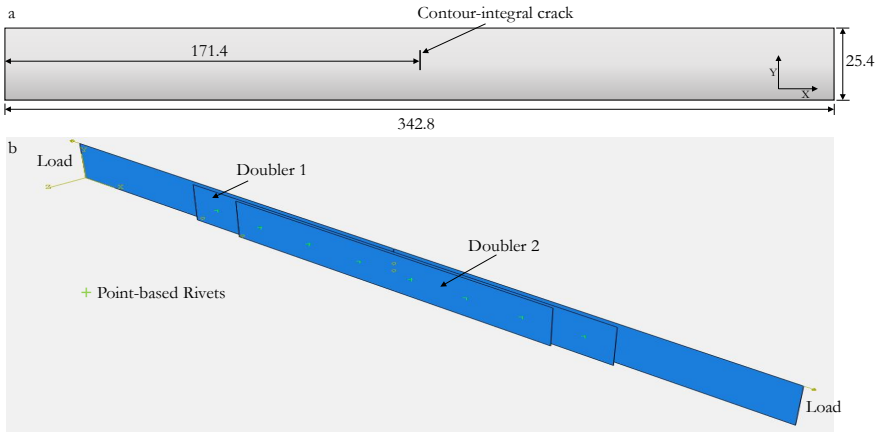

Figure 4.12: *(a) Cracked substrate with location of crack (in mm), (b) FEA model of reinforced riveted model [75].*

Joint Configuration	SIFs for AA 2024-T3–AA 2024-T3 (MPa · m$^{0.5}$)			SIFs for AA 2024-T3–CFRE (MPa · m$^{0.5}$)		
	Crack length			Crack length		
	1 mm	5 mm	10 mm	1 mm	5 mm	10 mm
Unreinforced	1.76	4.02	6.16	1.76	4.02	6.16
Riveted reinforcement	1.55	3.51	5.33	1.57	3.55	5.42
Adhesive Bonded reinforcement	1.52	2.96	3.95	1.55	3.12	4.04

Table 4.2: *SIF computed with ABAQUS for unreinforced, riveted reinforced and adhesive bonded reinforced joints.*

Joint Configuration	AA 2024-T3–AA 2024-T3			AA 2024-T3–CFRE		
	Crack length			Crack length		
	1 mm	5 mm	10 mm	1 mm	5 mm	10 mm
Riveted vs Unreinforced	-11.93%	-12.69%	-13.47%	-10.8%	-11.69%	-12.01%
Adhesive bonded vs Unreinforced	-13.64%	-26.37%	-35.88%	-11.93%	-22.39%	-34.42%
Adhesive Bonded vs Riveted	-1.94%	-15.67%	-25.89%	-1.27%	-12.11%	-25.46%

Table 4.3: *SIF comparison for riveted vs unreinforced, adhesive bonded vs unreinforced and adhesive bonded vs riveted reinforced.*

Joint Configuration	Crack Length		
	1 mm	5 mm	10 mm
Riveted	1.29%	1.14%	1.69%
Adhesive bonded	1.97%	5.41%	2.28%

Table 4.4: *SIF comparison for metal and composite doublers under riveted and adhesive bonded reinforcements.*

There are no significant differences in the SIF results for riveted reinforced and adhesive bonded reinforced joints for cracks of 1 mm length (see Table 4.3). Moreover, the SIF computed for each case with composite doubler is slightly higher than that of the corresponding case with metal doubler as shown in Table 4.4 (so, from this standpoint, metal doublers perform better). However, the SIF do not vary significantly with the doubler material: the largest difference in SIF computed for composite doubler compared to that of metal doubler is 5.4%. When comparing the SIF computed for adhesive bonded joints with those for riveted joints, the former perform better, with their SIF values being smaller than the SIF of the riveted joints.

4.1.2 Fatigue analysis

Fatigue analysis using numerical methods is quite complex compared to static analysis. In this thesis, numerical fatigue analysis in ABAQUS CAE is represented by strain energy release rate (SERR), which represents energy available for the crack growth and 'G' can be related to the crack growth parameter 'da/dN' [78]. Indeed, the FCG rate is proportional to the SERR. Using this information, adhesive bonded and hybrid joints are modelled by artificially placing cracks of various lengths along the bondline. Computing SERR for various crack lengths will determine the relative CGR. This will provide information on the effect of the fasteners on the fatigue performance of the hybrid joints.

Adhesive bonded and hybrid models are modelled using Virtual Crack Closure Technique (VCCT). VCCT uses Linear Elastic Fracture Mechanics (LEFM) principles, which assumes brittle crack propagation between pre-defined surfaces. VCCT is based on SERR, and assumes that strain energy released for crack extension is same as the energy required for crack closure. VCCT works only in ABAQUS/standard algorithm for 3-dimensional solid and shell elements. Cracks of VCCT are defined in the interaction module where adhesive bonded surfaces are defined. The definition of crack properties is based on adhesive properties. In this analysis, Araldite adhesive has a critical energy of 2 kJ/m^2 in mode I and 4 kJ/m^2 in modes II and III.

Predefined crack lengths of 15, 30, 45, 60, 75 and 90 mm are inserted in the adhesive interface. For specified crack lengths, energy released at the crack front is computed and compared for adhesive bonded and hybrid configurations. Adhesive bonded and hybrid joint models are the same as those discussed in Chapter 2. One-end of the joints is assigned symmetry boundary condition in x-axis, and a load of 4 kN is applied on the other-end (all the joints are loaded under same conditions). Table 4.5 shows the obtained SERR results for various crack lengths in mode I and mode II, for metal-metal adhesive bonded and hybrid joints. Particularly, the reported SERR values are the summation of mode I and mode II. The energy in mode III is much lower than in mode I and mode II. Hence, the energy values in mode III are neglected.

Crack length (mm)	Adhesive Bonded joint SERR (J/m²)	Hybrid joint SERR (J/m²)
15	1132	869
30	1257	456
45	1288	263
60	1321	184
75	1350	108
90	1363	120

Table 4.5: *Strain energy release rate (SERR) in mode I and mode II directions for metal-metal adhesive bonded and hybrid joints.*

For adhesive bonded joints, as the debonding crack length increases from 15 to 90 mm, the SERR as well increases. The highest SERR is observed for 90 mm crack length with 1363 J/m^2 and the lowest for 15 mm crack length with 1132 J/m^2. From 15 mm to 90 mm crack length, an increase of 11%, 2.55, 2.5%, 2.2% and 1% is observed for crack incremental of 15 mm. An increase of only 20% of SERR is observed between 15 mm to 90 mm crack length. Conversely, for hybrid joints, the SERR diminishes with increasing debonding crack length. For 15 mm debonding, SERR is 869 J/m^2 and subsequently magnitude of energy drops to 120 J/m^2 for 90 mm debonding. This reduction can be due to the effect of rivets as the load is shared between rivets and adhesive layer.

Similarly, SERR for metal-composite adhesive bonded and hybrid joints are shown in Table 4.6. Magnitude of SERR increases with increase in crack length for adhesive bonded joints. An increase of 293% of SERR is observed for metal-composite adhesive bonded joints. From 15 mm to 90 mm crack length, an increase of 38%, 15%, 19%, 24% and 25% is observed for crack incremental of 15 mm. Hybrid joint with 90 mm debonding of adhesive layer has released an energy of 243 J/m^2, whereas for adhesive bonded joint with same debonding crack length energy released is 2904 J/m^2. The reduction in SERR for hybrid joints with increase in crack length can be due to the presence of rivets, which helps in arresting the crack growth in adhesive layer and thereby improves fatigue life of the joints.

Crack length (mm)	Bonded joint SERR (J/m²)	Hybrid joint SERR (J/m²)
15	990	751
30	1370	188
45	1570	341
60	1872	284
75	2318	197
90	2904	243

Table 4.6: *Strain energy release (SERR) in mode I and mode II directions for metal-composite adhesive bonded and hybrid joints.*

On comparison between metal-metal and metal-composite adhesive bonded and hybrid configurations, hybrid configuration of metal-composite has lower SERR. Thus, hybrid configuration metal substrate with composite doublers have better fatigue performance compared to other configurations.

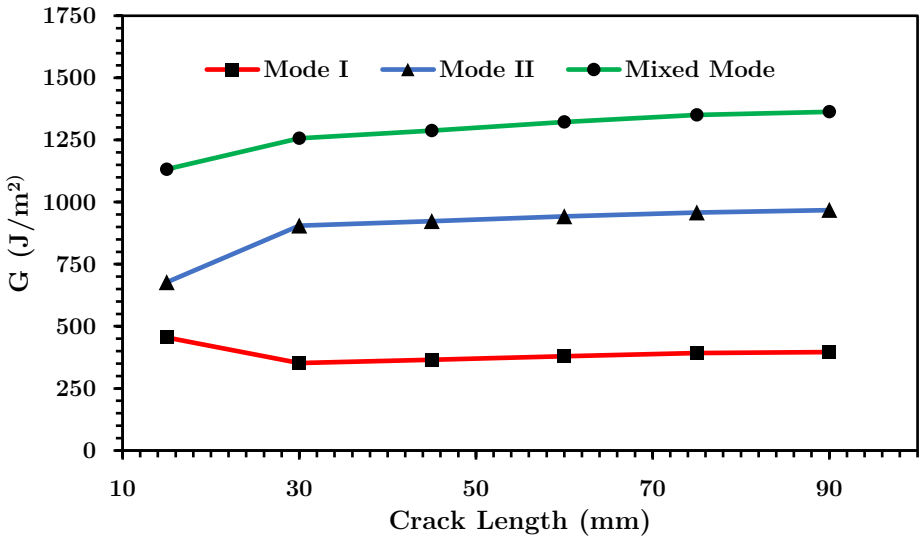

Figure 4.13: *SERR for metal-metal adhesive bonded joint in mode 1, mode 2 and mixed-mode.*

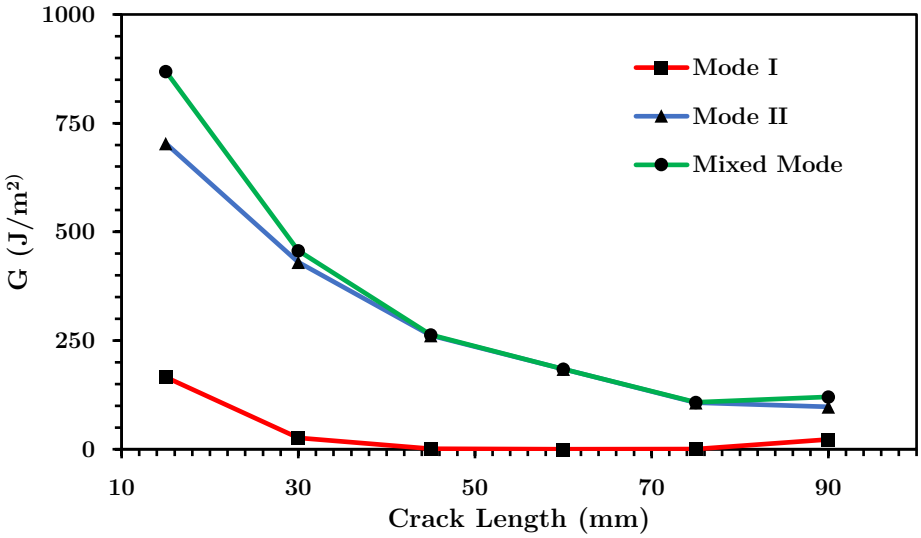

Figure 4.14: *SERR for metal-metal hybrid joint in mode 1, mode 2 and mixed-mode.*

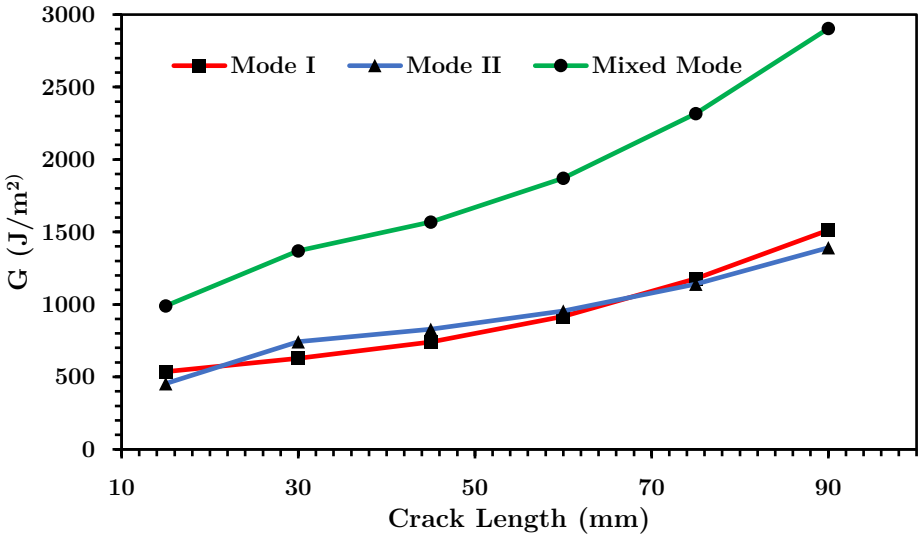

Figure 4.15: *SERR for metal-composite adhesive bonded joint in mode 1, mode 2 and mixed-mode.*

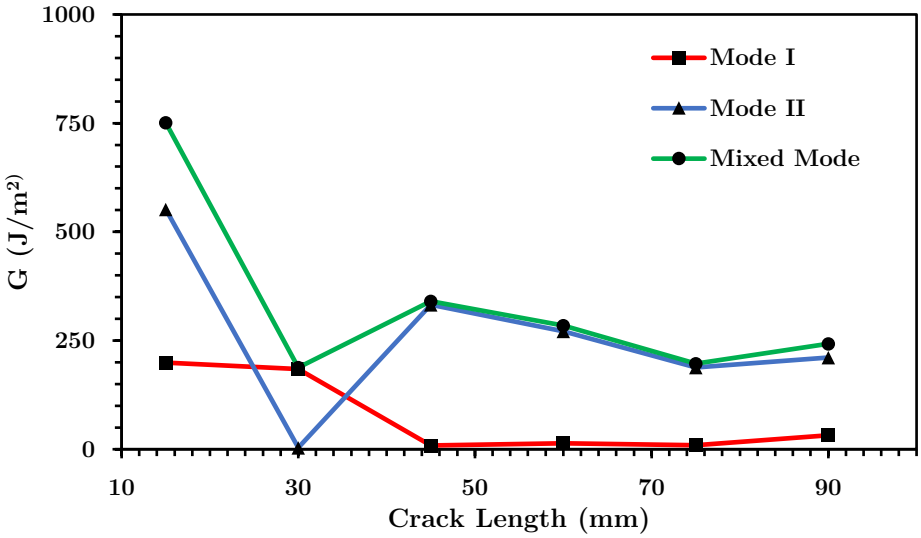

Figure 4.16: *SERR for metal-composite adhesive bonded joint in mode 1, mode 2 and mixed-mode.*

For metal-composite joints, the SERR for crack length of 15 mm are lower than for metal-metal joints, but SERR for crack length of 90 mm are higher for metal-composite joints compared with for metal-metal joints. This means that: 1) for metal-composite adhesive bonded joints, SERR increases much faster with crack length, compared with metal-metal adhesive bonded joints; 2) conversely, for metal-composite hybrid joints, SERR decreases much slower with crack length, compared with metal-metal hybrid joints. This can be due to the presence of rivets in the hybrid joints, which can arrest the crack growth in adhesive layer.

4.2 CFRE Substrates

In this section, the FEA results on joints with composite substrates are described. The models of riveted, adhesive bonded, and hybrid joints used in this FEA were discussed in Chapter 2. The only differences between the models are due to the materials: the composite materials of the substrate and doublers are modelled as composite laminas with layup directions.

4.2.1 Static analysis

Static analysis of the models is performed using same boundary conditions as experiments. Fig. 4.17 and 4.18 show load-displacement curves as obtained from experiments and FEA for composite-composite and composite-metal joints. Remarkably, the error between FEA and experimental results (measured peak load at failure displacement) is, in all cases, under 1.5%, and the lowest error (0.23%) is observed for riveted joints.

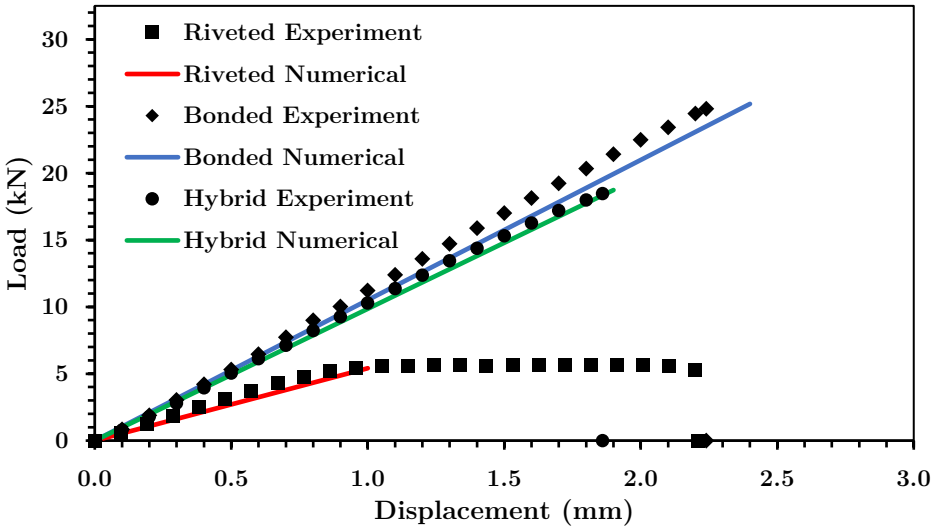

Figure 4.17: *Experimental and numerical load-displacement curves for composite-composite.*

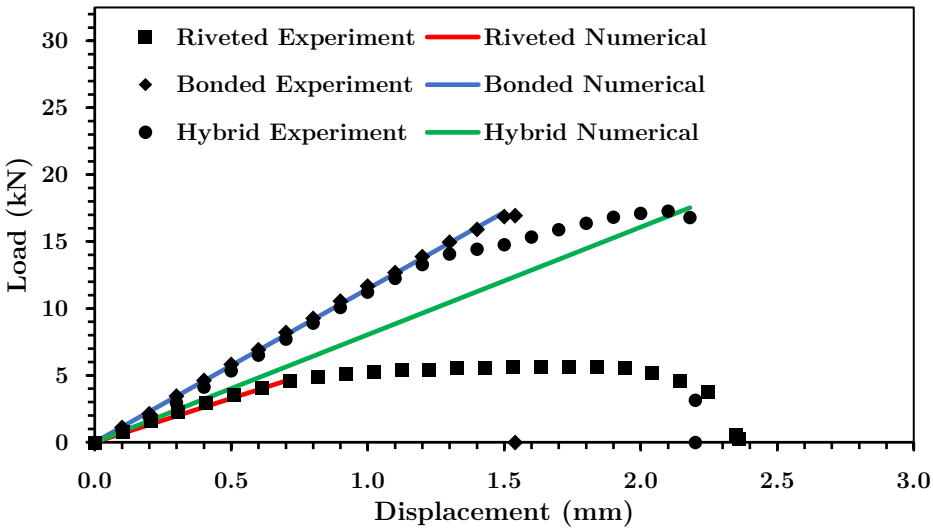

Figure 4.18: *Experimental and numerical load-displacement curves for composite-metal joints.*

In Fig. 4.18 note, the significant difference between the experimental results and the numerical results obtained from FEA for hybrid joints. The experimental curve shows significantly higher stiffness than the FEA curve. This may be due to the elastic model used for the point-based fasteners as well as the CZM for the adhesive layer. Table 4.7 shows a comparison of the ultimate loads for riveted, adhesive bonded, and hybrid joints with composite-composite and composite-metal configurations, as obtained from the FEA and experiments, and the error between experimental and numerical results.

Joint Configuration		**Numerical Strength (kN)**	**Experimental Average Strength (kN)**	**% difference**
CFRE-CFRE	Riveted Joint	5.2	5.10	0.2
	Adhesive Bonded Joint	25.2	24.8	1.3
	Hybrid Joint	18.7	18.5	1.4
CFRE-AA 2024-T3	Riveted Joint	4.9	4.6	0.9
	Adhesive Bonded Joint	17.2	17.0	1.5
	Hybrid Joint	17.5	17.3	1.4

Table 4.7: *Strength of the studied joints as obtained from numerical analysis and experiments, and error between numerical and experimental results.*

Stress analysis of riveted joints

As mentioned before, riveted joints are the most commonly used repair technology for airframe composite structures. Most of these structures are loaded in tensile direction. Hence, the tensile stress response of composite-composite and composite-metal riveted joints is studied with FEA. Particularly, in this analysis, a load of 4.2 kN is applied to the riveted joints. This load vale is chosen because it corresponds to the average elastic limit of composite substrate riveted joints. Results are shown in Fig. 4.19, 4.20 and 4.21 where the overlap distance is the distance with respect to the *yz* symmetry plane of the joint, and each stress peak corresponds to a rivet row. Note that each rivet row shows tensile as well as compressive stresses.

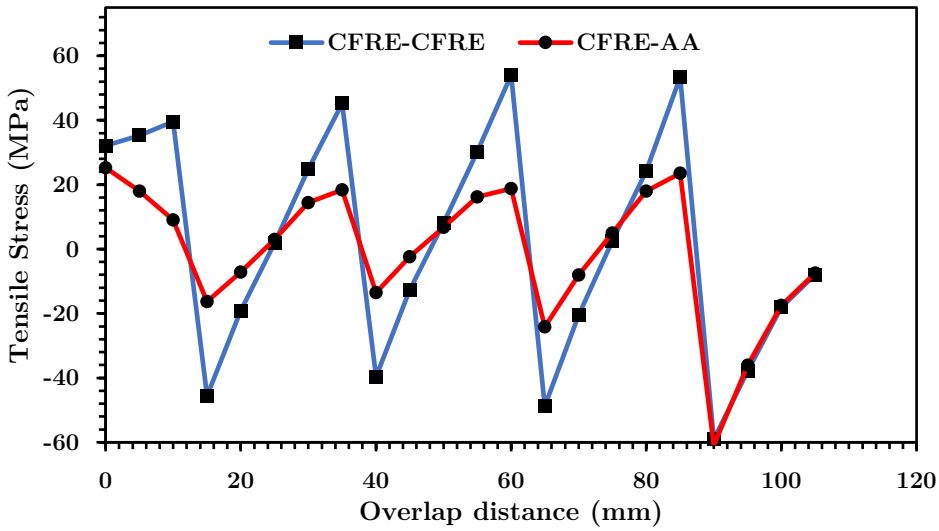

Figure 4.19: *Tensile stress vs overlap distance for substrate for composite-composite and composite-metal riveted joints, as obtained from FEA at a load of 4.2 kN.*

The tensile stresses in the composite substrate are significantly higher in absolute terms when using composite doublers compared to metal doublers. On the other side, the composite doublers have in most cases lower tensile stresses than the metal doublers. This is because composites are brittle and stiffer in nature compared to metals, which are ductile and with lower stiffness. For the substrate, the lowest stresses are observed at the first rivet row from the symmetry plane, while the following rivet rows have in general slightly increasing stresses up to fourth rivet row. After the fourth rivet row, the

stresses in the substrate for the composite-composite and composite-metal joint are identical. Composite substrate with composite doublers has higher tensile stresses (compressive in nature due to being negative) on substrate from first to third rivet row compared to metal doublers. At first rivet row composite substrate with composite doublers, have 280% of stresses compared to composite substrate with metal doublers and subsequently 290% and 200% for second and third rivet rows. At fourth rivet row, tensile stresses are nearly same (see Fig. 4.19).

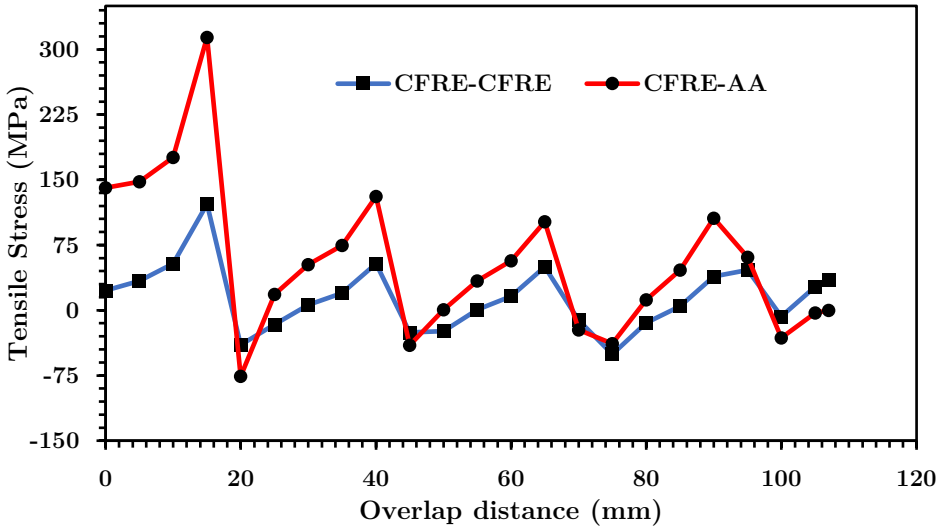

Figure 4.20: *Tensile stress vs overlap distance for doubler 1 for composite-composite and composite-metal riveted joints, as obtained from FEA at a load of 4.2 kN.*

For doubler 1 (see Fig. 4.20), high stresses are observed for the composite-metal joint. This may be due to using dissimilar materials and their different load transfer behaviour, since composites are usually more brittle and stiffer than metals, which are ductile. For both composite-composite and composite-metal riveted joints, the stresses drop from first to fourth rivet row. Particularly, tensile stresses are much higher at the first rivet row compared to the second rivet row (nearly three times higher). This suggests that the load shared by first rivet row is higher than the subsequent rivet rows. Composite substrate repairs with metal doublers have higher tensile stresses on metal doublers. At first rivet row, metal doublers have 257% higher stress magnitude compared to composite doublers. Subsequently a higher magnitude of 245%,

200% and 272% of tensile stresses are observed at second, third and fourth rivet row for metal doubler 1 compared to composite doubler 1.

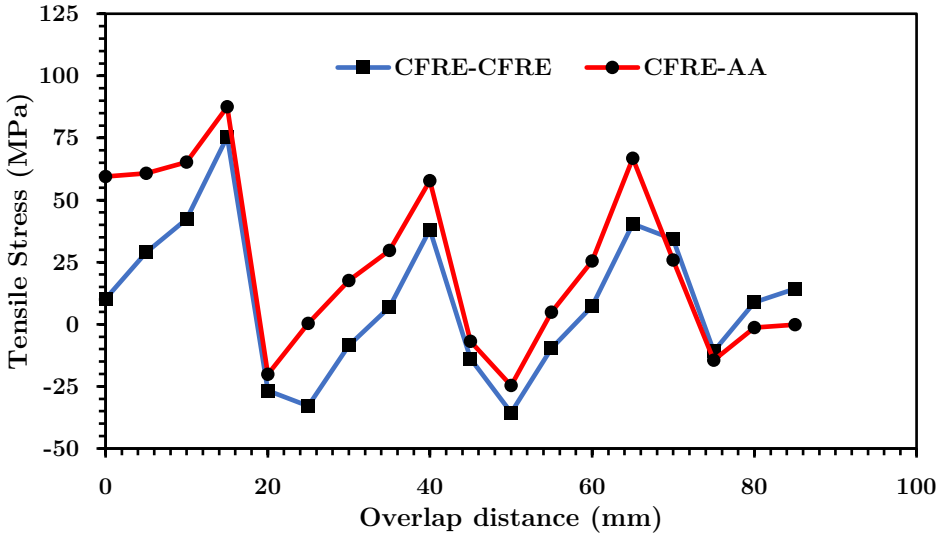

Figure 4.21: *Tensile stress vs overlap distance for doubler 2 for composite-composite and composite-metal riveted joints, as obtained from FEA at a load of 4.2 kN.*

For doubler 2 (see Fig. 4.21), the tensile stresses at the first rivet row are slightly higher compared to the second and third rivet rows, but anyway there is not much difference in the tensile stresses in any of the rivet rows and between composite-composite and composite-metal joints, for doubler 2. Similarly, there are no large deviations in the tensile stresses in the composite substrate at the second, third, and fourth rivet rows between the case with composite doublers and the case with metal doublers. However, the first rivet row has higher stresses by 116% for metal doublers compared to composite doublers. At second and third rivet row, tensile stresses are higher by 152% and 165% for metal doubler 2 compared to composite doubler 2.

Hence, from this analysis, two observations are made for composite-composite and composite-metal riveted joints. Low tensile stresses on substrate is observed for composite-metal riveted joint whereas low tensile stresses on both the doublers is observed for composite-composite riveted joint.

4.2.2 Fatigue analysis

Numerical fatigue analysis results for composite-composite and composite-metal joint configurations are obtained using VCCT technique. The methodology for obtaining fatigue models is the same as discussed in Section 4.1.2. The SERR results for composite-composite and composite-metal adhesive bonded and hybrid joints are reported in the Tables 4.8 and 4.9.

For composite-composite configurations, the energy released for adhesive bonded joints is significantly higher than that for hybrid joints. For an initial de bond crack 15 mm, adhesive bonded joint has available energy of 1930 J/m^2. For the same 15 mm crack length, hybrid joints have 1348 J/m^2, which is 29% lower than that for adhesive bonded joint. As the crack length increases for adhesive bonded joints, available energy 'G' increases with maximum at 90 mm crack. From crack lengths 15 mm to 90 mm, an increase of 18%, 10%, 13%, 18% and 21% is observed for crack incremental of 15 mm. Whereas for hybrid joints, energy released is not in relation with crack length and this is due to the presence of rivets. In case of hybrid joints, both adhesive and rivets share and transfer load.

Crack length (mm)	**Adhesive Bonded joint (J/m^2)**	**Hybrid joint (J/m^2)**
15	1930	1348
30	2284	761
45	2517	445
60	2835	395
75	3348	0.6
90	4056	311

Table 4.8: *Strain energy release in mode I and mode II directions for composite-composite adhesive bonded and hybrid joints.*

Figures 4.22 and 4.23 show energies released in mode I, mode II and mixed mode (mode I+ mode II) for adhesive bonded and hybrid joints.

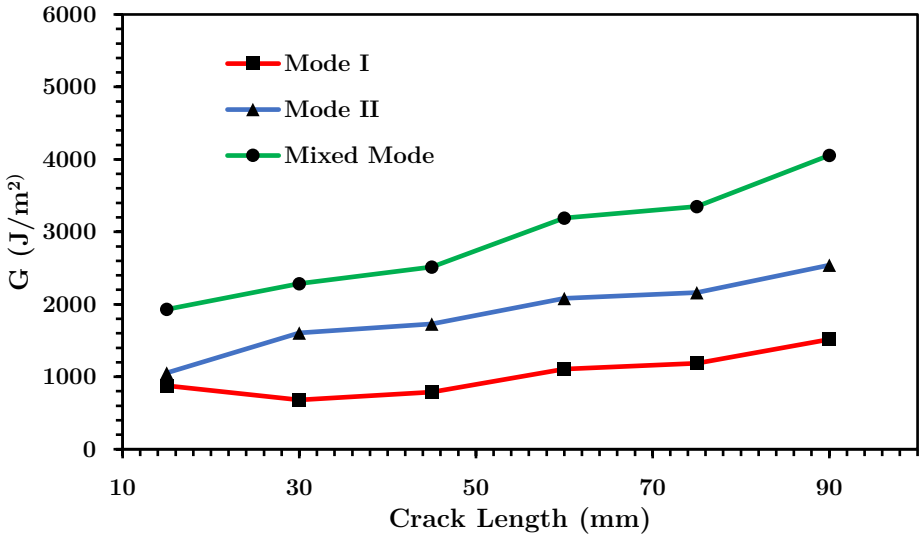

Figure 4.22: *SERR for composite-composite adhesive bonded joint in mode 1, mode 2 and mixed-mode.*

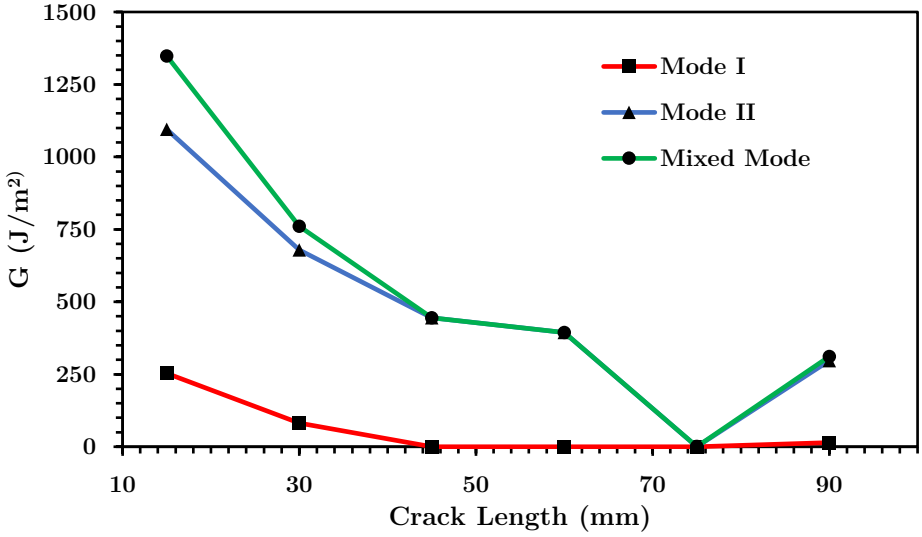

Figure 4.23: *SERR for composite-composite hybrid joint in mode 1, mode 2 and mixed-mode.*

SERR for composite-metal configurations are shown in Table 4.9. One can notice that adhesive bonded joints have much higher magnitude of 'G' compared to hybrid joints. As the crack length increases from 15 to 30 mm, there is an increase of SERR, and for cracks higher than 30 mm, SERR decreases. However, a huge difference is not observed for the SERR from 30 to 90 mm when compared to 15 mm crack length. Whereas hybrid joint have a

reduction in SERR from 15 mm to 60 mm. At 75 mm crack length, SERR is zero and increases by 157% for crack length 90 mm.

Crack length (mm)	Adhesive Bonded joint (J/m²)	Hybrid joint (J/m²)
15	2264	1501
30	2326	722
45	2312	416
60	2271	309
75	2181	0
90	2022	157

Table 4.9: *Strain energy release in mode I and mode II directions for composite-metal adhesive bonded and hybrid joints.*

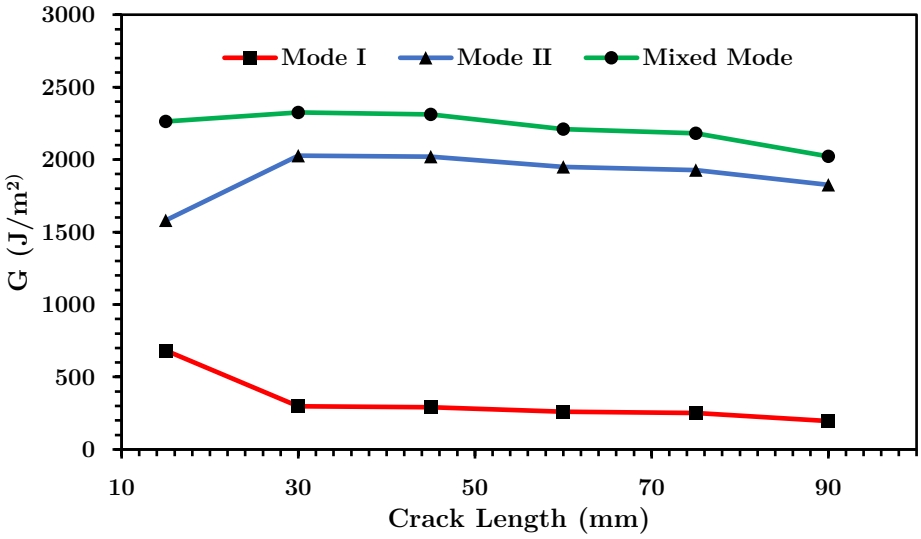

Figure 4.24: *SERR for composite-metal adhesive bonded joint in mode 1, mode 2 and mixed-mode.*

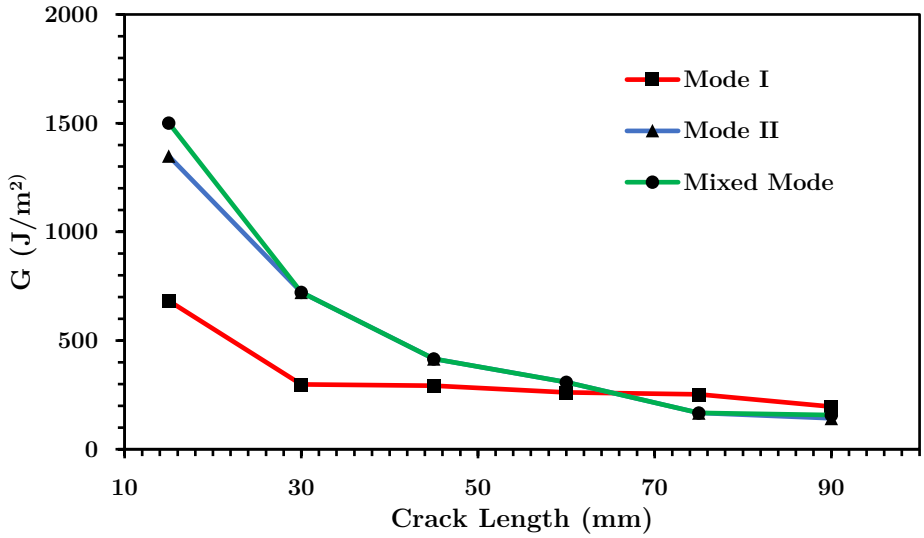

Figure 4.25: *SERR for composite-metal hybrid joint in mode 1, mode 2 and mixed-mode.*

4.3 Fatigue analysis in FRANC2D/L

Fatigue life analysis of un-repaired and repaired metallic substrates is performed with FRANC2D/L. The substrate and doublers in this analysis are made of AA 2024-T3. The dimensions of the joint are shown in Fig. 4.26. The procedure followed for modelling in FRANC2D was described in Chapter 2.

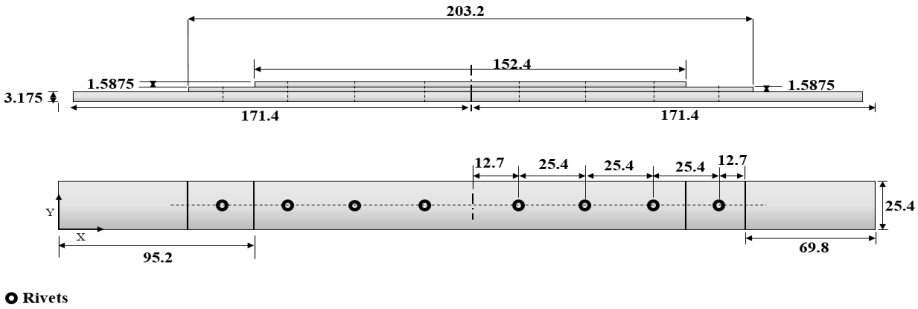

Figure 4.26: *Dimensions of metal-metal riveted joint (units are in mm) [76].*

In particular, SIF for un-repaired substrate and substrate repaired with riveted and adhesive bonded joints were computed in FRANC2D/L. Among the studied joints, the un-repaired substrate shows high values of Δk compared to repairs with riveted and adhesive bonded joints. Differences in SIFs (Δk)

are observed between cyclic stress of 60.7 MPa and 6.07 MPa. Fig. 4.27 shows the stress distribution in the substrate repaired with riveted joint at 60.7 MPa.

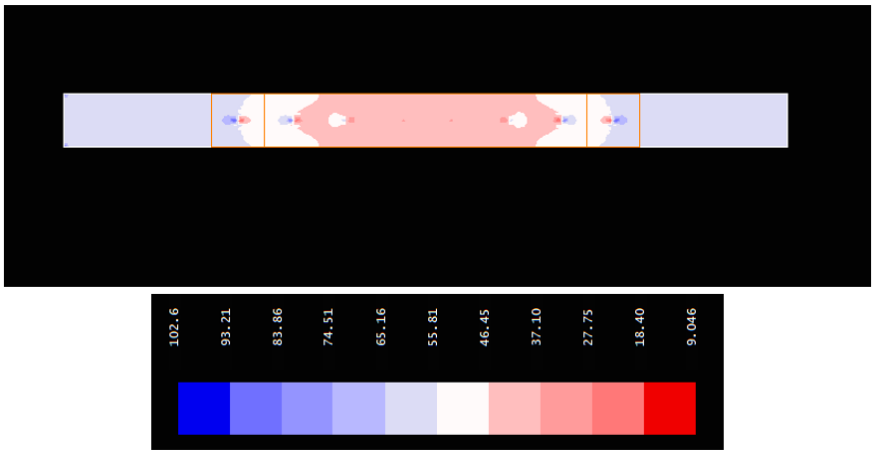

Figure 4.27: *Stress distribution on substrate of repaired-riveted joint at 60.7 MPa [76].*

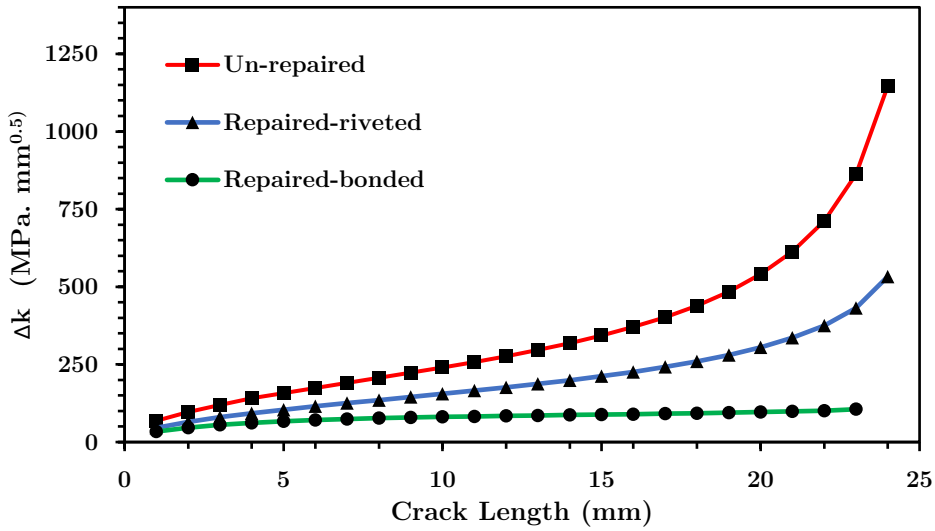

Figure 4.28: *Δk vs crack length (in mm) for un-repaired, repaired-riveted and repaired-adhesive bonded joints.*

The un-repaired metal substrate exhibits highest Δk (862.7 MPa.mm$^{0.5}$) for a crack length of 23 mm, whereas the substrate repaired with riveted (adhesive bonded) joint has 431.8 MPa.mm$^{0.5}$ (72 MPa.mm$^{0.5}$), as shown in Fig. 4.28. From the SIF, the fatigue life of the joints can be computed using the Paris law:

$$\frac{da}{dN} = C(\Delta k)^m \qquad 4\text{-}1$$

In the above equation, C and m for AA 2024 T3 at stress ratio 0.1 are 2.22×10^{-11} m/cycle and 3.545, respectively [75]. Substituting these values in the Paris equation gives the fatigue life of the joints, as shown in Fig. 4.29. Namely, for the applied stress levels for an initial crack length of 1 mm, the fatigue life of the substrate repaired with adhesive bonded joint is 3.5×10^6 cycles. For a crack length of 23 mm, the fatigue life of the substrate repaired with adhesive bonded joint is approximately 6×10^5 cycles. Whereas the un-repaired substrate fails after 365 loading cycles and the substrate repaired with riveted joint fails after 4255 cycles. Fatigue life for riveted joints is lower than adhesive bonded joints and it can be said that rivets cause higher SIF because the load transfer is concentrated in few rivets while the load transfer with adhesive is less concentrated as it is distributed in a much wider area.

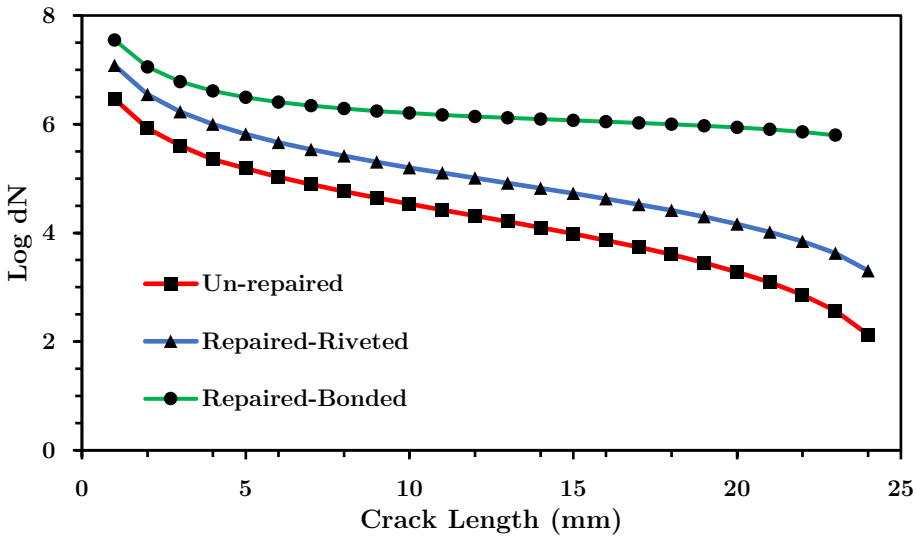

Figure 4.29: *Fatigue cycles in logarithmic scale vs crack length (in mm) for un-repaired, repaired-riveted and repaired-bonded joints.*

4.4 FRANC3D

FCG for riveted and adhesive bonded joints is compared using FRANC3D and FEA tool ABAQUS. Cracked AA 2024-T3 plate is analysed in FRANC3D for crack lengths of 1, 2, 5, 10 and 12.7 mm. Fatigue life of repaired riveted and repaired adhesive bonded is compared.

A simple 3D FEA model is created in ABAQUS with material properties and boundary conditions. The load is applied in the form of two different stresses on one end of the substrate plate: 93.6 MPa and 140 MPa. Once the material properties and boundary conditions are set, the model from ABAQUS is imported to FRANC3D. Later, cracks of different lengths are inserted in the model as shown in Fig. 4.30. FRANC3D has inbuilt meshing algorithm to mesh the crack fronts with an option to refine depending on complexity of the model, as shown in Fig. 4.31.

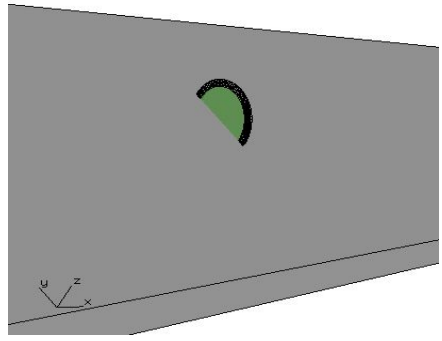

Figure 4.30: *Crack insertion in FRANC3D [75].*

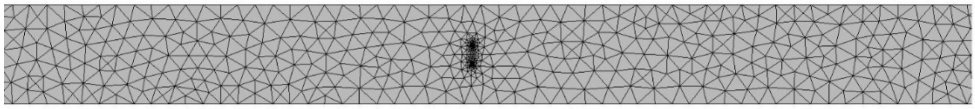

Figure 4.31: *Mesh generation in FRANC3D [75].*

Initial analysis comprises of static analysis to obtain SIF at the crack fronts. Cracks are grown under quasi-static power law criterion. Based on the given input conditions, fatigue life of the plate is computed in FRANC3D using NASGRO 3 equation [75]. Table 4.10 shows fatigue life computed for AA 2024-T3 substrate.

Crack length (mm)	Fatigue Life (N_f) for 93.6 MPa	Fatigue life (N_f) for 140 MPa
1	314362	48193
2	178451	30024
5	14447	3670
10	1206	616
12.7	576	126

Table 4.10: *Fatigue life of AA 2024-T3 substrate obtained from FRANC3D.*

SIF's for repaired-riveted and repaired-adhesive bonded are computed in ABAQUS CAE using contour integral cracks. Riveted and adhesive bonded models in FEA are explained in Chapter 2. Contour integral cracks are inserted in the substrate with seam length equal to crack length as shown in Fig. 4.32. SIFs for crack fronts from history outputs are requested at maximum energy release rate.

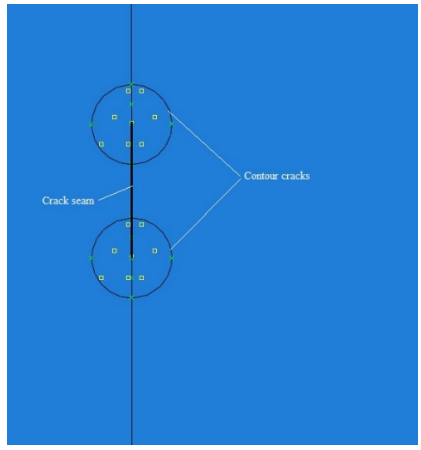

Figure 4.32: *Contour integral crack in FEA model.*

SIFs obtained for repaired-riveted and repaired-adhesive bonded 3D models is shown in Fig. 4.33 and 4.34. For crack sizes of 1 and 2 mm, SIF solution for repaired-riveted and repaired-adhesive bonded joints is nearly same. At 93.6 MPa, the repaired-riveted joint has SIF of 26 MPa.mm$^{0.5}$ and repaired-adhesive bonded joint has 17.6 MPa.mm$^{0.5}$.

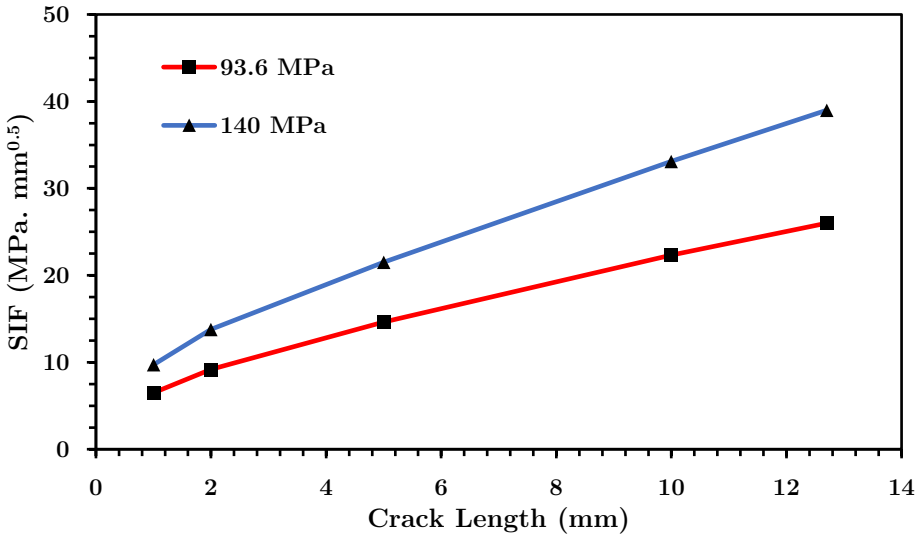

Figure 4.33: *SIF solution for AA 2024-T3- AA 2024-T3 repaired-riveted joint.*

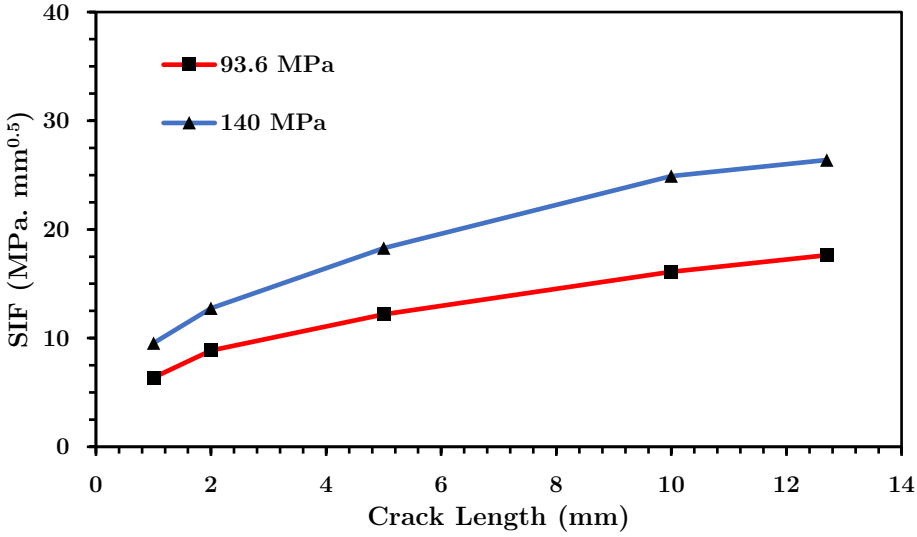

Figure 4.34: *SIF solution for AA 2024-T3- AA 2024-T3 repaired- adhesive bonded joint.*

4.5 Helius composites

A simple substrate model of CFRE is created in Helius Autodesk Composite tool. This tool is implemented to analyse ply stress/load distributions, first-ply failure with PFA, and failure envelopes in various longitudinal, transversal, and through-thickness directions. An applied load on

composite laminate will determine stress distributions in the plies and understanding local stress concentration in plies eliminates chances of failure. Once the ply stress distributions are computed, first-ply failure is performed to calculate the maximum stresses in longitudinal, transversal, and shear directions.

After first-ply failure analysis, failure propagation to other plies is analysed. Hence, PFA is performed to visualise ply failure occurrence and their mode of failure (fibre or matrix). Particularly, Christensen's failure criterion formulated in the Helius Autodesk Composites tool is implemented to predict the failure of the CFRE substrate.

In this analysis, the CFRE substrate consists of twelve plies with ply orientations as described in Chapter 2, and results are computed for various loads: 5, 10, 15, 20, and 30 kN. For these loads, the stress distributions obtained with Helius Autodesk Composites tool in the longitudinal and transverse directions for the composite substrate plies are shown in Fig. 4.35 and 4.36.

It can be noticed that longitudinal stresses are highest in 0/90 plies, that is, plies 2 to 5 and 8 to 11 have highest stresses in the loading direction. While low longitudinal stresses are observed in the outer plies (plies 1 and 12) and central plies (plies 6 and 7), as they are in 45/135 layup direction, not aligned with the loading direction. On the contrary, transverse stresses are highest in 45/135 plies; particularly, transverse stresses for plies 1, 6, 7, and 12 are positive, while for the remaining plies (with orientation 0/90) compression is observed.

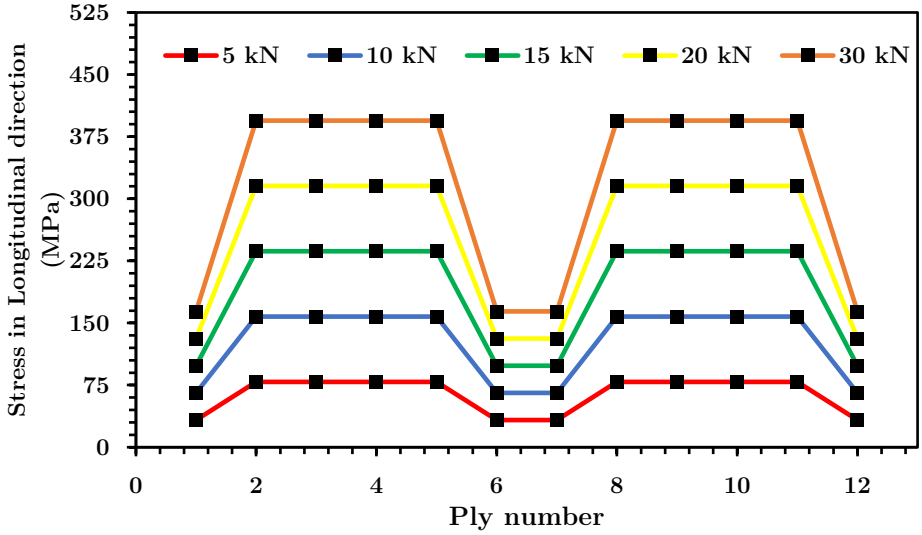

Figure 4.35: *Longitudinal stress distribution for plies of composite substrate.*

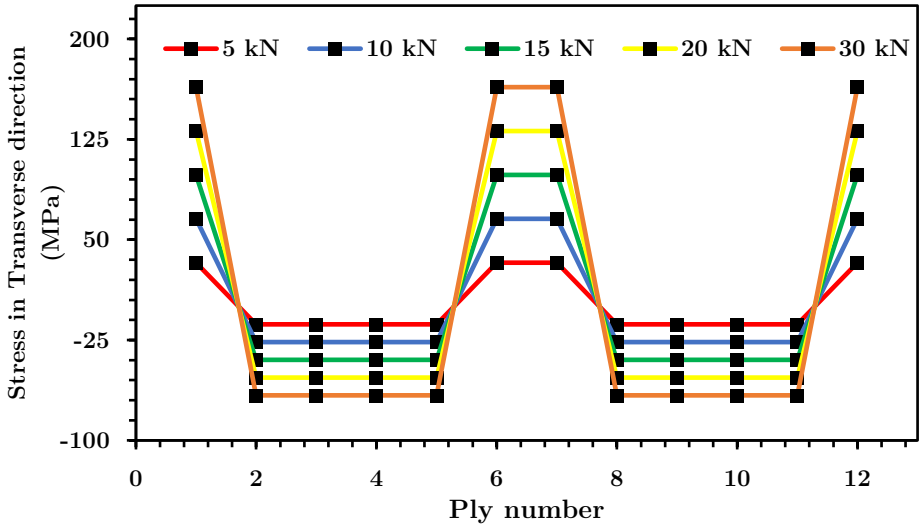

Figure 4.36: *Transverse stress distribution for plies of composite substrate.*

The stress distributions of the substrate plies provide information about ply load distribution but not about their failure mode. Hence, PFA is done with Helius Autodesk Composite tool to the understand failure mode of composite substrate. Fig. 4.37 shows the PFA results for the composite substrate. These results suggest that the first failure occurs at stress of 678 MPa and strain 0.011 in the plies 2 to 5 and 8 to 11 (i.e., plies with orientation 0/90). Once failure occurs in 0/90 plies, the load carrying capacity of the

substrate falls to 156 MPa. At this point and up to 226 MPa, only the plies with orientation 45/135 take the load. Final failure of the plies 1, 6, 7, and 12 (and thus complete failure of the substrate) occurs ultimately at stress of 226 MPa and strain 0.016. Failure of plies with orientation 0/90 is caused by fibre failure, while plies with orientation 45/135 failed due to matrix failure. Christensen's failure criterion was used in this PFA to find the failure mode of plies, as explained in Chapter 2.

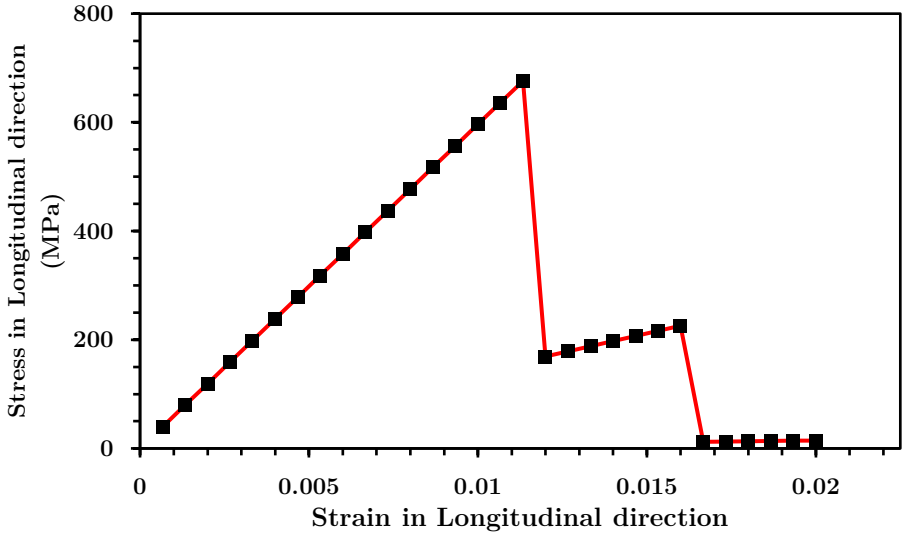

Figure 4.37: *Stress vs strain in longitudinal direction for composite substrate.*

Finally, the failure envelopes obtained with Helius Autodesk Composites tool for the composite substrate are presented in Fig. 4.38 and 4.39. These envelopes provide the operational limits of the composite substrate in longitudinal, transverse, and shear direction. The plots in Fig. 4.38 and 4.39 provide complete information on stresses for the composite substrate.

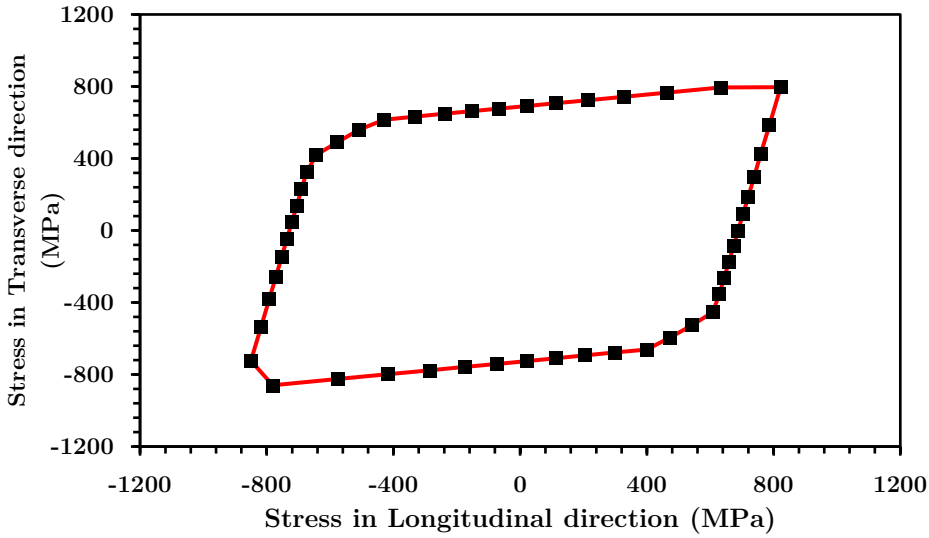

Figure 4.38: *Failure envelope in transverse vs longitudinal direction for composite substrate.*

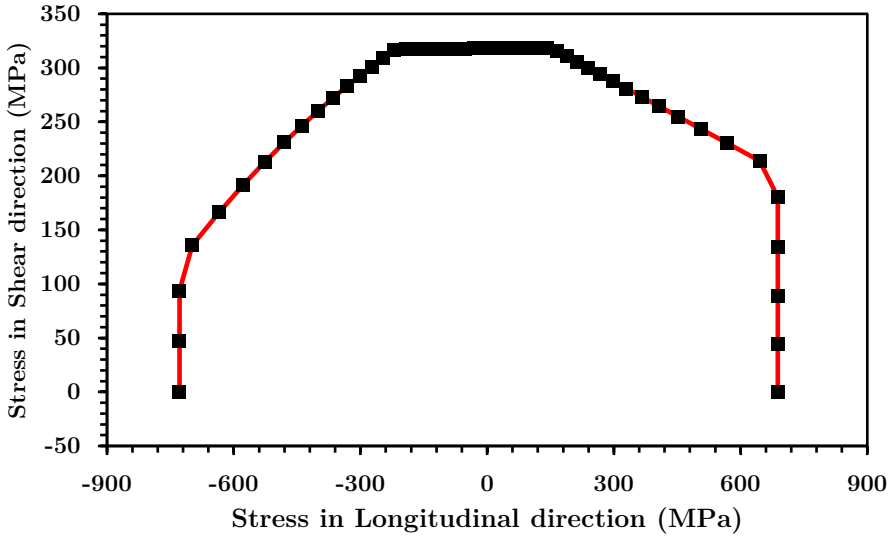

Figure 4.39: *Failure envelope in shear to longitudinal direction for composite substrate.*

4.6 Summary of static analysis in FEA

In this section, a summary of static analysis performed in finite element tool ABAQUS is discussed. Table 4.11 shows a comparison of peak strength of the metal-metal and metal-composite joints.

Joint configuration		**AA–AA**			**AA–CFRE**		
		Riveted	Adhesive Bonded	Hybrid	Riveted	Adhesive Bonded	Hybrid
AA 2024-T3–AA	Riveted	X	439%	479%	103%	447%	359%
	Adhesive Bonded	23%	X	109%	24%	102%	82%
	Hybrid	21%	92%	X	22%	93%	75%
AA–CFRE	Riveted	97%	424%	463%	X	432%	347%
	Adhesive Bonded	22%	98%	107%	23%	X	80%
	Hybrid	28%	122%	133%	29%	124%	X

Table 4.11: *Comparison table of FEA peak strengths of AA 2024-T3–AA 2024-T3 and AA 2024-T3–CFRE joints of riveted, adhesive bonded, and hybrid joints.*

From FEA, for metal-metal joints, the hybrid joint has highest peak strength, which is 479% higher than that of the riveted joint and 109% of that of the adhesive bonded joint. For metal-composite joints, the adhesive bonded joint has highest peak strength, which is 432% higher than that of the riveted joint and 124% higher than that of the hybrid joint. This shows the importance of the adhesive bond in hybrid joints (from FEA point of view) and in adhesive bonded joints.

Among metal-metal and metal-composite joints, metal-metal hybrid joints have the best performance, followed by metal-composite adhesive bonded joints. From FEA results, it can be said that metal-metal hybrid joints are the best option for repairs of metal substrate with metal doubler, while adhesive bonded joints are the best option for repairs of metal substrate with composite doublers. The same was observed in experimental results where metal-metal hybrid joints and metal-composite adhesive bonded joints have highest average static peak strengths compared to their other joints.

The results from detailed stress analysis in FEA of metal-metal and metal-composite joints predict that, in both cases, hybrid joints will show the lowest Von-Misses stresses on both substrate and doublers.

Results from FEA analysis of metal cracked substrates with riveted and adhesive bonded reinforcements predict that:

- For crack length of 10 mm, adhesive bonded reinforcements have 25% lower SIF compared to riveted reinforcements.
- Among metal and composite doublers, lower SIFs are observed for metal doublers compared to composite doublers.

Joint configuration		**CFRE–CFRE**			**CFRE–AA**		
		Riveted	Adhesive Bonded	Hybrid	Riveted	Adhesive Bonded	Hybrid
CFRE–CFRE	Riveted	X	485%	360%	94%	331%	337%
	Adhesive Bonded	21%	X	74%	19%	68%	69%
	Hybrid	28%	135%	X	26%	92%	94%
CFRE–AA	Riveted	106%	514%	382%	X	351%	357%
	Adhesive Bonded	30%	147%	109%	28%	X	102%
	Hybrid	30%	144%	107%	28%	98%	X

Table 4.12: *Comparison table of FEA peak strengths of CFRE–CFRE and CFRE-AA 2024 joints of riveted, adhesive bonded, and hybrid joints.*

From Table 4.12, for composite-composite joints, adhesive bonded joints have highest static peak strength, which is 485% higher than that of riveted joints, and 135% higher than that of hybrid joints. On the other side, for composite-metal joints, hybrid joints and adhesive bonded joints have nearly the same static peak strength but the lowest peak strength is observed for riveted joints, which is 28% of that of hybrid and adhesive bonded joints. This shows the importance and significance of static peak strength of adhesive layer in adhesive bonded and hybrid joints.

Among composite-composite and composite-metal, composite-composite hybrid joints have the highest static peak strength. From FEA results, it can be concluded that adhesive bonded joints are the best option for repairs of composite substrates with composite doublers and hybrid joints are the best option for repairs of composite substrates with metal doublers.

From static FEA analysis of composite-composite and composite-metal riveted joints, it is observed that the lowest tensile stresses on composite substrate are observed for composite-metal riveted joints, whereas the lowest tensile stresses on doublers are observed for composite doublers of composite-composite riveted joints.

4.7 Summary of fatigue analysis in FEA

In this section, a summary of fatigue analysis in FEA is discussed. Table 4.13 shows a comparison of SERR for metal-metal, metal-composite adhesive bonded and hybrid joints.

Crack Length (mm)	**AA-AA**	**AA-CFRE**	**AA-AA vs AA-CFRE**
	Adh. Bonded vs Hybrid	Adh. Bonded vs Hybrid	Adh. Bonded
15	130%	132%	114%
30	276%	728%	92%
45	489%	460%	82%
60	717%	659%	71%
75	1250%	1177%	58%
90	1136%	1195%	47%

Table 4.13: *Comparison of SERR of AA-AA adhesive bonded vs hybrid, AA-CFRE adhesive bonded vs hybrid and AA-AA vs AA-CFRE adhesive bonded.*

From the Table 4.13, one can notice that adhesive bonded joints have higher SERR for both metal-metal and metal-composite joints. The lower SERR for hybrid joints can be explained due to the presence of rivets, which arrest the crack growth in these joints. Among metal-metal and metal-composite adhesive bonded joints, except for crack length of 15 mm, metal-metal adhesive bonded joints have lower SERR compared to metal-composite

adhesive bonded joints. This suggests under fatigue loading metal-metal hybrid joints have better performance.

The low SERR can be related to the experimental results, which showed better fatigue life of metal-metal and metal-composite hybrid joints compared to metal-metal and metal-composite adhesive bonded joints.

Crack Length (mm)	**CFRE-CFRE**	**CFRE-AA**	**CFRE-CFRE vs CFRE-AA**
	Adh. Bonded vs Hybrid	Adh. Bonded vs Hybrid	Adh. Bonded
15	143%	151%	85%
30	300%	322%	98%
45	565%	556%	109%
60	717%	735%	125%
75	3348%	2181%	154%
90	1304%	1288%	201%

Table 4.14: *Comparison of SERR of CFRE-CFRE adhesive bonded vs hybrid, CFRE-AA adhesive bonded vs hybrid and CFRE-CFRE vs CFRE-AA adhesive bonded.*

From Table 4.14, one can notice that SERR for adhesive bonded joints is higher than that of hybrid joints. The highest SERR for composite-composite and composite-metal adhesive bonded joints is observed for crack length of 75 mm, which is in between third and fourth rivet row in hybrid joint. This suggests that the crack in adhesive is arrested by third rivet in the hybrid joints. Among composite-composite and composite-metal joints, composite-composite hybrid joint have lowest SERR for crack lengths 15 and 30 mm compared to composite-metal hybrid joint. This suggests the crack growth for composite-composite hybrid joint is slower up to crack length 30 mm and for crack lengths larger than 30 mm, composite-metal joint have slightly lower FCG propagation. When FEA fatigue analysis is compared to experimental results, composite-composite hybrid joint have superior fatigue life.

Chapter 5: Conclusion

The objective of this thesis was to investigate and compare static strength and fatigue resistance of several aircraft repair patches made for metal and composite substrates. The substrates are repaired with metal and composite doublers under riveted, adhesive bonded, and hybrid joining methods. In this study, four joint combinations (metal substrate-metal doubler, metal-composite, composite-composite and composite-metal) were investigated experimentally and numerically. For each of these 12 joint configurations, three specimens were tested under static loads and three under fatigue loads. The results of a set of 36 static tests and 36 fatigue tests are thus reported in this thesis, and the main conclusions of this research are as follows:

Static response:

For, metal-metal and metal-composite configurations, adhesive bonded joints have thrice the average peak strength compared to riveted joints. However, metal-metal hybrid joints have higher average peak strength than riveted and adhesive bonded joints. Among composite substrate joints, riveted joints have also lower average peak strength than adhesive bonded and hybrid joints. Thus, for all the studied repair configurations, hybrid joints appear to be the most performing under static loading.

All the tested riveted joint specimens failed due to rivet shear. This clearly indicates that the rivets are the weakest elements in these joints. Hence, it appears that the strength of riveted joints can be easily improved by using rivets with higher strength.

All the tested specimens of metal-metal, metal-composite, and composite-metal adhesive bonded joint failed due to adhesive failure. Hence, it appears that the strength of adhesive bonded joints can be easily improved by using adhesives with higher strength. Conversely, two out of three composite-composite adhesive bonded joint specimens failed due to cohesive failure, and one specimen failed due to doublers failure.

Finally, hybrid joints failed mostly due to net-section failure, although some samples of metal-metal and composite-metal hybrid joints failed due to rivet shear and adhesive failure. The mentioned net-section failure occurred always in the composite plates (depending on the case, it occurred in the composite substrate or the composite doublers, like for metal-composite joints), indicating significant vulnerability of composites to rivet holes.

Fatigue response:

For all the studied repair configurations under fatigue loading, hybrid joints have highest life compared to riveted and adhesive bonded joints, except for composite-metal joints. The lowest fatigue lives were observed for riveted joints, while adhesive bonded joints have fatigue lives in between riveted and hybrid joints.

As in the static tests, most of the hybrid joint specimens failed due to net-section failure, except one specimen of metal-composite joint, which failed due to rivet shear and adhesive failure. However, none of the composite-composite joint specimens had failed at 600k loading cycles, and the tests were not further continued. Thus, no information is reported in this work about the failure mode of composite-composite joints under fatigue loading. All riveted joint specimens failed due to rivet shear, while all specimens of adhesive bonded joint failed due to adhesive failure. This clearly confirms the conclusions from the static test results pointing that the rivets and the adhesive are the weakest elements in the riveted and adhesive bonded joints, respectively.

Numerical analysis of each joint configuration was performed using commercial FEA tool ABAQUS, and the FEA results were compared with experiments. Point-based fasteners and Cohesive Zone Model were implemented in the numerical models for the rivets and the adhesive, respectively. The numerical results for static strength agree with experimental results with a maximum margin of 5%. Adhesive bonded reinforcements for metal-metal and metal-composite joints have 35% lower strength than riveted reinforcements.

(SERR) for the studied joint configurations are computed and compared for the adhesive bonded and hybrid joint fatigue analysis models. SERR results for hybrid joints are lower compared to adhesive bonded joints.

Fatigue life prediction tools such as FRANC2D/L and FRANC3D were used to predict fatigue lives of riveted and adhesive bonded joints. Helius composites tool is used to characterise material properties of composite substrate. Results from FRANC3D predicted that no significant difference in stress intensity factor is observed between metal-metal riveted and adhesive bonded joints. Results from FRANC2D/L predicted that for 23 mm crack length, metal-metal adhesive bonded joint have fatigue life of 600k cycles compared to riveted joint with just 4255 cycles.

Finally, the mechanical properties of the studied composite substrate are computed using Helius Autodesk Composite tool. Progressive failure analysis predicted that the initial failure of the substrate occurs in the 0/90 plies at 678 MPa, and that the complete substrate failure occurs at 226 MPa in the 45/135 plies. The failure of the 0/90 plies is due to fibre failure, while the failure of the 45/135 plies is due to matrix failure.

Chapter 6: Future Works

In this section, some of the possible future works for continuation of the project are discussed:

As adhesive bonding is a complex process which is highly dependent on adhesive layer thickness, bond area, and type of adhesive, apart from the manufacturing process, the debonding process in adhesive bonded joints could be further studied under static and fatigue loading.

Recent adhesives with carbon fibre nanoparticles embedded show very interesting mechanical properties. These adhesives can be implemented for airframe structural applications and further studying their performance in typical airframe repairs is challenging. High strength rivets can also be implemented in future studies of riveted and hybrid joints to obtain different failure modes.

Finally, the numerical analysis of the riveted joints in this thesis is based on an elastic rivet model, but in the future rivet plastic models could be used for a more accurate numerical analysis.

References

[1] Micheal Chun YN. Fasteners and Structural Joints. Micheal Chun YN (ed). *Airframe Structural Design*, 2nd ed. California: Conmilit Press Ltd.; **1988**: pp. 207-243.

[2] Faagov. *Damage Tolerance and Fatigue Evaluation of Structure Document Information. https://www.faa.gov/regulations_policies/advisory_circulars/index.cfm/go/document.information/documentID/865446 (accessed 13 July 2019).*

[3] Federal Aviation Regulation. *PART 25—AIRWORTHINESS STANDARDS: TRANSPORT CATEGORY AIRPLANES. https://www.faa.gov/regulations_policies/advisory_circulars/index.cfm/go/document.information/documentID/865446 (accessed 13 July 2019).*

[4] Hertel H. *Ermüdungsfestigkeit der Konstruktionen*. Germany: Springer; **1988**.

[5] Russell HW, Jackson LR, Grover HJ, Beaver WW. *Fatigue Strength and Related Characteristics of Aircraft Joints I- Comparison of spot-weld and rivet patterns in 24S-T AlClad sheer-Comparison of 24S-T AlClad and 75S-T AlClad*. Washington: NACA Wartime Reports; **1944**.

[6] Smith CR, Lindeneau GD. Riveted-Joints Fatigue Strength. (ed). *Fatigue of Aircraft Structures*. Philadelphia: ASTM International; **1957**: pp. 10-28. https://doi.org/10.1520/STP46290S

[7] Schije J. *The Fatigue Strength of Riveted Joints and Lugs*. Washington: NACA Technical Memorandum 1395; **1954**.

[8] Smith CR. Fatigue Resistance. *Aircraft Engineering and Aerospace Technology* **1960**; 35(5): 142-144. https://doi.org/10.1108/eb033250

[9] BENOIT, G.: Zum Gedächtnis an W.A . Julius Albert und die Erfindung seines Drahtseiles. Berlin: VDI-Verlag **1935**.

[10] Michael Chun YN. Airframe Structural Design. California: Conmilit Press Ltd; **1988**.

[11] Hartman A, Duyn GC. *A comparative investigation on the fatigue strength at fluctuating tension of several types of riveted lap joints, a series of bolted and some series of glued lap joints of 24 ST Alclad*. Amsterdam: NLR Report M.1857; **1952**.

[12] Oldersma A. *Fatigue of riveted joints- A literature survey and statistical analysis of existing test data*. Amsterdam: NLR Report CR 92401 L; **1992**.

[13] Hartman A. *A comparative investigation on the investigation on the influence of sheet thickness, type of rivet and number of rivet rows on the fatigue strength at fluctuating tension of riveted single lap joints of 24 ST Alclad sheet and 17 S rivets*. Amsterdam: NLR Report M.1943; **1954**.

[14] ESDU data sheet No. 79031. Endurance of riveted lap joints (aluminium alloy sheets and rivets). Engineering Science Data Unit, London; **1979**.

[15] United States Department of Transportation. Chapter 4: Aircraft Metal Structural Repair. (ed). *Aviation Maintenance Technician Handbook—Airframe*. United States: Federal Aviation Administration; **2018**.

[16] Skorupa A, Skorupa M. Production Variables Influencing the Fatigue Behaviour of Riveted Lap Joints. Gladwell GML (ed). *Riveted Lap Joints in Aircraft Fuselage*. Dordrecht: Springer; **2012**: pp. 27-28.

[17] Schijve J. *Fatigue of Structures and Materials*, 2nd ed. Amsterdam: Springer Netherlands; **2009a**.

[18] Schijve J. *The fatigue life of unnotched and notched 2024-T3 Alclad sheet material from different manufacturers*. Amsterdam: Report NLR TR 68093U; **1968**.

[19] Schijve J, de Rijk P. *The fatigue crack propagation in 2024 T-3 Alclad sheet materials from seven different manufacturers*. Amsterdam: Report NLR M.2162; **1966**.

[20] Hartman A, Jacobs FA, Van der Vet WJ. *Constant amplitude and programme fatigue tests on single lap joints in clad 2024-T3 and 7075-T6 aluminium alloy with two rows of rivets or huckbolts*. Amsterdam: Report NLR TN M.2147; **1965**.

[21] Hoffer K. *Permanent Fasteners for Light-Weight Structures*. Dusseldorf: Aluminium Verlag; **1984**.

[22] Barret RT. *Fastener Design Manual*. United States: NASA Reference Publication 1228; **1990**.

[23] Skorupa A, Skorupa M. Production Variables Influencing the Fatigue Behaviour of Riveted Lap Joints. Gladwell GML (ed). *Riveted Lap Joints in Aircraft Fuselage*. Dordrecht: Springer; **2012**: pp. 42-43.

[24] Hartman A. *The influence of manufacturing procedures on the fatigue life of 2024-T3 Alclad riveted single lap joints*. Netherlands: Report NLR TR 68072 U; **1968**.

[25] Schra L, Ottens HH, Vlieger H. *Fatigue crack growth in simulated Fokker 100 lap joints under MSD and SSD conditions*. Netherlands: Report NLR CR 95729 C; **1995**.

[26] Simpson A. The use of modern fastening systems to enhance the fatigue life of thin sheet structures. In: Berkovits, A. (ed.) Proceedings of the 15th ICAF Symposium, Aeronautical Fatigue in the Electronic Era, Jerusalem, Israel, 21–23 June 1989, pp. 243–262. EMAS, Warley **1989**.

[27] Atre A. *A finite element and experimental investigation on the fatigue of riveted lap joints in aircraft applications*. Ph.D. thesis, Georgia Institute of Technology, Atlanta; **2006**.

[28] Szymczyk E, Jachimowicz J, Agnieszka D. Numerical study of the influence of shape imperfections on residual stress fields in a rivet hole. *Journal of KONES Powertrain and Transport* **2007**; 14(2): 465-473.

[29] Leon A. Benefits of split mandrel cold working. *International Journal of Fatigue* **1998**; 20(1): 1-8.

[30] Chakherlou TN, Vogwell J. The effect of cold expansion on improving the fatigue life of fastener holes. *Engineering Failure Analysis* **2003**; 10(1): 13-24.

[31] Rans C, Straznicky PV, Alderliesten R. Riveting process induced residual stress around solid rivets in mechanical joints. *Journal of Aircraft* **2007**; 44(1): 323-329.

[32] Chakherlou, TN, Mirzajanzadech M, Saaedi, KH. Fatigue crack growth and life prediction of a single interference fitted holed plate. *Fatigue and Fracture of Engineering Materials and Structures* **2010**; 33(10): 633-644.

[33] Rodman, GA, Creager, M. Split mandrel vs split sleeve coldworking: dual methods for extending the fatigue life of metal structures. *In: Harris, Ch.E. (ed.) Proceedings of FAA/NASA International Symposium on Advanced Structural Integrity Methods for Airframe Durability and Damage Tolerance Hampton, 4–6 May 1994, NASA-CP-3274* **2010**: pp. 1078-1086.

[34] Park, JH, Atluri SN. Fatigue growth of multiple cracks near a row of fasteners holes in a fuselage lap-joint. *Computational Mechanics* **1993**; 13(3): 189-203.

[35] Krasnowski BR, Reddy DJ, Franada BG, Reid L, Restis J. Fatigue strength and damage tolerance of thin sheet riveted lap/splice joints with cold-expanded holes. *In: Rouchon, J. (ed.) Proceedings of 21st ICAF Symposium, Design for Durability in the Digital Age, Toulouse, France* **2001**: 195-207.

[36] Hartman A. *The influence of manufacturing procedures on the fatigue life of 2024-T3 Alclad riveted single lap joints.* Amsterdam: Report NLR TR 68072 U; **1968**.

[37] Fredell RS. *Damage tolerant repair techniques for pressurized aircraft fuselages.* : Ph.D. thesis, TU Delft; **1994**.

[38] Wanhill RJH. *Some practical considerations for fatigue and corrosion damage assessment of ageing aircraft.* Amsterdam: Report NLR TP 96253 L; **1996**.

[39] Schijve J, Jacobs FA, Meulman AE. *Effect of an anti-corrosion penetrant on the fatigue life in flight-simulation tests on various riveted joints.* Amsterdam: Report NLR TR 77103 U; **1977**.

[40] Schütz W. *Zeitfestigkeit einschnittiger Leichtmetall-Nietverbindungen Bericht Nr. F-47.* Darmstadt: Laboratorium für Betriebsfestigkeit; **1963**.

[41] Müller, RPG. *An experimental and analytical investigation on the fatigue behaviour of fuselage riveted lap joints. The significance of the rivet squeeze force, and a comparison of 2024-T3 and Glare 3.* Delft: Ph.D. thesis, TU Delft; **1995**.

[42] de Rijck JJM. *Stress analysis of fatigue cracks in mechanically fastened joints. An analytical and experimental investigation.* Delft: Ph.D. thesis, TU Delft; **2005**.

[43] Li G, Shi G. *Investigation of residual stress in riveted lap joints: experimental study.* Ottawa: Institute for Aerospace Research, NRC Report LTR-SMPL- 2003-0099; **2003**.

[44] Li G, Shi G. Effect of the riveting process on the residual stress in fuselage lap joints. *CASJ* **2004**; 50: 91-105.

[45] Megson THG. Structural components of aircraft. Megson THG (ed). *Aircraft Structures for Engineering Students.* United Kingdom: Elsevier Ltd.; **2013**: pp. 407-408.

[46] John Hart-Smith L. Adhesively Bonded Joints in Aircraft Structures. Lucas FM da Silva, Öchsner A, Robert DA (eds). *Handbook of Adhesion Technology.* Berlin: Springer; **2011**: pp. 1278-1279.

[47] Lehman GM, Hawley AV. *Investigation of Joints and Cutouts in Advanced Fibrous Composites for Aircraft Structures - Joint and Attachment Investigation*. Ohio: Air Force Flight Dynamics Laboratory; **1969**.

[48] Advanced Development of Boron Composite Wing Structural Components. AFML-TR-70-26I; **1970**.

[49] Advanced Composite Wing Structures - Vol. I Engineering. AFML-TR-70-231; **1970**.

[50] Hart-Smith LJ. *Adhesively-bonded double-lap joints*. Langley: Research Department NASA CR-112235; **1973**.

[51] Kelly LJ. Introductory Chapter. Baker AA, Jones R (eds). *Bonded Repair of Aircraft Structure*. Dordrecht: Martinus Nijhoff Publishers; **1988**: pp. 4-5.

[52] Kelly LJ. Introductory Chapter. Baker AA, Jones R (eds). *Bonded Repair of Aircraft Structure*. Dordrecht: Martinus Nijhoff Publishers; **1988**: pp. 7-9.

[53] Advanced Composite Repair Guide, Prepared by Northrop Corporation for United States Air Force, Air Force Wright Aeronautical Laboratories; **1982**.

[54] Kelly LJ. Introductory Chapter. Baker AA, Jones R (eds). *Bonded Repair of Aircraft Structure*. Dordrecht: Martinus Nijhoff Publishers; **1988**: pp. 9-10.

[55] Shannon RW, Stifel P, Beger R, Hughes EJ. *Primary Adhesively Bonded Structure Technology (PABST) General Material Property Data*, AFFDL-TR-77-107; **1978**.

[56] Bikales, Norbert M. *Adhesion and Bonding*. New York: John Wiley &Sons Inc; **1972**.

[57] Charles VC. *Adhesive bonding: techniques and applications*. New York: McGraw-Hill; **1968**.

[58] Reinhart TJ. Surface treatments for bonded repairs of metals . (ed). *Bonded Repair of Aircraft Structure*. Dordrecht: Springer; **1988**: pp. 19-30.

[59] Houwink R, Salomon G. *Adhesion and Adhesives*, 2nd ed. Amsterdam, London and New York: Elsevier Publishing Company; **1965**.

[60] Douglas FW, Bruno EJ. *Adhesives in Modern Manufacturing*. Indianapolis: Mishawaka; **1970**.

[61] Smith T. *Surface Treatment for Aluminum Bonding*. Rockwell Science Center, Report SC5180- 17FTR; **1979**.

[62] Hart-Smith LJ. Bolted and Bonded Joints. Daniel BM, Steven LD (eds). *Composites*. California: ASM Handbook; **2001**: pp. 167-176.

[63] Kweon JH, Jung JW, Kim TH, Choi JH, Kim DH. Failure of carbon composite-to-aluminum joints with combined mechanical fastening and adhesive bonding. *Composite Structures* **2006**; 75(1-4): 192-198.

[64] Sun C, Bhawesh K, Wang P, Sterkenburg R. Development of Improved Hybrid Joints for Composite Structures. *Composite Structures* **2005**; **35**: 1-20.

[65] Hart-Smith LJ. Bonded-Bolted Composite Joints. *Journal of Aircraft* **1985**; 22(11): 993-1000.

[66] Kelly G. Load transfer in hybrid (bonded/bolted) composite single-lap joints. *Composite Structures* **2005**; 69(1): 35-43.

[67] Paroissien E, Sartor M, Huet J. Analytical two-dimensional model of a Hybrid (Bolted-Bonded) Single-Lap Joint. *Journal of Aircraft* **2007**; 44(2): 573-582.

[68] Barut A, Madenci E. Analysis of bolted-bonded composite single-lap joints under combined in-plane and transverse loading. *Composite Structures* **2009**; 88(4): 579-594.

[69] Matsuzaki R, Shibata M, Todoroki A. Improving performance of GFRP/aluminium single lap joints using bolted/co-cured hybrid method. *Composites Part A- Applied Science and Manufacturing* **2008**; 39(2): 154-163.
[70] Pitta S, Carles VDLM, Roure F, Crespo D, Rojas JI. On the static strength of aluminium and carbon fibre aircraft lap joint repairs. *Composite Structures* **2018**; 201(1): 276-290.

[71] Benzeggagh ML, Kenane M. Measurement of Mixed-Mode Delamination Fracture Toughness of Unidirectional Glass/Epoxy Composites with Mixed-Mode Bending Apparatus. *Composite Science and Technology* **1996**; 56(4): 439-449.

[72] Camanho PP, Davila CG. Mixed-Mode Decohesion Finite Elements for the Simulation of Delamination in Composite Materials. *NASA/TM-2002–211737*, **2002**: 1–37.

[73] Sadowski T, Knec M, Golewski P. Experiment investigations and numerical modelling of steel adhesive joints reinforced by rivets. *International Journal of Adhesives and Adhesion* **2010**; 30(5): 338-346.

[74] Campilho RDSG, de Moura MFSF, Domingues JJMS. Using a cohesive damage model to predict the tensile behaviour of CFRP single-strap repairs. *International Journal of Solids Structures* **2008**; 45(5): 1497-1512.

[75] Pitta S, Rojas JI, Crespo D. Comparison of fatigue crack growth of riveted and bonded aircraft lap joints made of Aluminium alloy 2024-T3- A numerical study. *Journal of Physics: Conference Series* **2017**; 843(1): 1-10.

[76] Pitta S, Rojas JI, Crespo D, Abdel WM. Fatigue life analysis of un-repaired and repaired metallic substrate using FRANC2D. Abdel WM (ed). *Proceedings of the 7th International Conference on Fracture Fatigue and Wear. FFW 2018.* Singapore: Lecture Notes in Mechanical Engineering, Springer; **2018**. pp. 558-565.

[77] Helius Composite. *Christensen Criterion. https://knowledge.autodesk.com/support/helius-composite/learn-explore/caas/CloudHelp/cloudhelp/2017/ENU/ACMPDS/files/GUID-5FA2C5F8-51F7-4568-87C7-5C6EE4AF138C-htm.html (accessed 13 July 2019).*

[78] Chowdhury NM, Chiu WK, Wang J, Chang P. Experimental and finite element studies of bolted, bonded and hybrid step lap joints of thick carbon fibre/epoxy panels used in aircraft structures. *Composites: Part B Engineering* **2016**; 100: 68-77.

[79] Gohardani AS, Doulgeris, Singh R. Challenges of future aircraft propulsion: Areview of distributed propulsion technology and its potential application for the all electric commercial aircraft. *Progress in Aerospace Sciences* **2011**; 47(1): 369-391.